

Validation and identification of tumour endothelial markers and their uses in cancer vaccine

by
Xiaodong Zhuang

A thesis submitted to
The University of Birmingham
for the degree of
DOCTOR OF PHILOSOPHY



Molecular Angiogenesis Group
Department of Immunity and Infection
College of Medical and Dental Sciences
The University of Birmingham
September 2012

UNIVERSITY OF
BIRMINGHAM

University of Birmingham Research Archive

e-theses repository

This unpublished thesis/dissertation is copyright of the author and/or third parties. The intellectual property rights of the author or third parties in respect of this work are as defined by The Copyright Designs and Patents Act 1988 or as modified by any successor legislation.

Any use made of information contained in this thesis/dissertation must be in accordance with that legislation and must be properly acknowledged. Further distribution or reproduction in any format is prohibited without the permission of the copyright holder.

Abstract

The abnormal tumour microenvironment, which is typically hypoxic, acidic and with poor blood flow, induces the endothelial expression of genes not found on normal microvessels. By selectively targeting these tumour endothelial markers (TEMs) it is possible to induce tumour regression, presenting a potential strategy for therapeutic intervention. Potential TEMs were predicted by bioinformatics data mining. Validation of these TEM candidates identified a novel TEM CLEC14A. Functional characterization suggests a regulatory role of CLEC14A in endothelial cell migration. Inhibition of endothelial migration by CLEC14A antisera or monoclonal antibody holds therapeutic promise for the treatment of cancer. Differential gene expression analysis of freshly isolated lung tumour endothelium by 2nd generation sequencing identified 13 putative TEMs. Subsequent validation work confirmed six of which to be expressed on lung tumour vasculature. Finally, a pre-validated marker, Robo4, was investigated as a cancer vaccine. A strong antibody response was induced by delivery of pure mouse Robo4 protein or a Robo4 conjugate. The *in vivo* sponge assay in Robo4 vaccinated mice showed a significant reduction in vessel invasion. Tumour implantation experiments in vaccinated mice showed a marked delay in tumour growth.

Acknowledgements

My deepest thanks go to Professor Roy Bicknell for being an inspirational mentor and for sharing his scientific insights. I sincerely thank him for helping me through many difficulties in the past six years.

I would like to thank my co-supervisor, Dr. Zsuzsa Nagy for her guidance, advice, support and encouragement during the course of my PhD study.

I thank Gordon Ryan, Jane Steele, James Beesley, Rajeeb Swain and Victoria Heath for teaching me essential lab techniques and skills.

I express my gratitude to John Herbert for being a great friend and adventuring the TEM hunting with me. I extremely appreciate his excellent bioinformatics work that enabled us to generate interesting data.

I also express my thanks to Cancer Research UK and KTP for their funding.

My heartfelt thanks go to my wonderful wife Xue Lin for her endless support, constant encouragement and friendship.

I am equally indebted to my grandmother and my parents for their continuous support throughout these years.

List of contents

Introduction	1
1.1 Endothelial cells.....	2
1.2 Angiogenesis.....	3
1.3 Tumour angiogenesis.....	6
1.4 Anti-angiogenic therapy.....	8
1.5 VEGF as a target.....	9
1.6 Tumour vascular targeting.....	14
1.7 Tumour endothelial markers (TEMs).....	16
1.8 Identification of novel TEMs in lung cancer.....	23
1.9 Targeting tumour vasculature by vaccination.....	27
1.10 Aims and objectives.....	32
Materials and methods	34
2.1 Materials.....	35
2.2 Molecular biology methods.....	44
2.3 Mammalian cell isolation and culture.....	50
2.4 Transfection and transduction of mammalian cells.....	54
2.5 Protein analysis methods.....	57
2.6 Protein purification and Fc fragment removal.....	59
2.7 Methods used in expression analysis.....	60
2.8 Gene expression profiling methods.....	62
2.9 <i>In vitro</i> angiogenesis assays.....	64
2.10 <i>In vivo</i> angiogenesis assay.....	65
2.11 Generation of CLEC14A Knockout mice.....	66
2.12 Immunogenicity assay.....	67
2.13 Mouse immunization.....	68
2.14 Bioinformatics websites and programs.....	70

2.15 Statistical methods	71
Validation of potential TEMs	72
3.1 Introduction	73
3.2 CLEC14A is predominantly expressed in endothelial cells	74
3.3 CLEC14A siRNA knockdown in HUVEC.....	76
3.4 CLEC14A is expressed on vessels in tumours but not those in healthy tissue.....	77
3.5 Confirmation of CLEC14A as a tumour endothelial marker by immunohistochemistry..	85
3.6 GBP4 is highly expressed on tumour vessels and on vessels in some adjacent tissue.....	88
3.7 GBP4 is absent from vessels in healthy tissue	93
3.8 Validation of an IKBKE antibody by siRNA knockdown.....	96
3.9 Immunofluorescence of IKBKE on tissue samples.....	97
3.10 Conclusions.....	102
Functional chareacterization of CLEC14A	103
4.1 Introduction.....	104
4.2 CLEC14A knockdown inhibits endothelial cell migration	105
4.3 Polyclonal antisera to CLEC14A inhibits endothelial cell migration	107
4.4 Production of human and mouse CLEC14A protein using lentivirus	109
4.5 Generation of monoclonal antibodies to both human and mouse CLEC14A	111
4.6 Papain cleavage of CLEC14A-Fc protein and Fc fragment depletion	112
4.7 Evaluation of the CLEC14A monoclonal antibodies	114
4.8 Monoclonal antibody to CLEC14A inhibits endothelial cell migration.....	116
4.9 Overexpression of CLEC14A in HUVEC using a lentiviral system.....	118
4.10 Overexpression of CLEC14A inhibits HUVEC migration	120
4.11 Generation of germline transmission mice carrying a CLEC14A knockout allele.....	122
4.12 Generation of CLEC14A knockout mice	123
4.13 Confirmation of CLEC14A knockout in mice at the protein level.....	124
4.14 Conclusions.....	126

Identification of TEMs in lung cancer	127
5.1 Introduction.....	128
5.2 Laser microdissection approach.....	130
5.3 Endothelial isolation using <i>Ulex</i> coated beads.....	138
5.4 RNA-seq of lung endothelium	140
5.5 Microarray of biological replicates	142
5.6 Identification of lung TEM candidates.....	144
5.7 Validation of lung TEM candidates in EC isolated from NSCLC patients	146
5.8 Expression of TEM candidates in angiogenic tissue and lung cancer.....	148
5.9 Conclusions.....	151
Robo4 as a cancer vaccine	152
6.1 Introduction.....	153
6.2 Papain cleavage of human Robo4-Fc.....	154
6.3 Depletion of Fc fragments after papain digestion of human Robo4-Fc protein.....	156
6.4 Generation of a standard curve for assay of Robo4 antibodies in serum	158
6.5 Assay for Robo4 antibody in serum from cancer patients and healthy individuals	160
6.6 Expression of mouse Robo4-Fc in 293T cells after calcium phosphate transfection.....	162
6.7 Generation of a stable cell line expressing mouse Robo4 using lentivirus	164
6.8 Immunization with Robo4 in mice using protein vaccination.....	166
6.9 Sponge implantation assay in Robo4 immunized mice.....	168
6.10 Expression of Robo4 in the vasculature of the Lewis lung carcinoma tumour.....	172
6.11 Effect of Robo4 vaccination on growth of Lewis lung carcinoma in mice	174
6.12 Increased vascular leakage and neutrophil infiltration in tumours grown in Robo4 vaccinated mice.....	175
6.13 Soluble Robo4 conjugated to a carrier protein can induce a rapid protective antibody response in the absence of adjuvants	177
6.14 Tissue screen of Robo4 vaccinated mice.....	179
6.15 Conclusions.....	181

Discussion	182
Appendix	203
References	204

List of illustrations

Chapter one

Figure 1.1 Sprouting and intussusceptive angiogenesis.	5
Figure 1.2 Tumour angiogenesis	6
Figure 1.3 VEGF and its receptor system.	11
Figure 1.4 Structures of members in the endosialin family.	19
Figure 1.5 Structure of Robo4	23

Chapter two

Figure 2.1 Targeting strategy for generation of CLEC14A knockout mice.	67
--	----

Chapter three

Figure 3.1 Expression analysis of CLEC14A in primary cell isolates by real-time PCR.	75
Figure 3.2 Western blot of CLEC14A siRNA knock-down in HUVEC.	77
Figure 3.3a-c Confocal microscopic images (63X) of a human cancer tissue array stained with CLEC14A antibody.	79
Figure 3.4 Summary of CLEC14A expression in cancer and matched adjacent healthy tissue arrays.	82
Figure 3.5a-b Confocal microscopic images (63X) of healthy tissues stained with CLEC14A antibody.	83
Figure 3.6 Immunostaining of human liver showing adjacent healthy liver and hepatocellular carcinoma in the same section.	86
Figure 3.7 Comparison of CLEC14A immunostaining of healthy and tumor	87
Figure 3.8 Western blot on HUVEC of GBP4 siRNA knock-down.	89
Figure 3.9a-c Confocal microscopic images (63X) of a human cancer array with GBP4 antibody.	90
Figure 3.10 Summary of GBP4 expression in cancer and matched adjacent healthy tissue arrays	93
Figure 3.11a-b Confocal microscopy images (63X) of healthy tissues with GBP4 antibody.	94
Figure 3.12 SiRNA knock-down of GBP4 in HUVEC.	96
Figure 3.13a-c Confocal microscopy images (63X) of healthy tissues with IKBKE antibody.	98
Figure 3.14 Confocal microscopy images (63X) of cancer tissues with IKBKE antibody.	101

Chapter four

Figure 4.1 siRNA knockdown of CLEC14A inhibits endothelial cell migration.	106
--	-----

Figure 4.2 CLEC14A polyclonal antisera inhibits cell migration.	108
Figure 4.3 Purification of mouse CLEC14A-Fc protein.	110
Figure 4.4 Western blot of purified human and mouse CLEC14A-Fc protein.	110
Figure 4.5 Papain cleavage of human/mouse CLEC14A-Fc following Fc fragment depletion.	113
Figure 4.6 Confirmation of the specificity of monoclonal antibodies to human and mouse CLEC14A protein.	115
Figure 4.7 A monoclonal antibody to CLEC14A inhibits endothelial cell migration.	117
Figure 4.8 Western blot of CLEC14A transfected cells.	119
Figure 4.9 Overexpression of CLEC14A inhibits cell migration.	121
Figure 4.10 Chimera No.15 was identified carrying CLEC14A KO in the germline cells.	122
Figure 4.11 PCR on wild type and crossed arm of target vector and CLEC14A in wild type, CLEC14A heterozygous and KO mice.	123
Figure 4.12 Confirmation of CLEC14A KO at the protein level.	125

Chapter five

Figure 5.1 Scheme of strategies to identify TEMs in lung cancer.	129
Figure 5.2 Comparison of Cresyl violet and CD31 staining in the use of vessel dissection and RNA preservation.	131
Figure 5.3 Mapping strategy to obtain high quality RNA from laser microdissected samples.	133
Figure 5.4 Microarray of laser microdissected samples.	135
Figure 5.5 Potential difficulties for laser microdissection of normal and tumour lung.	137
Figure 5.6 Confirmation of endothelial enrichment and RNA integrity of <i>Ulex</i> -coated bead isolated endothelial samples.	139
Figure 5.7 RNA-seq confirmation of endothelial enrichment and elevation of MMPs and angiogenic associated genes.	141
Figure 5.8 Microarray of endothelial isolates from multiple patient samples.	143
Figure 5.9 Deep sequencing and microarray for the identification of putative lung TEMs	145
Figure 5.10 Quantitative real-time PCR validation of lung TEM candidates in EC isolated from NSCLC patients	147
Figure 5.11 Immunohistochemistry of lung TEM candidates on placental tissue.	149
Figure 5.12 Immunohistochemistry of lung TEM candidates on lung cancer tissue.	150

Chapter six

Figure 6.1 Optimization of papain cleavage of recombinant human Robo4-Fc.	155
Figure 6.2 Depletion of Fc fragments from papain cleaved human/mouse Robo4-Fc.	157
Figure 6.3 Standard curves for the assay of Robo4 antibodies in serum.	159

Figure 6.4 Assay of Robo4 antibody levels in serum from cancer patients.	161
Figure 6.5 Coomassie stain and western blot of Robo4 fractions from FPLC purified mouse Robo4-Fc.	163
Figure 6.6 Generation of a stable cell line expressing Robo4 and the purification of recombinant Robo4 protein.	165
Figure 6.7 Vaccination of mice with mouse Robo4 generates a Robo4-specific IgG response.	167
Figure 6.8 Sponge implantation assay in Robo4 vaccinated mice.	170
Figure 6.9 Comparison of vessel size between the sponges from Robo4 vaccinated and control mice.	171
Figure 6.10 Expression of Robo4 in the vasculature of the Lewis lung carcinoma tumour.	173
Figure 6.11 Tumour growth in Robo4 vaccinated mice.	174
Figure 6.12 Staining of fibrinogen and neutrophils in Lewis lung tumour from control and Robo4 vaccinated mice.	176
Figure 6.13 Induction of protective Robo4-specific antibody in carrier-primed animals	178
Figure 6.14 H+E staining of tissues from control and Robo4 vaccinated mice.	180

List of tables

Table 1 Monoclonal antibodies to human and mouse CLEC14A	111
Table 2 Number of offspring of each genotype from CLEC14A heterozygous parents.	123
Table 3 Comparison of protein production by calcium phosphate transfection and lentiviral expression systems	165

List of abbreviations

ANOVA	Analysis of variance
bFGF	Basic fibroblast growth factor
BSA	Bovine serum albumin
cDNA	Complementary DNA
CGG	Chicken Gamma Globulin
CRT	Cancer Research Technology
CRUK	Cancer Research UK
DAPI	4,6-diamidino-2-phenylindole
DLL4	Delta like ligand 4
DMSO	Dimethyl sulfoxide
ECs	Endothelial cells
ECSCR	Endothelial cell-specific chemotaxis receptor
EDTA	Ethylenediaminetetraacetic acid
EGFR	Epidermal growth factor receptor
ELISA	Enzyme-Linked ImmunoSorbent Assay
EPCAM	Epithelial cell adhesion molecule
FACs	Fluorescence-activated cell sorting
FCS	Fetal calf serum
FDA	Food and Drug Administration
FITC	Fluorescein isothiocyanate
FPLC	Fast protein liquid chromatography
GFP	Green fluorescent protein
GM-CSF	Granulocyte-macrophage colony-stimulating factor
H&E	Hematoxylin and eosin stain
HASMC	Human aortic smooth muscle cells (HASMC)
HBE	Human bronchial epithelial cells
HDMEC	Human dermal microvascular endothelial cells
HUVEC	Human Umbilical Vein Endothelial Cell
IFN	Interferon
IRES	Internal ribosome entry site
KD	Knockdown
KDR	Kinase insert domain receptor
KO	Knockout
LB	Lysogeny broth
LCM	Laser capture microdissection
LLC	Lewis lung carcinoma
mAb	Monoclonal antibody
MHC	Major histocompatibility complex
MMPs	Metalloproteinases
MWCO	Molecular Weight Cut-off
NF	Nuclease Free
NSCLC	Non-small cell lung cancer
OD	Optical density
PAGE	Polyacrylamide gel electrophoresis

PBMC	Peripheral blood mononuclear cell
PCA	Principal component analysis
PCR	Polymerase chain reaction
PDGFR	Platelet-derived growth factor
PIGF	Placental growth factor
PMSF	phenylmethanesulfonyl fluoride
qPCR	Quantitative real time PCR
RIN	RNA integrity number
RT	Room temperature
SAGE	Serial Analysis of Gene Expression
SDS	Sodium dodecylsulfate
SEM	Standard error of the mean
siRNA	Small interfering RNA
SSC	saline-sodium citrate
TEM	Tumour endothelial marker
TKIs	Tyrosine kinase inhibitors
TNF	Tumor necrosis factor
UV	Ultraviolet
VEGF	Vascular endothelial growth factor
VEGFR	Vascular endothelial growth factor receptor

Chapter one

Introduction

1.1 Endothelial cells

Endothelial cell

Endothelial cells line the inner surface of all blood and lymphatic vessels, forming a barrier between the circulating blood or lymph and the rest of the vessel wall or tissue.

The thin monolayer of endothelium controls the transport of proteins, solutes and gases as well as cells across the blood vessel wall [1, 2]. All vascular endothelium is supported by a basement membrane. A lumen of capillaries is formed by 2 to 5 endothelial cells and is partially covered by pericytes. Unlike capillaries, arteries and veins are surrounded by vascular smooth muscle cells and collagenous connective tissue. The mural cells not only provide a structural support to the vasculature but also cross-talk with the endothelial cells and restrict endothelial motility [3].

Endothelial cells are involved in various aspects of vascular biology, including blood coagulation, functional barrier, vasoconstriction/vasodilation and inflammation [4].

Furthermore, *de novo* vascular development and angiogenesis are processes that are orchestrated by endothelial cells [5]. ECs are normally quiescent in healthy tissue but are sensitive to signaling molecules from the extracellular environment. Inadequate activation or inactivation of endothelial cells by these signals has been associated with a variety of vascular disorders and disease [6].

Types of endothelial cells

Following the seminal work of Gerhardt and Betsholtz, the concept of endothelial tip

and stalk cells [7] and later the stabilized phalanx cell were introduced [8]. When growth factors reach the vessels, only a subpopulation of endothelial cells acquire the tip cell phenotype. Tip cells pioneer the formation of new blood vessels, termed angiogenesis, by projecting sprouts and talking to the guidance cues in the extracellular environment. Next to the tip cells, the stalk cells with less filopodia are actively proliferative to build up a lumen supporting the elongation of the new sprout. Unlike tip and stalk cells, phalanx cells are quiescent endothelial cells, which form a tight barrier to maintain vascular stability and control permeability. These cells rarely project filopodia and show poor motility. As active angiogenesis initiates with tip cells, much interest has centered on what switches a stabilized phalanx cell into a stalk or tip cell.

1.2 Angiogenesis

The human vascular network supplies nutrients and oxygen to almost all organs throughout the body while removing metabolic waste. Angiogenesis describes the formation of new blood vessels from the pre-existing ones [9]. In all adults, physiological angiogenesis occurs in the wound healing process. While in women, it also takes place in the menstrual cycle and during pregnancy. Since the vessels connect to every part of the body, abnormal growth of vessels leads to numerous pathological conditions. So far, there are more than a hundred disorders have been implicated to be angiogenesis dependent. For instance, insufficient vessel growth or

vessel regression causes stroke, ischaemic heart disease, ulcerative disorders and neurodegeneration whilst excessive angiogenesis leads to rheumatoid arthritis, pulmonary hypertension, age-related macular degeneration and tumour progression in cancer [5].

Vasculogenesis is the formation of a primitive vasculature and is a process that occurs before angiogenesis. During embryonic development, when diffusion of nutrients is no longer sufficient to meet the growth rate, mesoderm derived endothelial precursors, known as angioblasts, assemble into new vessels and differentiate into a primitive vascular network [10]. Angiogenesis further remodels the initial vasculature into arteries and veins by sprouting [11]. Mural cells, such as pericytes and smooth muscle cells, are then recruited to stabilize the vessel wall and allow perfusion [12, 13].

Types of angiogenesis

Sprouting angiogenesis was the first described pattern of angiogenesis (**Figure 1.1**). This type of angiogenesis proceeds with the activation of surface receptors on the endothelial cells within the pre-existing vasculature by growth factors such as vascular endothelial growth factor (VEGF). The activated endothelial cells become unstable and invasive and change their morphology by protruding filopodia. These cells then begin to secrete proteolytic enzymes to dissolve the basement membrane supporting the existing blood vessels [14, 15]. This is followed by proliferation and migration, where endothelial cells form an entirely new lumen towards the source of

the growth factors. Pericytes are subsequently recruited to stabilize the newly formed vessels [16].

Besides sprouting angiogenesis, other vessel growth patterns exist through different mechanisms. For example intussusceptive angiogenesis is the splitting of an existing vessel into two, initiated by the establishment of an endothelial cell junction within the capillary [17]. Since this type of angiogenesis can dramatically expand the capillary without increasing the number of endothelial cells, it is particularly important during embryonic development where the number of endothelial cells is limited [18]. Circulating endothelial precursor cells can also contribute to the expansion of the existing vasculature [19]. Despite the existence of these other vessel growth patterns, therapeutics targeting the tumour vasculature have focused on inhibiting sprouting angiogenesis or targeting the established vasculature within the tumour.

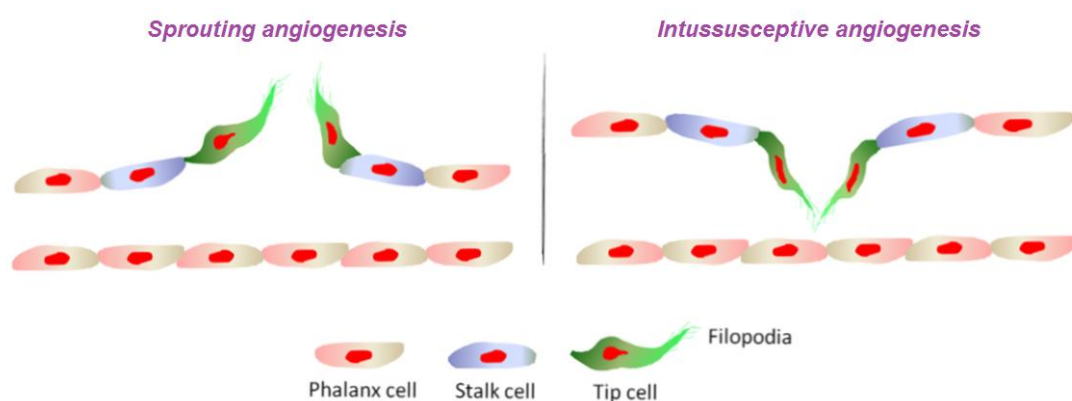


Figure 1.1 Sprouting and intussusceptive angiogenesis. Sprouting angiogenesis; the formation of new blood vessels through degradation of basement membrane by proteases released from the activated endothelial cell, followed by migration and tube formation. Intussusceptive angiogenesis; the splitting of an existing vessel into two, initiated by the establishment of an endothelial cell junction within the capillary.

1.3 Tumour angiogenesis

Like healthy organs, a tumour needs blood vessels to acquire oxygen and nutrients to allow its growth. Initially, micro-tumours survive by local diffusion. However, when a tumour reaches a certain size, approximately 3 mm^3 , diffusion is no longer sufficient to meet its growth rate. At this stage, the avascular tumour could become dormant for an indefinite period of time. However, tumours can overcome this inadequacy by building up a new blood supply through recruitment of new vessels from the adjacent existing vessels. This process is called tumour angiogenesis (**Figure 1.2**).

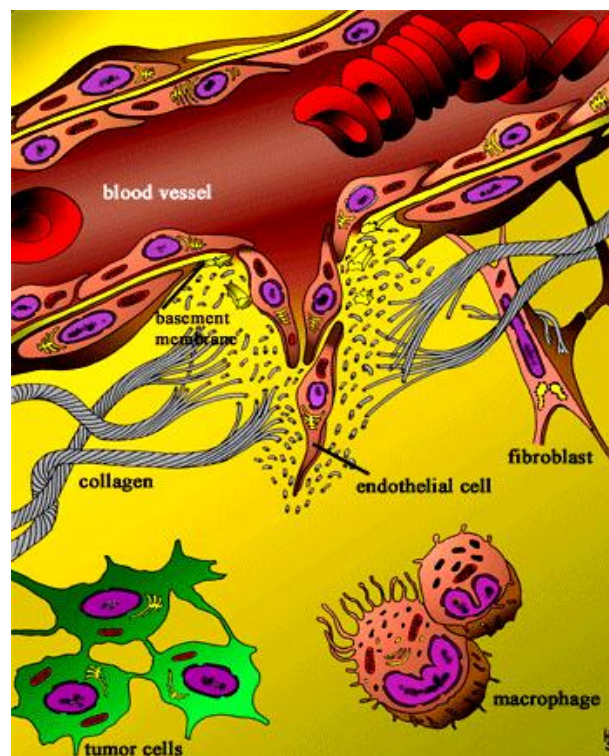


Figure 1.2 Tumour angiogenesis Endothelial cells secrete proteolytic enzymes that dissolve the basement membrane surrounding the existing blood vessels. Small capillaries form by the migration and proliferation of endothelial cells orchestrated by angiogenic growth factors. Stabilization of the newly formed vessels is achieved by secretion of basement membrane extracellular matrix [20]. Image used with permission.

Tumour cells secrete growth factors (pro-angiogenic factors) such as IL8, bFGF and VEGF that diffuse into the surrounding tissues. The existence of soluble angiogenic factors was elusive until Folkman and his colleagues proved it in a rabbit cornea model in the early 1970s. In that study, a small piece of tumour, about 0.5 mm³, was implanted into the stromal layers of a rabbit cornea away from the limbal edge. 10 days later, new blood vessels from the limbus had reached the tumour. However, the tumour implanted into the centre of the cornea expanded slowly until the edge of the tumour extended to less than 2 mm from the limbus and the recruitment of new blood vessels eventually occurred [21].

Endothelial cells express many tyrosine kinase receptors that are highly sensitive to angiogenic factors. The binding of growth factors to their receptors activates intracellular signaling involved in endothelial migration and proliferation. As described earlier, upon activation, the quiescent endothelial cells start to form sprouts to sense the guidance cues. Later, a newly formed vessel is extended towards the source of the stimuli, a starving tumour. In order to survive, the tumour vasculature is being constantly remodeled. Therefore, like the proliferation of cancer cells, once occurred, tumour angiogenesis becomes an ever progressing process. It is widely accepted that blocking this process could starve the tumour and lead to regression [22-24].

1.4 Anti-angiogenic therapy

Besides surgical removal of the malignant tissue, there exist two major therapies to treat cancer patients: chemotherapy and radiotherapy. Chemotherapy was designed to induce apoptosis of rapid proliferating tumour cells by disrupting their DNA replication or transcription. Radiotherapy uses photons or charged particles to damage the DNA chain, which subsequently causes cell death. Although chemotherapy and radiotherapy have been successful in reducing primary tumour burden, these two approaches rarely achieve lasting benefits for those with advanced or metastasized disease. This is mainly due to their unspecified toxicity that not only harms the rapid growing cancer cells but also healthy tissues that have relatively high proliferative rates; especially hair follicles and bone marrow. An ideal therapy for cancer should be able to kill tumours beyond its primary site but spare healthy tissue. Anti-angiogenic therapy has the advantage in both counts and has drawn much attention as a strategy to treat cancer.

In 1971, Folkman and colleagues proposed that angiogenesis inhibitors can stop tumour growth by choking off its blood supply and that anti-angiogenesis held therapeutic potential in the treatment of cancer [25]. Since then anti-angiogenic therapy became an active field attempting to prevent or destroy tumour vasculature by manipulating the growth of new blood vessels. In principal, anti-angiogenic therapy would have a number of advantages over the traditional anti-cancer therapies. Firstly, cancer cells are genetically unstable which results in drug resistance. In contrast,

anti-angiogenic therapies mainly target the endothelial cells which have a much lower mutation rate, therefore drug resistance is less likely to develop. Secondly, one endothelial cell supports the survival of tens to hundreds of cancer cells. It is conceivable that taking one endothelial cell out could lead to a 10 – 100 fold increasing death of cancer cells that relied on it [26]. Thirdly, anti-cancer agents are difficult to deliver into the tumour because of the interstitial pressure. However, this problem could be avoided as the endothelial cells have direct contact with the blood stream which is highly accessible for anti-angiogenic agents. Finally, all tumours need angiogenesis to allow their growth and expansion. This indicates that anti-angiogenic agents have the ability to inhibit a wide range of tumour types [27]. Taken together, anti-angiogenic therapy is a promising strategy with many advantages over conventional treatments and development of such therapy is ongoing.

The VEGF pathway has been the focus of this field and therefore extensively pursued for the last three decades [28, 29]. Accumulating evidence shows that blocking this pathway by neutralizing VEGF or disrupting their cognate receptor tyrosine kinases results in reduced tumour burden and increased survival [30].

1.5 VEGF as a target

Tumour angiogenesis is a complicated process that involves multiple regulators in which the most prominent one is vascular endothelial growth factor – VEGF (also

called VEGF-A). VEGF-A is a pro-angiogenic molecule that stimulates endothelial proliferation, migration, tube formation and survival [31-33]. Deletion of VEGF-A in mice is embryonic lethal due to abnormal development of blood vessels, suggesting VEGF-A is essential for the development of normal vasculature [34, 35].

The VEGF family comprises VEGF-A, VEGF-B, VEGF-C, VEGF-D, VEGF-E and placental growth factor (PlGF). VEGF receptors (VEGFRs) are single transmembrane proteins that belong to the receptor tyrosine kinase superfamily. The extracellular region of VEGFRs contains 7 immunoglobulin-like domains and the intracellular region composed of a split tyrosine kinase domain and a C-terminal tail. The receptors dimerize when cognate VEGF members bind to them on the cell surface, which is followed by phosphorylation and activation of the tyrosine kinase domain (**Figure 1.3**).

All VEGF(R) members are involved in angiogenesis and/or lymphoangiogenesis and have therapeutic potential. Among the VEGF members, VEGF-A is the most potent pro-angiogenic growth factor which strongly induces physiological and pathological angiogenesis by signaling through VEGFR-2 (also called FLK-1, KDR) [36]. The hypoxic environment of a tumour significantly induces the expression of VEGF-A [37]. As angiogenesis can be directly induced by the binding of VEGF to VEGFR2, this pathway provides an attractive pharmaceutical target for various vascular diseases, especially cancer. Expression of VEGFR2 is also found in lymphatic endothelium

which implied a role of VEGF-A in lymphoangiogenesis [38, 39]. VEGF-A also binds to VEGFR1 with a higher affinity but this receptor triggers a weaker phosphorylation signal compared to VEGFR2 [40, 41]. Since VEGFR1 has been involved in inflammation and cancer, this pathway has also offered a useful target [42-44]. VEGF-C and VEGF-D and their cognate receptor VEGFR3 are deeply involved in lymphoangiogenesis and have proven a critical system for lymph node metastasis [45, 46]. VEGF-E specifically binds to VEGFR2 to induce angiogenesis [47]. VEGF-E has been investigated in proangiogenic therapy and showed less side effects compared with patients treated with VEGF-A [48, 49].

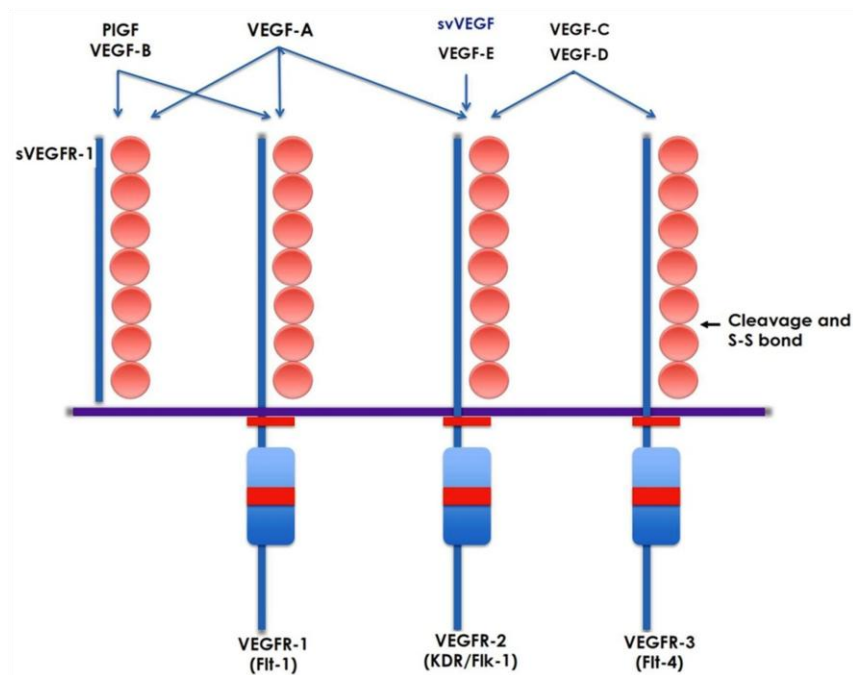


Figure 1.3 VEGF and its receptor system. Major signals of angiogenesis are generated from VEGFR2. Although VEGFR1 has a weak tyrosine kinase activity, it also stimulates angiogenesis via recruitment of bone marrow-derived mononuclear cells. VEGFR1 plays an important role in inflammation and atherosclerosis. Soluble VEGFR1 is involved in placental regulation and avascularity in the cornea. Figure was adapted from [50].

VEGF clinical achievements and challenges

Owing largely to the essential role played by VEGF in vascular development and tumour angiogenesis, significant efforts have been invested to explore the therapeutic use of VEGF blocking agents. Numerous pre-clinical studies have shown that in either orthotopic or ectopic human xenograft tumour models, the disruption of VEGF signaling led to a dramatic reduction of tumour progression [51]. Collective evidence has paved the way for anti-angiogenic drugs towards clinical application. In 2004, the Food and Drug Administration (FDA) approval of Avastin, the first anti-angiogenic drug, led to a boost in the development of several drugs that target the VEGF signaling pathway, namely VEGF(R) blockers.

Avastin is a humanized monoclonal antibody to VEGF-A that was designed for inhibiting tumour angiogenesis by neutralizing VEGF-A. Nowadays the use of Avastin has extended to metastatic non-squamous non small cell lung cancer, metastatic breast cancer and metastatic renal cell carcinoma in the form of chemotherapy or cytokine therapy combination or to recurrent glioblastoma multiforme as a monotherapy [52]. Another group of VEGF(R) blockers are multi-targeted tyrosine kinase inhibitors (TKIs) including sorafenib (targeting VEGFR2 and 3, PDGFR, Raf), sunitinib (targeting VEGFR2, PDGFR & c-kit²⁷) and pazopanib (targeting VEGFR 1-3, PDGFR & c-kit⁹²) and most of these have been approved for treating metastatic renal cell carcinoma. More recently, vandetanib (targeting VEGF1-3, PDGFR, EGFR & RET^{30, 95}) has been approved to treat

unresectable or metastatic medullary thyroid cancer but the clinical outcome has not yet been released. These VEGF(R) blockers generally provide an improvement of progression-free survival of up to a few months in cancer patients [5]. Besides the treatment of cancer, Avastin and two other anti-VEGF drugs: pegaptanib (VEGF aptamer) and ranibizumab (VEGF Fab antibody), have been approved to treat age-related macular degeneration that often causes blindness due to damage to the vasculature [53-56].

Despite these successes in the treatment of cancer, the clinical data has shown that the use of anti-angiogenic therapy was not as potent as it was hoped for. The initial goal of the anti-angiogenic therapy was to inhibit angiogenesis and reduce the vascular supply to the tumour. However, their benefit was limited by the insufficient capability or the initial refractoriness and later, resistance [57]. Increasing evidence from pre-clinical and clinical studies suggests that VEGF blockers cause normalization of the tumour vasculature and that the conversion of abnormal tumour vessels into functional ones has become a complementary therapeutic paradigm [58]. This is mainly because the normalized tumour vessels can facilitate the delivery of chemotherapeutic drugs and immune cells [59]. This also explained, to some extent, why cancer patients have not benefited from single agent anti-angiogenic treatment.

More recent studies have shown that VEGF targeting strategies, including anti-VEGFR2 and VEGFR tyrosine kinases, suppressed primary tumour growth but

also accelerated metastasis and shortened survival time in mice [60, 61]. One possible mechanism is that these anti-angiogenic drugs often increase tumour hypoxia due to their efficiency of pruning the tumour vasculature, in turn leading to a hypoxic niche, facilitating the selection of more aggressive, hypoxia-resistant cancer cell clones [62]. Ebos et al. also reported that pre-treating healthy mice with VEGF inhibitors caused increased metastasis in ectopic tumour models [60]. These findings implied a pre-conditioning of the blood vessel system, which, possibly due to an unknown effect on the normal vasculature, facilitates tumour cell seeding and revascularization.

1.6 Tumour vascular targeting

Targeting the tumour vasculature is different from anti-angiogenic therapy. Vascular targeting aims to limit tumour growth by specifically destroying the established vasculature that supports tumour survival, expansion and metastasis, while exempting the normal vasculature from the same effects. Instead of preventing neo-vessels from growing, the established vasculature in tumours has been explored as a target for cancer treatment.

The study which provided proof of principle that vascular targeting can be used to eradicate solid tumours in mice came from the work of Burrows and Thorpe in 1993 [63]. In this study, a neuroblastoma tumour line was engineered to secrete interferon gamma (IFN- γ) that is known to induce the expression of MHC class II antigens on

endothelial cells residing in the tumour. They then coupled ricin to an anti-mouse MHC class II antibody and showed that a single injection resulted in extensive haemorrhagic necrosis and elimination of the tumours [63]. A later study supported this strategy by directing a thrombogen, tissue factor to the tumour vasculature, which led to complete tumour eradication in mice [64]. A recent study targeting phosphatidylserine that is normally intracellular but exposed on the luminal surface of tumour endothelial cells, also showed inhibitory effects on tumour growth, again supporting a vascular targeting strategy [65].

Despite success in animal models, the translation of vascular targeting agents to the clinic has been slow, owing largely to the absence of a rigorously characterized tumour vascular target in man. The success of antibody and vaccine approaches will be reflected by the specificity of the target for tumor endothelium, and this has prompted the search for well-defined targets. Indeed, as targeting can be achieved with antibodies, antibody conjugates, and more recently, vaccines and modified T cells (reviewed in [22]; [66, 67]), a naturally occurring marker of tumor endothelial cells would provide significant therapeutic promise. Unfortunately, the expression of some of these targets is not as widespread as was hoped for [22], and there remains a need to identify novel and improved tumour endothelial molecular targets.

1.7 Tumour endothelial markers (TEMs)

Fundamental differences between tumour and normal vasculature present unique targets for anti-cancer therapy [68]. A major cause of these differences is the influence of the extracellular environment on the endothelial transcriptome. Endothelial cells resident within a tumour are exposed to an extracellular environment markedly different from that of endothelial cells resident in healthy tissue. For example, an endothelial cell within the tumour microenvironment will experience hypoxia and that alone can change the expression of up to 2000 genes [69]. Tumours also show glucose deprivation, acidic extracellular pH, high interstitial pressure [70], excess of pro-angiogenic factors and increased mechanical compression [71]. Each of these factors may influence the transcriptome of the endothelial cells residing within tumours. Considerable effort has been invested to identify and validate the genes that are restricted to the tumour vessel, known as Tumour Endothelial Markers (TEMs). Although the putative TEMs to date have not been studied in clinical trials, the investigation of their potential in the treatment of cancer has raised wide interest [23].

Identification of TEMs

Numerous endothelial specific genes have now been identified and functional studies have shown that many play a role in angiogenesis [72, 73]. Attempts to identify TEMs have included construction of SAGE libraries from freshly isolated endothelium [74], use of microarray platforms [75], proteomic analysis of freshly isolated endothelial

cell membranes [75, 76] as well as bioinformatics data mining [77, 78]. These efforts succeeded in identifying candidates including the EDB domain of fibronectin, a series of numbered TEM's, annexin A and Robo4 reviewed in [79]. There nevertheless remains an urgent need to identify novel and improved vascular targets.

In order to identify the genes that are only expressed in tumour endothelium but not that in normal tissue, our group have predicted novel putative tumour endothelial markers by bioinformatics data mining in public EST and SAGE libraries [78]. In brief, endothelial genes were firstly identified by in-silico subtraction of genes expressed in endothelial cells versus those in non-endothelial cells. Tumour genes were then identified by subtracting bulk tumour libraries from bulk normal ones. The genes present in both lists were considered putative tumour endothelial markers [78]. In this study, three putative TEMs have been chosen for validation based on the level of association with endothelial cells, previously published work, intellectual property, sites of expression and relation to known genes with interesting functional properties.

Putative TEMs

CLEC14A

CLEC14A (C-type lectin domain family 14 member A), also called EGFR5 or C14orf27, is a type I transmembrane protein that belongs to the C-type lectin domain family. A C-type lectin is a type of sugar-binding protein domain [80]. The C-type

originated from the requirement of calcium for carbohydrate binding. Proteins containing the C-type lectin domain have a wide range of biological functions such as cell-cell contact, immune response to pathogens [81] and apoptosis [82]. CLEC14A is a member of the Endosialin family that has three other members: Endosialin, CD93 and thrombomodulin (**Figure 1.4**). Endosialin was originally reported to be found in small blood vessels in tumours, however its expression was later found on fibroblasts and pericytes [83]. CD93 is expressed on endothelium, myeloid cells, platelets and stem cells and is involved in leukocyte and endothelial cell adhesion. It also can have a role in the regulation of phagocytosis of apoptotic cells and antibody production [84]. Thrombomodulin is an endocytic receptor expressed in endothelial cells. It is involved in sequestration of thrombin and the activation of protein C [85, 86]. The function of CLEC14A remains unknown.

Full length CLEC14A is a 51.6 kDa protein which has 490 amino acids. The extracellular domain (amino acids 23 to 398) includes a C-type lectin domain or carbohydrate recognition domain and a single EGF-like domain. The transmembrane domain of amino acids 399 to 421 is followed by a small cytoplasmic tail of 69 amino acids. Bioinformatic analysis of potential sites of glycosylation predicted one highly conserved N-glycosylation site and nine poorly conserved potential O-glycosylation sites.

Previous work in our group has shown selective expression of CLEC14A in

endothelial cells by PCR on various cell lines. Weak expression was detected in fibroblasts and placenta (site of active angiogenesis). No expression could be detected in a variety of primary cells or cell lines. We also found that the expression of CLEC14A was induced by low shear stress which strongly correlates with the reduced blood flow in ill formed tumour vessels [87].

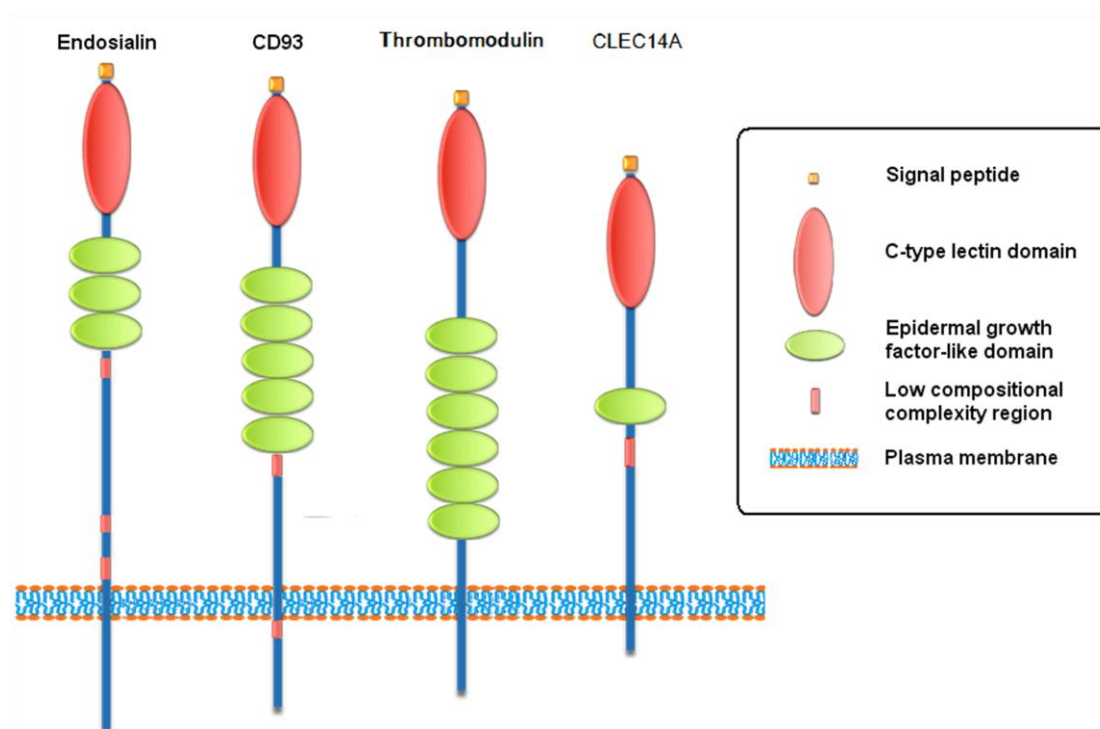


Figure 1.4 Structures of members in the endosialin family. C-type lectin domain (pink). 1-6 EGF domains (green). Pro/Ser/Thr rich domain (pink bar). A transmembrane domain (blue).

GBP4

GBP4 (Guanylate binding protein 4) is a member of the guanylate binding protein family which belongs to the GTPase superfamily. Seven members have been discovered in man: hGBP1-7 and all members are expressed by endothelial cells and

inducible by IFN- γ [88].

GBP1 is the best characterized member in the family. *In vitro* studies showed that GBP1 can be induced by many inflammatory cytokines including IFN- γ , interleukin-1 β (IL-1 β), IL-1 α and TNF- α [89]. Emerging evidence demonstrated that GBP1 plays a role in angiogenesis and cancer. The helical domain of GBP1 is tightly associated with the inhibition of endothelial cell proliferation and invasion induced by inflammatory cytokines [90]. The most recent publication demonstrated that induction of GBP1 by doxycycline inhibits tumour growth in mice [91]. GBP2 was recently characterized as a p53-regulated tumour marker in esophageal squamous cell carcinomas [92]. Three GBP5 splicing variants (gbp-5a, -5b and -5ta) that lead to two proteins: GBP-5a/b and GBP-5ta were identified in cutaneous T-cell lymphoma and melanoma cell lines at a high expression level [93].

The whole GBP4 gene is 6160 bp with 10 exons (Cds 1923 bp), located on chromosome 1. Its protein product contains 640 aa and the molecular weight is predicted to be 73 kDa. It has a GTP binding site motif at aa 60-67 and aa 112-116 and a coiled-coil domain at aa 498-612. In endothelial cells, GBP4 can be induced by IFN- γ but not TNF- α . Its subcellular localization was revealed in both the cytoplasm and the nucleus [88]. At present, there is little known about GBP4 in respect of tumour specificity or its function in endothelial biology.

IKBKE

IKBKE (Inhibitor of kappa light polypeptide gene enhancer in B cells, kinase epsilon), also named IKKi or IKK ϵ , belongs to the IKK family which includes another three members: IKK α , IKK β and a regulatory subunit IKK γ (NEMO) that play a key role in the NF- κ B signaling pathway [94].

In the classic NF- κ B pathway, IKK α , IKK β and NEMO form a core IKK complex that is firstly activated by the upstream stimuli and subsequently phosphorylates the NF- κ B inhibitory protein I κ B α . This leads to the ubiquitination of I κ B α and allows NF- κ B to translocate into the nuclear and activates the transcription of target genes [94].

IKBKE is a serine/threonine protein kinase which consists of 716 amino acids with predicted molecular weight of 70 kDa. The protein sequence of IKBKE shares 33% and 31% homology to IKK α and IKK β respectively. Although IKBKE processes the function in the activation of NF- κ B, it was not induced by TNF- α and IL-1 like IKK α and IKK β but it is activated by interferon, phorbol12-myristate 13-acetate or the T-cell receptors. Therefore IKBKE has also been described as a non-canonical IKK family member [95-97].

In 2007, IKBKE was characterized as a breast cancer oncoprotein using integrative genomic approaches. The gene was overexpressed in over 30% of breast carcinomas

and breast cancer cell lines [98]. The same group later reported that serine 418 of the tumour suppressor CYLD was directly phosphorylated by IKBKE and promotes cell transformation [99]. IKBKE has also been associated with tumour progression and cisplatin resistance in ovarian cancer [100]. These findings suggested a link between the IKBKE pathway and the initiation and progression of cancer where active angiogenesis is strongly involved.

A validated TEM

Robo4

Robo4 was first identified as an endothelial specific gene in 2000 [77] and later shown by our group and others to be a gene preferentially expressed in the tumour compared to healthy tissue endothelium [73]. Robo4 is the smallest member of the roundabout family and the only one to have restricted tissue expression. The other Roundabouts were originally identified and are primarily characterized as axon guidance receptors [101], although there is increasing evidence that they are also involved in angiogenesis [102]. Robo4 contains two of the five Ig like regions and two of the three fibronectin like regions present in the Robo1~3 extracellular domain, a transmembrane domain and an intracellular region with two conserved motifs for intracellular signal transduction (**Figure 1.5**). Multiple functions have been identified for Robo4, reviewed in [103]. Robo4 is specifically expressed in endothelial cells *in vitro*, is involved in endothelial motility, which is an essential process in tumour

angiogenesis [104-107]. The over expression of Robo4 in placenta, as determined by in situ hybridization, indicates that Robo4 is preferentially expressed at sites of active angiogenesis. More importantly, in adult tissues, Robo4 is abundantly present on the endothelium in a wide range of solid tumours whereas it is almost or completely absent in normal tissues [73, 108, 109]. A recent study showed that in a B16/F10 mouse melanoma model, Robo4 antibody coupled nanoparticles targeted vasculature associated with the tumour periphery, revealed by magnetic resonance image technology [110].

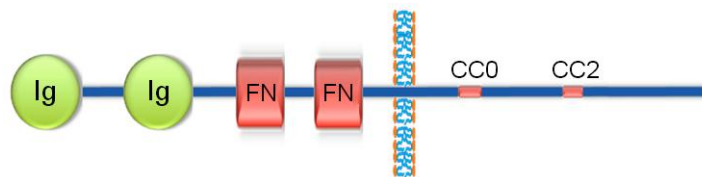


Figure 1.5 Structure of Robo4 Robo4 is comprised of two Ig and two fibronectin domains in the extracellular region, one transmembrane region and two conserved motifs in the intracellular region.

1.8 Identification of novel TEMs in lung cancer

Lung cancer remains the leading cause of cancer related death in the world and there is still a lack of an effective treatment. Platinum-based chemotherapies achieved a modest improvement of survival time for 6 months however most patients subsequently developed progressive disease. Although tyrosine kinase inhibitors of EGFR initially showed promising outcomes in several trials, resistance eventually developed in all patients [111]. The ineffectiveness of the classic treatments prompted

the search for alternative approaches for non-small cell lung cancer. More recently, the development of anti-angiogenic drugs such as VEGF (receptor) blockers has drawn greater focus to the tumour vasculature. The use of such drugs or compounds in treating NSCLC patients have been investigated in early clinical trials. Profiling differentially expressed genes in lung tumour will not only enhance our understanding of the molecules involved in this disease but may also provide biomarkers or targets that have therapeutic potential.

Isolation of endothelial cells

The first successful isolation and culture of primary human endothelial cells was achieved in the early 1970s, independently by Gimbrone et al. [112] and Jaffe et al. [113]. These findings paved the way for detailed research in vascular biology. However conventional tissue culture involved multiple factors such as a lack of flow and acidic stress that have profound effects on the transcriptome of endothelial cells. In rat, 40% of the original endothelial surface proteins in lung disappeared when in culture [114]. Thus a prerequisite for success in molecular profiling of endothelium is to obtain a pure endothelial specimens from *in vivo* physiological and pathological samples. To profile differential gene expression of endothelial cells in normal and tumour lung, endothelial cells need to be isolated from the whole tissue.

Laser capture microdissection

Laser capture microdissection (LCM), often called microdissection, is a technology to isolate specific microscopic regions of tissue. The LCM isolating process involves a pre-lineation of desired regions from a tissue slide. Then a laser beam, in most cases a UV laser, follows the defined trajectory to microdissect the region of interest. This region is then transported into a cap by a laser pressure catapult. This technology has the advantage of maintaining the chemistry of the dissected sample, which permits an effective retrieval of DNA and RNA and in some cases protein. For this reason, LCM has been widely used for molecular profiling downstream work. LCM can precisely dissect and collect the desired tissue at a cellular level which is particularly useful as endothelium only accounts for a minor proportion of the whole tissue. There are a number of endothelial profiling studies published using this technology [115-117]. The main challenge for LCM is to obtain enough high quality RNA material to perform gene expression profiling analysis.

Ulex-bead approach

Ulex europaeus agglutinin I is a lectin that specifically binds to L-fucose residues on the human endothelial surface [118, 119]. Previous studies have shown high purity of endothelial isolates using *Ulex*-conjugated beads [120-124].

The *Ulex*-bead isolation approach is preferentially performed on fresh tissue,

therefore requiring a fresh clinical specimen. A major benefit from this approach is that the RNA integrity is high and the yield is good. Therefore, the bead isolation approach permits studies using 2nd generation sequencing platforms, whereas the laser microdissection technique, due to its low RNA yield, is only suitable for microarray analyses.

Although both techniques have been previously described in isolating endothelium from various types of tissue [115, 117, 125-127], an attempt in lung cancer has not yet been reported and remains a challenge.

2nd generation sequencing (Deep sequencing)

RNA-seq deep sequencing or 2nd generation sequencing is a parallel sequencing method for transcriptome analysis. It facilitates RNA snapshots of a tissue by sequencing millions of short reads that can be assembled into a transcriptome and be used to measure differential gene expression. The two major systems of 2nd generation sequencing are Applied Biosystems SOLiD4 and Illuminas Gene Analyser II/HiSeq sequencers [128]. These technologies have the advantage of querying both known and previous undescribed transcripts and therefore, unlike microarrays, do not rely on prior knowledge of transcripts. In the same way, it neither suffers from probe cross hybridization of closely similar genes. Deep sequencing also provides rich information splice variants, isoform switching and non-coding RNAs such

microRNAs and pseudogenes.

1.9 Targeting tumour vasculature by vaccination

Cancer immunotherapy

Immunotherapy is the use of the host immune system to treat disease, often involving the elicitation, enhancement or suppression of an immune response. Cancer immunotherapy is particularly designed to stimulate a cancer patients' immune system to kill malignant cells and in turn, achieve tumour regression. Administration of therapeutic antibodies can direct one's immune system to specifically attack tumour cells. Cell based immunotherapy involves *in vivo* or *ex vivo* activation of immune cells including natural killer (NK) cells, cytotoxic T cells (CTL) and dendritic Cells (DCs) followed by transfusing them back into patients.

Immunotherapy that targets the tumour vasculature has been explored in the last two decades. Although the use of VEGF blockers in combination with chemotherapies have shown clear clinical benefit, in certain types of cancer resistance eventually developed and disease progressed in almost all patients [129]. Cancer vaccination is a strategy to boost the patient's own immune system against tumour cells by inducing an immune response that can recognize antigens present on the tumour cells.

Cancer vaccine

The vaccine approach has been used to protect people from diseases for decades, for instance: measles, chicken pox and the flu. The idea of a cancer vaccine is to treat existing cancer or prevent cancer occurring in people at high risk. At present, two vaccines have been approved by the FDA for preventing cancer but only one cancer vaccine, Sipuleucel-T, was approved by FDA for the treatment of metastatic hormone-refractory prostate cancer [130]. Although promising, the development of an effective cancer vaccine is slow and proven difficult. A major obstacle for developing an effective vaccine is the choice of appropriate targets.

Most identified vascular targets associated with tumour angiogenesis are endogenous proteins, which are considered a self-antigen for immunization. These self-antigens normally have considerably low immunogenicity of which the immune surveillance often are unaware so that the cells that express them are well tolerated and easily escape immunity [131]. Therefore, it is essential to develop an effective strategy to break the immunogenic tolerance to such molecules.

A vaccine against tumour vasculature

Advanced knowledge of the molecular signatures of the tumour vasculature has provided several promising targets that can be used as the vaccine immunogen. These targets are specifically present on the new formed tumour vasculature but low in or

absent from normal vasculature. Accumulating pre-clinical data suggests that vaccination against these molecules is a feasible and promising strategy that holds therapeutic potential [132, 133]. Compared to the anti-angiogenic drugs, such as monoclonal antibodies or inhibitors, vaccination is particularly preferential because of its long lasting effects and low cost.

Vaccination against VEGF receptors provided first proof of principle of this strategy. As described earlier, VEGF is a critical signaling molecule involved in physiological and tumour angiogenesis. All members of the VEGF family activate the cellular signaling pathways by a ligand-binding to their corresponding tyrosine kinase receptors present on the cell membrane. VEGFR2 is upregulated in activated endothelial cells in tumours and involved in critical steps in angiogenesis such as endothelial cell proliferation, migration and survival. VEGFR2 targeting by oral DNA vaccination showed significant inhibition of tumour growth and increase of the median survival rate in mice [134-136]. Similar effects were also observed when mice were immunised with VEGFR1 or VEGFR2 derived peptides [137, 138]. However, the wide expression of VEGF receptors in many healthy tissues might raise a safety concern when considering their uses in the clinic [139]. Other targets that are preferentially expressed on the tumour vasculature have been investigated as a vaccine and resulted in anti-angiogenic and anti-tumour effects. These targets are fibroblast growth factor receptor-1 [140], endothelial specific Tie2 [141], endoglin [142], integrin- α v β 3 [143] and angiomin (the receptor of angiostatin) [144].

More recently, encouraging results were seen in vaccination against targets that are predominantly present on the tumour vasculature. Olsson and colleagues demonstrated that vaccination against the extra domain-B of fibronectin evoked antibody response which, resulted in a 70% tumour size reduction in mice [67]. Listeria-based vaccination directly against CD105 led to a 20% prevention of tumour occurrence in an autochthonous breast cancer model [145]. Targeting delta-like ligand 4 that is present in endothelial tip cells by plasmid DNA vaccination dramatically decreased orthotopically implanted tumour growth [146]. No evidence of adverse effects on physiological angiogenesis were found from the above studies which further prove that selective targeting of the tumour vasculature holds clear therapeutic potential.

Compared to currently available anti-angiogenic drugs such as small molecule tyrosine kinase inhibitors or monoclonal antibodies, vaccination is a less advanced but a promising approach that has many advantages. Instead of using externally administered drugs, vaccination induces anti-angiogenic effects by the immune system within individual patients and such immunity provides long-term protection. Such protection otherwise can only be achieved by repeated administration of anti-angiogenic substances. Potentially, the specificity of the immune response elicited by a vaccine is expected to be more restricted to the target which means less toxicity than many angiogenesis inhibitors.

Targeting the tumour vasculature has many attractive advantages compared with a vaccine against cancer cells. As mentioned earlier, endothelial cells are genetically more stable than cancer cells and thus the chance of developing resistance to the vaccine is minimized when endothelial cells are used as the target. Targeting tumour vasculature may also be effective in a wider spectrum of cancer patients, because the angiogenic processes are similar in different tumour types. In contrast, vaccination against cancer cells tends to be more specific to the cancer type due to the restriction of their expressed cancer associated antigens. Finally, the immune cells are much more accessible to the vasculature compared to tumour cells. To target the tumour cells, multiple tissues or cell layers need to be crossed to reach the targeted cells.

1.10 Aims and objectives

Validation of putative tumour endothelial markers

A list of putative TEMs, CLEC14A, GBP4 and IKBKE will be validated by IHC or IHF on human tissue arrays or clinical samples.

Functional characterization of CLEC14A in endothelial cell biology

The aim is to determine the function of CLEC14A in endothelial cell biology. Silencing or overexpression of CLEC14A in HUVEC will be achieved with siRNA or lentiviral system respectively. Manipulated cells were studied in a scratch wound assay to determine CLEC14A's role in endothelial migration. Polyclonal antisera to CLEC14A will also be tested in a wound healing assay. Recombinant CLEC14A protein will be purified to enable the generation of monoclonal CLEC14A antibodies. To facilitate future in vivo functional work, a CLEC14A KO mouse will be generated.

Identification of novel TEMs in non-small cell lung carcinoma

Two methods, laser microdissection and *Ulex*-bead isolation will be compared in their success in isolating endothelial cells from frozen and fresh tissue respectively. Gene expression in the isolated endothelial cells from normal and tumour lung tissue will be analysed by deep sequencing and microarray analysis. Data derived from both technologies will be merged and a list of lung TEM candidates will be generated.

Investigation of Robo4 as a cancer vaccine

This will explore the possibility of using the validated TEM Robo4 as a cancer vaccine. As Robo4 is a self-antigen, the immune tolerance will be broken by protein immunization with adjuvants. The effect of vaccination on angiogenesis will be investigated in a rodent sponge assay. Whether vaccination against Robo4 has an effect on tumour growth will also be tested in Lewis lung carcinoma model.

This thesis covers a broad area of tumour vascular targeting, ranged from validation of identified putative TEMs, functional characterization of a validated TEM in endothelial biology, using deep sequencing to identify novel TEMs in lung cancer and exploring the use of a pre-validated TEM as a cancer vaccine. These objectives are interlinked and build a picture of tumour vascular targeting; from discovery to exploring their potential clinical use.

Chapter two

Materials and methods

2.1 Materials

2.1.1 Equipment

Centrifuge	Source
Bench centrifuge Biofugepico	Heraeus, Newport Pagnell, UK
Mikro 22R Centrifuge	Hettich Zentrifugen, Tuttlingen, Germany
Biofuge Primo Centrifuge	Heraeus, Newport Pagnell, UK
Avanti J-20 XP	Beckman Coulter, Brea, USA
MC 6 Centrifuge	Sarstedt, Leicester, UK

Microscopes	Source
DM 1000 light microscope	Leica, London, UK
USB 2.0 2M Xli camera	Xli, Carrollton, US
Leica MZ 16	Leica, London, UK
Leica DME	Leica, London, UK
Axiovert 100M laser confocal microscope	Carl Zeiss, Göttingen, Germany

Plate reader and spectrophotometer	Source
1420 Multilabel Coulter	VICTOR ³ , Singapore
ND-1000 Spectrophotometer	Nanodrop Technologies, Wilmington, USA
ELISA plate reader	VICTOR ³ , Singapore

Equipment for biochemistry	Source
XCell SureLock™ Mini-Cell electrophoresis apparatus	Invitrogen, Paisley, UK
Xcell II™ Blot Module wet transfer apparatus	Invitrogen, Paisley, UK
Electrophoresis Power supply EPS 301	Amersham Biosciences, Sweden
Polyvinylidene difluoride membranes	Immobilon-P, Billerica, USA
Chromatography paper	Whatman, Brentford, UK
Block heater SBH 200D	Stuart, Stone, UK
AccuBlock™ Digital Dry Bath	Labnet International, Inc, Woodbridge, USA
Gyro-rocker SSL3	Stuart, Stone, UK
Rocker 25	Labnet International, Inc, Woodbridge, USA
Rotator SB3	Stuart, Stone, UK
Heating Magnetic stirrer FB15001	Fisher Scientific, Loughborough, UK
3510 pH meter	Jenway, Stone, UK
Scale EK-300i	A&D, Seoul, Korea
ROTO-SHAKE	Scientific Industries, New York, USA
Compact x4 X-ray film developer	Xograph Imaging System, Tetbury, UK
LKB Pump P-1	Pharmacia, Uppsala, Sweden

Hitrap Protein A column	GE Healthcare Life Sciences , Little Chalfont, UK
AKTA purifier (FPLC)	Biotech, London, UK

Equipment for molecular biology	Source
Gallenkamp Orbital Incubators	Gallenkamp, Loughborough, UK
BIO Imaging system	Gene Genius, UK
Electrophoresis tank	Jencons, Leighton Buzzard, UK
Incubator for Bacteria Cellstar	Borolabs, Basingstoke, UK
Peltier Thermal Cycler PTC-225	MJ Research, Waltham, USA
Rotor-Gene RG3000 thermal cycler	Corbett Research, Cambridge, UK
MilliQ water purification system	Millipore, Billerica, USA

Equipment for cell biology	Source
Cell culture sterile hood, Advanced Bio Safely Cabinet Class 2	Microflow, Andover, UK
Incubator, 37°C, 5% CO ₂ , 95% filtered air	Heraeus, Newport Pagnell, UK
BD FACSCalibur Flow Cytometer	Becton Dickinson, Franklin Lakes, USA
Water bath	Fisher Scientific, Loughborough, UK
Amaxa nucleofactor II	Amaxa, Wolverhampton, UK
20 µl filter tip	Starlab, Milton Keynes, UK
Glass cell counter	Marienfeld, Lauda-Königshofen, Germany
FastRead counting slides	Immune system, Devon, UK
Glass micro-well chambers	Nunc, Loughborough, UK

Facilities	Source
CRUK animal service	Clare Hall, London, UK
Histology units	NHS, Birmingham, UK
High speed cell sorter MoFlo	Beckman Coulter, High Wycombe, UK
Plasmid sequencing service	Technology Hub, Birmingham, UK
Microarray scanning	Technology Hub, Birmingham, UK
Microarray data analysis	Technology Hub, Birmingham, UK
Deep sequencing service (SOLiD 4 TM)	Technology Hub, Birmingham, UK
Deep sequencing data analysis	Technology Hub, Birmingham, UK

2.1.2 Consumables, chemicals and reagents

Biochemistry	Source
Bio-Rad D _c Protein assay	Bio-Rad, Hemel Hempstead, UK
Protein A Sepharose	Sigma, Gillingham, UK
Protein G Sepharose	Sigma, Gillingham, UK

Histoclear	National diagnostics, Hessle, UK
20x SSC	Eppendorf, Stevenage, UK
Ultra pure ProtoGel	GeneFlow, Lichfield, UK
Phosphate Buffered Saline tablets	Sigma, Gillingham, UK
Tween 20	Sigma, Gillingham, UK
Ponceau S	Sigma, Gillingham, UK
Enhanced chemiluminescent substrate	Amersham Biosciences, Amersham, UK
Hyperfilm MP	GE Healthcare Life Sciences , Little Chalfont, UK
Igepal (NP-40)	Sigma, Gillingham, UK
Precision plus protein standard 250 – 10 kDa	Bio-Rad, Hemel Hempstead, UK
Papain	Sigma, Gillingham, UK
L-Cysteine	Sigma, Gillingham, UK
Iodoacetic acid	Sigma, Gillingham, UK
OPD (o-Phenylenedia mine dihydrochloride)	Sigma, Gillingham, UK
Phosphate-citrate buffer tablets	Sigma, Gillingham, UK
Calcium chloride powder	Sigma, Gillingham, UK
Protease Inhibitor tablet	Sigma, Gillingham, UK
Ammonium persulphate	Amresco, Solon, USA
TEMED	Sigma, Gillingham, UK
PMSF	Sigma, Gillingham, UK
Azide	Sigma, Gillingham, UK

Molecular biology	
SensiMix™ NoRef	Bioline, London, UK
ProbeLibrary Real-time PCR Assay System	Exiqon, Woburn, USA
TRI reagent	Sigma, Gillingham, UK
Agarose	Sigma, Gillingham, UK
SYBR safe DNA gel stain	Invitrogen, Paisley, UK
10 mM dNTP	Fermentas, Cambridge, UK
6x DNA loading buffer	New England Biolabs, Herts, UK
High-Capacity cDNA Archive kit	Applied Biosystems, Paisley, UK
Fusion DNA polymerase	New England Biolabs, Herts, UK
Taq DNA polymerase	Bioline, London, UK
EcoRI	New England Biolabs, Herts, UK
NotI	New England Biolabs, Herts, UK
PacI	New England Biolabs, Herts, UK
PmeI	New England Biolabs, Herts, UK
T4 ligase	New England Biolabs, Herts, UK
α-Select competent cells Gold efficiency	Bioline, London, UK
α-Select competent cells Bronze efficiency	Bioline, London, UK

Cell biology	
Lymphoprep	Axis-Shield, Stockport, UK

Trypan blue	Sigma, Gillingham, UK
Lipofectamine RNAiMax	Invitrogen, Paisley, UK
Recombinant hRobo4-Fc protein	CRT, London, UK
Recombinant human IgG-Fc fragment	Bethyl, Montgomery, USA
Papain cleaved human / mouse Robo4	Bicknell lab, Birmingham, UK

2.1.3 Water

NF water was used in all molecular biology experiments, purchased from Qiagen, Crawley, UK. Solutions and buffers were made using MilliQ filtered water.

2.1.4 Antibodies and probes

Catalogue	Specificity	Characteristics	Appl. / dilution	Source
AF4968	Human CLEC14A	Sheep polyclonal antibody 0.2 mg/ml	WB: 1/1000 IF: 1/20 ELISA: 1/1000	R&D system, Abingdon, UK
ab70058	Human GBP4	Mouse polyclonal antibody 0.4 mg/ml	WB: 1/1000 IF: 1/40	Abcam, Cambridge, UK
I4907	Human IKBKE	Rabbit polyclonal antibody 0.5 mg/ml	WB: 1/1000 IF: 1/50	R&D system, Abingdon, UK
Ab5512	Human ROS1	Rabbit polyclonal antibody 0.25 mg/ml	IHC: 1/50	Abcam, Cambridge, UK
Ab117257	Human STEAP1	Rabbit polyclonal antibody 0.2 mg/ml	IHC: 1/40	Abcam, Cambridge, UK
Ab469	Human BIRC5	Rabbit polyclonal antibody 0.97mg/ml	IHC: 1/100	Abcam, Cambridge, UK
Ab38584	Human GJB2	Rabbit polyclonal antibody 0.25 mg/ml	IHC: 1/50	Abcam, Cambridge, UK
Ab55506	Human PCDH7	Mouse polyclonal antibody 0.5 mg/ml	IHC: 1/50	Abcam, Cambridge, UK
Ab118492	Human PROM2	Rabbit polyclonal antibody 0.5 mg/ml	IHC: 1/20	Abcam, Cambridge,

				UK
JC70	Human CD31	Mouse monoclonal antibody 0.5 mg/ml	IHC: 1/100	Dako, Glostrup, Denmark
Ab10547	Human/mouse Robo4	Rabbit polyclonal antibody 0.5 mg/ml	WB: 1/1000	Abcam, Cambridge, UK
MR7	Human Robo4	Mouse monoclonal antibody	WB: 1/1000 FACs: 1/1000	CRT, London, UK
81-8611	Sheep IgG (H+L)	Rabbit polyclonal antibody - FITC	IF: 10 µg/ml or 1/100	Zymax, Paisley, UK
81-6711	Mouse IgG (H+L)	Rabbit polyclonal antibody - FITC	IF: 10 µg/ml or 1/100	Zymax, Paisley, UK
A3673	Mouse IgG (γ-chain specific)	Rabbit polyclonal antibody peroxidase conjugated	ELISA: 1/10000	Sigma, Gillingham, UK
A6154	Rabbit IgG	Goat polyclonal antibody peroxidase conjugated	ELISA: 1/10000	Sigma, Gillingham, UK
A1949	Rabbit IgG (γ-chain specific)	Mouse monoclonal antibody peroxidase conjugated 6.5 mg/ml	WB: 1/10000	Sigma, Gillingham, UK
A8667	Human IgG	Goat polyclonal antibody peroxidase conjugated	ELISA: 1/10000	Sigma, Gillingham, UK
A6029	Human IgG (γ-chain specific)	Goat polyclonal antibody peroxidase conjugated 6.5 mg/ml	WB: 1/10000	Sigma, Gillingham, UK
A0080	Human/mouse fibrinogen	Rabbit polyclonal antibody 0.5 mg/ml	IF: 1/500	Dako, Glostrup, Denmark
553123	Mouse (Gr-1) Ly6G and Ly-6C	Rat monoclonal antibody 0.5 mg/ml	IF: 1/1000	BD Biosciences, Stockholm, Sweden
RL-1062	Endothelium	<i>Ulex europaeus</i> agglutinin I (UEAI)- rhodamine	IF: 10 µg/ml or 1/100	Vectorlabs, Orton Southgate, UK
P36935	Nucleus	Prolong gold anti-fade reagent including DAPI	Neat	Invitrogen, Paisley, UK

*WB: Western blot; IF: Immunofluorescence; IHC: Immunohistochemistry; ELISA: Enzyme-linked immunosorbent assay

2.1.5 DNA vectors and plasmids

Vector	Characteristics	Sources
pWPI	Lentivector, EF1 α promoter, separated GFP driven by IRES	Bicknell group, Birmingham, UK
pMD2G	Envelop plasmid for lentivirus expression system	Bicknell group, Birmingham, UK
psPAX2	Packaging plasmid for lentivirus expression system	Bicknell group, Birmingham, UK
pIG vector	Mammalian expression vector, human Fc tag in C-terminus with a short span	Bicknell group, Birmingham, UK
pcDNA3.1	Mammalian expression vector, human Fc tag in C-terminus	Invitrogen, Paisley, UK
pEGFP-N1	Mammalian expression vector, CMV promoter, GFP tag in C-terminus	BD Bioscience, Oxford, UK
Plasmids	Source / cloning strategy	Application
FL-hCLEC14A-pEGFP1	Bicknell group, Birmingham, UK	Template for sub cloning
FL-mCLEC14A-pCMV6	OriGene, Cambridge, UK	Template for sub cloning
FL-hCLEC14A-pWPI	PCR with PacI & SwaI overhangs primers	Transduction of HUVEC
Ex-hCLEC14A-pIG	PCR with EcoRI & NotI overhangs primers	Template for sub cloning into pWPI lentivector
Ex-mCLEC14A-pIG	PCR with EcoRI & NotI overhangs primers	Template for sub cloning into pWPI lentivector
Ex-hCLEC14A-Fc-pWPI	PCR with PmeI & PacI overhangs primers	Recombinant hCLEC14A-Fc protein production
Ex-mCLEC14A-Fc-pWPI	PCR with PmeI & PacI overhangs primers	Recombinant mCLEC14A-Fc protein production
Ex-mRobo4-pIG	CRT, London, UK	Template for sub cloning into pWPI lentivector
Ex-mRobo4-Fc-pWPI	PCR with PacI & SwaI overhangs primers	Recombinant mRobo4-Fc protein production

2.1.6 Oligonucleotides

Oligonucleotides	Application	Sequence
CLEC14A-qPCR Probe 24	qPCR	5'-CTGGGACCGAGGTGAGTG-3' 5'-CGCGATGCAAGTAACTGAGA-3'
CD31-qPCR	qPCR	5'-GCAACACAGTCCAGATAGTCGT-3'

Probe		5'-GACCTCAAACCTGGGCATCAT3'
TBGP-qPCR Probe 70	qPCR	5'-CGC-TAC-TCT-GGT-GGA-ACT-CA-3' 5'-CCT-CTT-CGC-CTC-TTG-TTG-G-3'
LMTK3-qPCR Probe 18	qPCR	5'-GCC-TTA-CGC-GGA-CTA-CTG-G-3' 5'-TGG-AGA-TCA-GAG-GCT-GAA-GG-3'
STEAP1-qPCR Probe 76	qPCR	5'-GGA-TTG-GCA-ATA-CTG-GCT-CT-3' 5'-GAA-ACA-ATT-CCT-AGC-TTG-CTC-TG-3'
TEM7-qPCR Probe 22	qPCR	5'-GAC-ACG-CTG-CCA-GAT-AAC-AG-3' 5'-GCC-ATA-GAG-ACG-GGA-CAC-AT-3'
ROS1-qPCR Probe 78	qPCR	5'-CGG-GAG-AAA-ATA-GCA-CCT-CA-3' 5'-ATT-TGG-GAA-TGC-CTG-GTT-TA-3'
BAMBI-qPCR Probe 71	qPCR	5'-CGC-CAC-TCC-AGC-TAC-ATC-TT-3' 5'-CAC-AGT-AGC-ATC-GAA-TTT-CAC-C-3'
GJB2-qPCR Probe 71	qPCR	5'-GAG-CAG-GCC-GAC-TTT-GTC-T-3' 5'-TGA-TCG-TAG-CAC-ACG-TTC-TTG-3'
SLCO1B3-qPCR Probe 59	qPCR	5'-CGG-CCT-AAC-CTT-GAC-CTA-TG-3' 5'-TGA-GTT-GCA-ATA-AGA-AAG-TGG-TAC-A-3'
SYT12-qPCR Probe 1	qPCR	5'-CGA-AGC-CAT-GAT-CTT-CTC-G-3' 5'-GCT-CTC-AGC-CAC-CGT-CAC-3'
BIRC5-qPCR Probe 36	qPCR	5'-TCT-GCT-TCA-AGG-AGC-TGG-A-3' 5'-AAA-GTG-CTG-GTA-TTA-CAG-GCG-TA-3'
PCDH7-qPCR Probe 15	qPCR	5'-CTA-CCA-CCA-GCC-AAC-ACA-TTT-3' 5'-TGT-ATG-GAT-GTA-GAC-GCA-TCT-GT-3'
PROM2-qPCR Probe 25	qPCR	5'-TGC-AGC-TCA-ACG-ACT-CCT-AC-3' 5'-ACT-CCT-GCC-GTA-GCT-TGT-TG-3'
Flotillin 2-qPCR Probe 28	qPCR	5'-TGTTGTGGTTCGACTATAAACAG-3' 5'-GGGCTGCAACGTCATAATCT-3'
Mouse CLEC14A 400/R600 Expected size: 200 bp	Genotyping	5'-CCACAACGTTCTGTACAGTG-3' 5'-GCTGCTCAGCCGGAAGGGAGC-3'
UNeo-Fwd/SD Expected size: 404 bp	Genotyping	5'-TCATTCTCAGTATTGTTTGGCC-3' 5'-GAATAGGAAAATGTCTCTTGCC-3'
CLEC14A duplex set:	siRNA	Duplex1: GAACAAGACAATTCAGTAA Duplex2: CAATCAGGGTCGACGAGAA
GBP4 duplex set:	siRNA	Duplex1: GAACAAGACAATTCAGTAA Duplex2: CAATCAGGGTCGACGAGAA
IKBKE duplex set:	siRNA	Duplex1: GGAACAAGGAGATCATGTA Duplex2: AGGAGTGCCTGCAGAAGTA
Negative control duplexes	siRNA	Scrambled
Ex-mRobo4-Fc PacI / SmaI	Cloning into pWPI vector	Forward: 5'-TAGTAGATTTAAATACCATGGGCTCTGGAGGAACG-3' Reverse: 5'-TAGTAGTTAATTAATCATTACCCGGAGACAGGGAGAG-3'
Ex-hCLEC14A EcoRI / NotI	Cloning into pIG vector	Forward: 5' - TAGTAGGAATCTATGAGCCGGCGTTCGCCCTGTGC - 3'

		Reverse: 5' – GCGGCCGCTGGAGGAGTCGAAAGCCTGAGGAGTGGC – 3'
Ex-mCLEC14A EcoRI / NotI	Cloning into pIG vector	Forward: 5' – TAGTAGGAATTCTATGAGGCCAGCGCTTGCCCTGTGC – 3' Reverse: 5' – GCGGCCGCTCGTGAAGAGGTGTCGAAAGTCAG – 3'
FL-hCLEC14A PacI / SmaI	Cloning into pWPI vector	Forward: 5'-TAGTAGTAAATTAAGAGAGAATGAGGCCGGCGTTC-3' Reverse: 5'-CTACTAGTTTAAACCTATGCATCACTAGAGCCAAG – 3'
Ex-hCLEC14A-Fc PmeI / PacI	Cloning into pWPI vector	Forward: 5'-TAGTAGTAAATTAAGAGAGAATGAGGCCGGCGTTC-3' Reverse: 5'-TAGTAGGTTTAAACTCATTACCCGGAGACAGGGAGAG -3'
Ex-mCLEC14A-Fc PmeI / PacI	Cloning into pWPI vector	Forward: 5' - TAGTAGTAAATTAATCCAGGATGAGGCCAGCGCTTGCCCTGTGC -3' Reverse: 5'-TAGTAGGTTTAAACTCATTACCCGGAGACAGGGAGAG -3'

2.1.7 Primary isolates, cell lines and culture media

Primary isolates	Source
Human umbilical vein endothelial cells (HUVEC)	Processed within Bicknell lab, Birmingham, UK
Human dermal microvascular endothelial cells (HDMEC)	TCS Cell Works, Buckingham, UK
Human aortic smooth muscle cells (HASMC)	TCS Cell Works, Buckingham, UK
Human bronchial epithelial cells (HBE)	TCS Cell Works, Buckingham, UK
Human lung fibroblasts (MRC5)	CRUK Central Services, London, UK
Human peripheral blood mononuclear cells (PBMCs)	University of Birmingham, Birmingham, UK
Hepatocytes	Dr Patricia Lalor University of Birmingham, Birmingham, UK
Cell lines	
293T cells	TCS Cell Works, Buckingham, UK
4T1 cell line	TCS Cell Works, Buckingham, UK
EL4	University of Birmingham, Birmingham, UK
SEND	University of Oxford, Oxford, UK
Lewis lung carcinoma cells	CRUK Central Services, London, UK
Media	
Fetal calf serum	CRUK Central Services, London, UK
M199 media	Sigma, Gillingham, UK
Large vessel endothelial cell growth supplement	TCS Cell Works, Buckingham, UK
Bronchial Epithelial cell medium	TCS Cell Works, Buckingham, UK

OptiMEM serum low media	Invitrogen, Paisley, UK
Collagenase type I A	Sigma, Gillingham, UK
Type I gelatin from porcine skin	Sigma, Gillingham, UK
Aim V serum low media	Invitrogen, Paisley, UK

2.1.8 Physiological and pathological specimens

Materials	Company
Normal / cancer tissues	CRUK Central Services, London, UK
Cancer / matching normal tissue array	SuperBiochips Inc, Seoul, Korea
Umbilical cords	NHS, Birmingham, UK
Fresh lung tissue	Heartlands hospital, Birmingham, UK
Heparinised whole blood	QEH, Birmingham, UK
Human serum	QEH, Birmingham, UK
Mouse serum	CRUK Central Services, London, UK
Basic fibroblast growth factor	R&D system, Abingdon, UK

2.1.9 Buffers and solutions

Buffer	Recipe
HBS buffer (2x)	2.73 mM NaCl, 48.5 mM KCl, 15.2 μ M Na ₂ HPO ₄ ·2H ₂ O, 0.11 mM Dextrose, 0.42 mM HEPES, pH 7.05; sterilized with 0.22-micron filter
NP40 lysis buffer	50 mM Tris-HCl, 150 mM NaCl, 1% NP-40, pH 8.0 with addition of protease inhibitors tablets
6x SDS Loading Buffer	30 % (v/v) glycerol, 0.25 % (w/v) bromophenol blue, 0.25 % (w/v) xylene cyanol FF
2x SDS Loading Buffer	100 mM Tris-Cl, pH 6.8, 20% (v/v) β -mercaptoethanol, 4% (w/v) SDS, 0.2% (w/v) bromophenol blue, 20% (v/v) glycerol
Coomassie staining buffer	40 % (v/v) methanol, 10 % (v/v) acetic acid, 0.2 g Coomassie Brilliant Blue dye
Running buffer	25 mM Tris, 250 mM glycine, 5% SDS
Transfer buffer	25 mM Tris, 192 mM glycine, 20% methanol pH 8.3
Tris-Buffered Saline Tween-20 (TBST)	1 M Tris pH 7.5, 5 M NaCl, 20% (v/v) Tween-20
Blocking buffer	5% dried skimmed milk in TBST
pH 3 buffer	Sodium Citrate 100 mM
pH 7 buffer	Sodium phosphate 20 mM
TAE buffer	40 mM Tris-base, 18 mM glacial acetic acid, 1

	mM EDTA
10x Papain buffer	1.5 M NaCl, 6.7 mM EDTA, 50 mM L-Cysteine, 100 mM Na ₂ HPO ₄ , pH 7.3
Tris buffer pH 9	CRUK Central Services
0.5M EDTA	CRUK Central Services

2.2 Molecular biology methods

2.2.1 DNA / RNA handling and quantification

All DNA and RNA work was carried out using sterile tips and NF water. DNA samples were resuspended in elution buffer (Sigma, Gillingham, UK) and stored at -20°C. RNA or siRNA duplexes were resuspended in nuclease free water and stored at -80°C. The quantification of DNA or RNA was performed on a Nano-drop spectrophotometer. The OD 260/280 ratio was used as a measure of sample purity.

2.2.2 DNA preparation

Mini-prep, Midi-prep or Maxi-prep kits (Sigma, Gillingham, UK) were used for different scales of DNA preparation according to manufacturer's instructions. In brief, a starting culture from a bacterial clone was initiated for 16 - 18 hs. The overnight culture was then subjected to alkaline lysis followed by the removal of RNA by treatment with RNase A. The debris and genomic DNA were removed by SDS precipitation. The eluted DNA was further concentrated by adding a DNA precipitation step using isopropanol. After 70% ethanol washing, plasmid DNA was

dissolved in elution buffer.

2.2.3 RNA extraction

Total RNA was isolated from primary cells or cell lines using TRI reagent (Sigma, Gillingham, UK) following manufacturer's instructions. In brief, for one well of a 6-well plate, 500 μ l of TRI reagent was applied to lyse the cells. 200 μ l of chloroform was added to the cell lysate and incubated on ice for 30 mins. Following 15 mins centrifugation at 14000 x g and 4°C, two phases were separated. RNA was precipitated from upper aqueous phase with 750 μ l of isopropanol. After washing once with 70% ethanol, the RNA pellet was dissolved in NF water.

2.2.4 Agarose gel electrophoresis

1% agarose gel was prepared in TAE buffer with appropriate dilution of SYBR safe DNA gel stain (Invitrogen, Paisley, UK). DNA or RNA samples were mixed with 6x loading buffer and loaded into each well. The loaded samples were run at 60 to 80 V for 1 h. A picture of the gel was then taken using the BIO Imaging system machine under ultraviolet light. These were further modified using GeneSnap software (Gene Genius, Cambridge, UK).

2.2.5 Polymerase chain reaction

For screening purpose

Reaction mix	μl	
Template	1	
10x NH ₄ buffer	5	
10 mM dNTPs	1	
Forward primer (10 μM)	0.5	
Reverse primer (10 μM)	0.5	
MgCl ₂ (50 mM)	2.5	
Taq polymerase	0.5	
H ₂ O	39	
Total	50	
PCR program		
Temperature	Time	Cycle
94 °C	2 min	1
94 °C	1 min	30
60 °C	30 sec	
72 °C	1 min	
72 °C	5 min	1
4 °C	Hold	

For cloning purpose

Reaction mix	μl	
Template	1	
5x buffer	10	
10 mM dNTPs	1	
Forward primer (10 μM)	0.5	
Reverse primer (10 μM)	0.5	
Fusion polymerase	0.5	
H ₂ O	36.5	
Total	50	
PCR program		
Temperature	Time	Cycle
98 °C	30 sec	1
98 °C	10 sec	24
60 °C	30 sec	
72 °C	1 min	
72 °C	5 min	1

4 °C	Hold	
------	------	--

2.2.6 Restriction enzyme digestion

Restriction enzymes were supplied with appropriate reaction buffers and 100x BSA. The digestion was performed following the manufacturer's instructions. In brief, 1 µg of DNA vector was mixed with 1 µl of enzyme (normally 10 units) for 5 hs at 37°C. An overnight incubation was used for PCR products to ensure complete digestion. A sequential digestion was performed when the double digestion was not feasible because of buffer incompatibility.

2.2.7 Genotyping of knockout mice

Ear clips were collected from mice for genotyping. Genomic DNA was isolated using extraction mix (25 mM NaOH, 0.2 mM EDTA; shake at 1200 rpm for 30 min at 98°C). PCR reactions were performed to identify wild type, heterozygous and homozygous mice. Two primer sets: F400/R600 (internal WT CLEC14A) and UNeo-Fwd/SD (selection from the cassette insert linked to downstream CLEC14A) were used to discriminate the genotype of mice. The PCR mix and program are shown below:

	1 x 20 µl reaction (µl)
Template	1
10 x NH4 buffer	2
10 mM dNTP	0.4
50 mM MgCl ₂	1
10 µM Primer 1	2

10 μ m Primer 2	2	
10 μ m Primer 3	2	
10 μ m Primer 4	2	
Taq polymerase	0.2	
H ₂ O	7.4	
Total	20	
PCR program		
Temperature	Time	Cycle
94 °C	5 min	1
94 °C	15 sec	35
62 °C	30 sec	
72 °C	1 min	
72 °C	5 min	1
15 °C	Hold	

2.2.8 Ligation

T4 ligase was used for the generation of all DNA constructs. A 20 μ l reaction was routinely carried out. The reaction mix was incubated at RT for 1 h followed by a heat-shock transformation (see below).

	Vector + Insert (μ l)	Vector only (μ l)
Insert	15	-
Vector	3	3
10x Buffer	2	2
T4 ligase	1	1
H ₂ O	0	15
Total	20	20

2.2.9 *E. coli* Transformation

‘Gold efficiency α -Select’ competent cells were used for cloning while ‘Bronze efficiency α -Select’ competent cells were used for the amplification of plasmid. A 50 μ l aliquot of frozen competent cells was thawed on ice for 30 mins. 10 μ l of the

ligation mix was added to the thawed competent cells and mixed well. Heat shock was achieved by placing the tube into a heated block at 42°C for 45 seconds. After 2 mins incubation on ice, 250 µl of LB was added and the tube was placed at 37°C on bacterial shaker at 220 rpm for 1 h. The mix was then spread on an LB agar plate with ampicillin or kanamycin antibiotic at 100 µg/ml.

2.2.10 Long-term bacteria storage

500 µl of overnight bacterial culture in LB broth was added to an equal volume of 30% glycerol in a cryovial and stored at -80°C.

2.2.11 Complementary DNA synthesis

In order to perform real time PCR analysis, RNA isolated from primary cells or tissues was converted to cDNA using a High-Capacity cDNA Archive kit (Applied Biosystems, Warrington, UK). In brief, RNA was diluted in NF water at 0.2 mg/ml. 2 µg of RNA was added to 10 µl of 2x RT master mix which was made up following the manufacturer's instructions. The synthesis reaction was performed in the PCR machine following the program below:

	Step 1	Step 2	Step 3	Step 4
Temperature	25 °C	37°C	85°C	4°C
Time	10 min	120 min`	5 sec	∞

2.3 Mammalian cell isolation and culture

2.3.1 HUVEC isolation from umbilical cords

HUVECs were isolated from umbilical cords donated by the NHS with donor consent and in accordance with UK Ethics approval from the Birmingham Biobank. Cords were dissected from placentas and the vein was washed with sterile PBS to remove blood. 1 mg/ml of collagenase type I A diluted in M199 medium was injected into the vein and then incubated at 37°C for 20 mins to detach the endothelial cells. HUVEC were collected by washing in M199 complete medium containing 10% FCS, 10% large vessel endothelial cell growth supplement, 4 mM L-glutamine and then seeded on plates coated with 0.1% Type 1 gelatin from porcine skin.

2.3.2 Adherent cell culture

Culture was performed at 37°C in a 5% CO₂ atmosphere. HUVEC and HDMEC were both cultured on a 1% gelatin coated plates with M199 media containing 10% FCS, 4 mM L-glutamine and 10% large vessel endothelial cell growth supplement. Cells were passaged 1 in 3 when they reached confluence. MRC5 and HASMC were cultured in DMEM media containing 10% FCS and 4 mM L-glutamine. Bronchial epithelial cell medium supplied by TCS Cell Works was used specifically for human bronchial epithelial cells culture. Cell lines including HEK 293T, SEND, 4T1 and Lewis lung carcinoma were cultured in DMEM media containing 10% FCS and 4

mM L-glutamine. These cell lines can be passaged 1 in 10 due to their fast growth rate.

2.3.3 Release by exposure to trypsin

Media was removed and the plate washed with sterile PBS. 2 ml of trypsin/EDTA was applied for one 10 cm tissue culture dish followed by 3 mins incubation at 37°C. Cells were totally detached by gently tapping the plate. 8 ml of PBS or complete media was used to neutralize the trypsin and wash the cells off the plate. After 5 mins centrifugation at 1000 rpm, the cell pellet was resuspended in an appropriate volume for cell counting.

2.3.4 Cell counting

Released adherent cells or non-adherent cells were resuspended in an appropriate volume of media. 10 µl of 5 x trypan blue was added to 40 µl of cell suspension and mixed well by pipetting up and down. 10 µl of the mix was loaded onto the glass cell counter or into a pocket of the FastRead counting slides when multiple samples needed to be counted. The cell number was calculated using the following formula: (average count from one 4 x 4 grid) x 10⁴ x dilution factor = cell number/ml

2.3.5 Freezing and thawing of mammalian cells

To cryo-preserve, released adherent cells or non-adherent cells were centrifuged at 1000 rpm for 5 min and resuspended in pre-cooled filtered FCS containing 10% DMSO. The cryovials were placed at RT in a freezing container (Thermo Scientific, Langenselbold, Germany) and immediately transferred to the -80°C freezer. The next day, the cells were transferred to the liquid nitrogen storage. When thawing cells, the cryovials were submerged in the waterbath at 37°C. Contents were transferred to a 15 ml tube, and diluted with 9 ml of media. Cells were spun down and then resuspended in 10 ml of DMSO free media after the two washes.

2.3.6 Blood sampling

Fresh blood from healthy donors or cancer patients was collected with patient consent and ethics approval (Project Licence PPL 70/6082). 60 ml of whole blood from each collection was mixed with 0.5 ml of 1000 U/ml preservative-free sodium heparin.

2.3.7 Preparation of PBMC and serum

Heparinised blood was diluted 1:1 in RPMI 1640 at 37°C. 25 ml of diluted blood was slowly layered onto 15 ml of lymphoprep and centrifuged at 1600 rpm for 30 min. The upper layer of the supernatant which contains the serum was collected and stored at -20°C. PBMC at the interface were collected and pooled followed by three washes

with warm RPMI. Cell number and viability was determined by trypan blue exclusion. PBMCs need a recovery procedure before putting into an assay. In brief, 10 ml of cell suspension after thawing was transferred into a 25 cm² flask and incubated at 37°C overnight.

2.3.8 Isolation of endothelial cells from lung tissues using *Ulex* magnetic beads

Surgically removed bulk lung tissues were obtained from Heartlands hospital with patient consent and ethics approval (Heartlands hospital, REC reference no. 07/MRE08/42). Tumour tissue was resected near the tumour core while the matched healthy tissue was resected at least 10 cm away from the tumour. The endothelial isolation procedure was performed within 2 hs. Tissues were weighed and minced, then digested for 1.5 h with DMEM containing 2 mg/ml collagenase type V (Sigma, Gillingham, UK), 7.4 mg/ml of actinomycin (Sigma, Gillingham, UK) and 30 kU/ml of DNase I (Qiagen, Crawley, UK) at 37°C on a shaker. Streptavidin-coated Dynabeads (Invitrogen, Paisley, UK) were incubated with 20 mg/ml of biotinylated *Ulex* lectin (Vectorlabs, Orton Southgate, UK) for 30min at 37°C on a shaker. The digested cell suspension was filtered through a 70 µm cell strainer following three washes with cold DMEM. Endothelial cells were then isolated by positive selection using *Ulex* coated beads and a magnet. This method was modified from previously described methods [121, 122].

2.3.9 Isolation of endothelial cells from lung sections using laser microdissection

Cresyl violet or CD31 stained slides were used for laser microdissection on a P.A.L.M. machine to collect blood vessels for downstream applications. In brief, the stained slides were air dried in a fume hood for 10 min then placed on the P.A.L.M. section platform. 20 µl of RNA extraction buffer from miRNeasy Mini kit (Qiagen, Crawley, UK) was pipetted into the inner ring of the cap to which the dissected tissue is catapulted. Upon completion of microdissection, the captured tissue was centrifuged for 1 min at 13000 rpm and stored at -80°C until RNA extraction. Due to the low yield of RNA, multiple laser dissected samples were pooled before RNA extraction.

2.4 Transfection and transduction of mammalian cells

2.4.1 Calcium-phosphate transfection

Calcium phosphate transfection is a transient transfection method and was used to transfect 293T cells. In brief, 3×10^6 of 293T cells were plated in a 10 cm tissue culture dish at 37°C overnight. Medium (DMEM, 10% FCS, 4 mM glutamine) was changed 1 h before the transfection. 5 µg of plasmid DNA, 63 µl of 2 M CaCl₂ and an appropriate volume of water were mixed to make up a final volume of 500 µl. An equal volume of 2x HBS was added to the mixture dropwise and left on ice for 10 mins. Media was replaced by complete media or OptiMEM low serum media the following day.

2.4.2 Lentivirus production

The gene of interest was cloned into the lenti-vector pWPI containing an untagged GFP expressed from an IRES site. A standard calcium phosphate method was used to produce Lentivirus from 293T cells. In brief, 3×10^6 of 293T cells were seeded in 10 cm dishes and transfected with 20 μg transfer vector (pWPI containing the gene of interest), along with 15 μg of the packaging plasmid (2nd generation, psPAX2) and 6 μg of the envelope plasmid (PMD2G). 48 h post-transfection, the supernatant which contains the virus was harvested and stored at -80°C .

	Normal cal-phosphate	Lentivirus
Vector with gene	5 μg	20 μg
psPAX2	-	15 μg
pMD2G	-	6 μg
CaCl ₂	63 μl	63ul
H ₂ O	Up to 500 μl	Up to 500 μl
2 x HBS	500 μl	500 μl
Total	1 ml	1 ml

2.4.3 Lentiviral transduction of 293T cells and HUVECs

To transduce 293T cells or HUVECs, the frozen viral supernatant was thawed at RT. 3 ml of the viral supernatant was added to 3×10^6 cells and incubated at 37°C for 7 h. The media was then replaced with complete media and the culture left for a further 48 hs.

2.4.4 Generation of lentivector containing human Fc tagged Robo4 or CLEC14A

The extracellular mouse Robo4-Fc was subcloned into a pWPI lentivector from the pIG vector using PacI and SmaI ended primers. The extracellular domain of human or mouse CLEC14A was first cloned into a pIG vector which contains a C-terminal Fc tag using EcoRI and NotI ended primer set. Then the human or mouse CLEC14A-Fc was subcloned into an empty pWPI lentivector containing a GFP expressed from an IRES site, using PacI and PmeI ended primers. In brief, inserts were amplified by PCR reaction using Fusion polymerase. EcoRI, NotI, PacI, PmeI or SmaI was chosen as the restriction sites for different inserts. A sequential or double digestion was performed to create the inserts and the open vector. Overnight ligation was performed using T4 ligase followed by a heat shock transformation using 'α-Select Gold efficiency' competent cells. Colonies were picked and screened by PCR reaction using EF1α primer which is from the vector and a reverse primer from the gene. Each generated lentivector with the Fc fused insert was verified by sequencing. The derived constructs were scaled up by maxi-prep and stored at -20°C.

2.4.5 Generation of a stable line expressing Fc fusion protein by FACs sorting

The procedure for lentivirus generation is described above. FACs sorting was used to generate a population that stably produces recombinant protein. Cells transduced with mRobo4-Fc-pWPI, hCLEC14A-Fc-pWPI or mCLEC14A-Fc-pWPI were passed through a MoFlo high speed cell sorter and GFP positive cells were collected and

cultured in 10 % FCS DMEM. The selected cells were then expanded for a large scale production of the Fc fusion protein. FACS sorting was also used to obtain a population of CLEC14A overexpressing cells for functional assays from FL-CLEC14A-pWPI transduced HUVEC.

2.5 Protein analysis methods

2.5.1 Protein quantification

Protein was quantified using either a Bio-Rad D_c protein assay or the Nano-drop machine. Bio-Rad assay was used when the protein sample was at a low concentration or a relative accurate readout was required. The Nano-drop machine was used for approximate concentrations.

2.5.2 Western blotting

Cell lysates were prepared using NP40 lysis buffer. Protein samples were mixed with 6x protein loading buffer and denatured by boiling for 3 mins before loading onto a SDS-PAGE gel. After SDS PAGE electrophoresis, the gel was blotted onto a PVDF membrane at 30 Volt for 2 hs at 4°C. The membrane was blocked with 5% milk in wash buffer (PBS 0.1% Tween-20) for 1 h at RT. The membrane was washed (4 x 5 min) and primary antibody diluted in blocking buffer was applied and incubated for 1 h at RT or overnight at 4°C. After washing, horseradish peroxidase conjugated

secondary antibody with 1 in 10000 dilution in blocking buffer was applied for 1 h at RT. Following antibody staining, the membrane was again washed and 400 μ l of ECL western blotting detection reagents was added for 3 mins. A piece of Hyperfilm was then exposed to the membrane for different lengths of time and the luminescence created by horseradish peroxidase detected.

2.5.3 Membrane antibody stripping

When a single membrane was to be probed with more than one antibody, a membrane stripping procedure was carried out. In brief, the membrane was washed 3 times with PBS 0.1% Tween-20 and incubated in stripping buffer at 70°C for 45 mins. The membrane was washed 3 times with PBS containing 0.1% Tween-20 followed by blocking with 5% milk for 1 h at RT.

2.5.4 Coomassie brilliant blue staining

Gels were stained with Coomassie brilliant in the microwave at high power for 1 min. The gel was destained by incubating with destain buffer on a rocker at RT as required.

2.6 Protein purification and Fc fragment removal

2.6.1 Purification of Fc fusion proteins using a protein A column

FACs sorted lentivirus transduced 293T cells (mRobo4-Fc, hCLEC14A or mCLEC14A) were expanded with complete media in 15 cm tissue culture dishes. Once 80% confluent, the old media was replaced with fresh OptiMem low serum media. 5 collections within 10 days produced 1~3 L of conditioned media. The collected media was adjusted to pH 8.0. 1 mM EDTA and a few PMSF crystals were added to inhibit serine proteases. A protein A column was prepared by washing with 20% ethanol and then equilibrated with pH 7 buffer (sodium phosphate 20 mM). Conditioned media was run through a Hi-Trap protein A column at 2 ml/min at 4°C followed by a 5x column volume wash with pH 7 buffer. pH gradient elution was achieved by FPLC chromatography using pH 3 buffer (sodium citrate 100 mM). The major products were eluted at pH 3.5 ~ 4. 0.1% Azide was added to the eluate to avoid potential bacterial contamination and stored at 4°C.

2.6.2 Papain cleavage of recombinant human or mouse Robo4-Fc

In brief, 10x buffer (1.5 M NaCl, 6.7 M EDTA, 5 mM L-Cysteine) was prepared and stored at -20 °C. Papain at 20 mg/ml was diluted 1 in 100 in PBS (0.2 mg/ml). The final mixture for a 1 ml reaction contained 1.6 µg/ml papain, 600 µg/ml of human or mouse Robo4-Fc protein in 1x buffer. Reaction was performed at 37°C for 40 mins.

For optimization of papain cleavage, samples were collected every 10 mins. 50 μ l of iodoacetic acid (130 mM, pH 6.8) was added to quench a 1 ml reaction [147, 148].

2.6.3 Depletion of Fc fragments from a papain reaction mix

To remove the Fc fragments from 1 ml of papain reaction mix, 50 μ l of cold PBS washed protein G beads were added to the mix and placed on a wheel at 4 °C for 2 hrs. Protein G beads were pelleted down and the supernatant was collected followed by a western blot to confirm cleavage and depletion. The supernatant containing the untagged protein was stored at 4°C. This protein was used for Robo4 antibody detection or monoclonal CLEC14A antibody screening.

2.7 Methods used in expression analysis

2.7.1 Real time PCR analysis

Following cDNA synthesis, the ProbeLibrary Real-time PCR Assay System was employed in the primary cell screening of gene expression. Flotillin 2 was chosen as the housekeeping gene to which the expression of each putative TEM was normalized. Primer and probe sets were designed by ProbeFinder software. Quantitative PCR was performed with the Rotor-Gene RG3000 thermal cycler. Reaction mix was prepared in triplicate for each primary cell type and 5 ng of cDNA was used in each reaction. The fold change of each primary isolate was normalized to HUVEC using the $\Delta\Delta C_t$

method.

2.7.2 Paraffin embedded section preparation for immunostaining

Paraffin embedded tissue arrays or single tissues (CRUK histology service, REC reference no. 06/Q2707/338) were used. Paraffin was removed by washing the slides three times with histoclear and re-hydrated by incubation in a series of ethanol, water and then PBS. For antigen retrieval, slides were placed in citrate buffer (pH 6.0) and microwaved at medium power for 5 min twice. When cooled, sections were washed with PBST 0.1% for 2 min twice followed by 1 h blocking with 10% FCS 3% BSA PBS.

2.7.3 Immunohistochemical staining

Antigen retrieved and serum blocked tissue was incubated with the diluted primary antibody in PBS for 1 h. For frozen lung tissue, sections were fixed in acetone at -20°C for 5 min before staining with primary antibodies. Following a PBS 1% Tween-20 wash, sections were visualized using Vector ImmPRESS universal antibody kit and Vector NovaRed chromagen (Vectorlabs, Orton Southgate, UK) following manufacturer's instructions. Finally sections were counterstained with Mayers hematoxylin (Surgipath, Peterborough, UK), dehydrated, cleared and mounted in distyrene-plasticizer-xylene (DPX, Surgipath, Peterborough, UK) resin. Slides were

examined on a Nikon Eclipse E400 microscope (Nikon, Kingston upon Thames, UK) and images captured with a Nikon Coolpix 995 camera. Cresyl violet staining was performed using the LCM Staining Kit (Ambion, Paisley, UK) following the manufacturer's instructions.

2.7.4 Immunofluorescence staining

For co-localization studies, slides were then incubated in primary antibodies at the appropriate concentration overnight at 4 °C. After 3 washes with PBS 1% Tween-20, sections were probed with 1 in 100 diluted fluorescence conjugated secondary antibodies. Endothelium was visualized with 1 in 100 diluted *Ulex europaeus* agglutinin I conjugated to rhodamine. Slides were permanently mounted with 'Prolong gold anti-fade' reagent with DAPI to counterstain cell nuclei. Sections were then examined using an Axiovert 100M laser scanning confocal microscope.

2.8 Gene expression profiling methods

2.8.1 Microarray

Total RNA extracted from laser microdissected or *Ulex*-bead isolated samples were first converted to cRNA, then subjected to amplification and labeling using Low Input Quick Amplification labeling kit (Agilent, Wokingham, UK) following the manufacturer's protocol. The input RNA samples were confirmed to be of good

quality (RIN > 7) on a Bioanalyzer machine prior to the array. The specific activity of Cy3 labeled cRNA samples was determined on a NanoDrop spectrophotometer. Labeled cRNA samples were then hybridized to an Agilent whole human gene expression microarray. After washing steps using Gene expression and hybridization and wash buffer kits (Agilent, Wokingham, UK), the slide was scanned for feature extraction using Agilent Feature Extraction software v.11.0.1.1 (Agilent, Wokingham, UK). The Bioconductor packages Core and Limma were used to back ground subtract and Quantile normalize probe signal intensities prior to performing differential gene expression analyses. Correlation distances, 2d-clustering and principle component analyses were performed in R.

2.8.2 Next generation sequencing and data analysis

Reads were mapped to the Human genome (University California Santa Cruz, version hg19) with Tophat 1.3.3 [149]. Default parameters for colour space mapping were used with the exception of the following;

1. `-g/--max-multihits` was set to 1 to only report best uniquely mapping reads
2. `-library-type` was set to `fr-secondstrand` to reflect the sequencing library preparation
3. `-G` provided Tophat with a model set of gene annotation genome positions from the Refseq hg19 transcriptome.

The Tophat output bam files were sorted using samtools (Version: 0.1.8, [150]), and

'HTSeq-count' version 0.4.7p4 [151] was used, in conjunction with the Human transcriptome GTF Refseq version 19, to assign gene counts to produce a tab delimited file of transcript/gene counts. Differential gene expression analysis and p-value generation on the count data was carried out using the R Bioconductor package DESeq v1.5 [152]. This method was provided by John Herbert (Bicknell group, Birmingham, UK).

2.9 *In vitro* angiogenesis assays

2.9.1 Small interfering RNA (siRNA) knockdown of HUVECs

2.5×10^5 HUVEC were seeded into one well of a 6-well plate the day before transfection. Two siRNA duplexes were designed by the online SMARTselection siRNA design software. Negative control duplexes (scrambled) were included in all experiments. The transfection was performed using 0.3% lipofectamine RNAiMax with 10 nM duplex in OptiMEM. The transfection mix was incubated with the cells for 4 hs before replacing with complete HUVEC media (antibiotic free). Cells were used 48 hs post transfection and knockdown of protein expression was assessed by western blotting.

2.9.2 Scratch wound assay

The scratch wound assay was performed on HUVECs in a 6-well plate. A scratch was

made with a 10 μ l sterile tip. Migration of HUVECs was assessed by acquiring images of wound closure at time 0, 8, 12 and 24 hs. Images were acquired with a Leica DM 1000 light microscope and USB 2.0 2M Xli camera. The open area of the wound was highlighted and quantitated using the ImageJ or Photoshop CS4 software.

2.10 *In vivo* angiogenesis assay

2.10.1 Sponge assays

C57BL/6 mice received a sponge subcutaneously under the dorsal skin. 200 μ l of 10 ng/ml of bFGF was injected into the sponge on alternate days. On day 14, sponges were excised, fixed in 4% formalin for no longer than 24 h followed by 70% ethanol. The fixed sponges were then paraffin embedded and sectioned. H&E staining was performed on the sections. Slides were then mounted with DPX. The picture of the whole sponge was acquired using a Leica MZ 16 microscope at 10x lens. The invasive edge of the sponge which was acquired using Leica DME microscope at 40X. The invaded area was highlighted and analysed using Photoshop CS4 and Image J software.

2.10.2 Tumour growth experiments

C57BL/6 mice were implanted with 10^6 Lewis lung carcinoma cells subcutaneously. Tumour size was measured at three day interval. Tumour size was measured twice

weekly. The tumour volume was calculated using the formula: length x width² x 0.4 [153]. ANOVA analysis was performed for comparison of tumour growth between Robo4 vaccinated and control mice.

2.11 Generation of CLEC14A knockout mice

ES cells containing CLEC14A targeting vector were purchased from the Knockout Mouse Project (KOMP, Davis, USA). The targeting vector contains a β -galactosidase coding sequence from the *E.coli* lacZ gene and a coding sequence for neomycin. To target the CLEC14A gene locus, 5' and 3' homology arms of 2 kb were used (**Figure 2.1**). The cryovial preserved targeted ES cells were expanded and injected into the inner cell mass of blastocysts which were then implanted into pseudopregnant C57BL/6 mice. Chimeric mice were mated to Albino mice to screen for germline transmission by color recognition of the offspring. This identified #15 mouse as having germline transmission. Mouse #15 was used to generate heterozygous offspring on a C57BL/6 background. Three pairs of CLEC14A heterozygous crossing were set up to generate complete CLEC14A knockout mice.

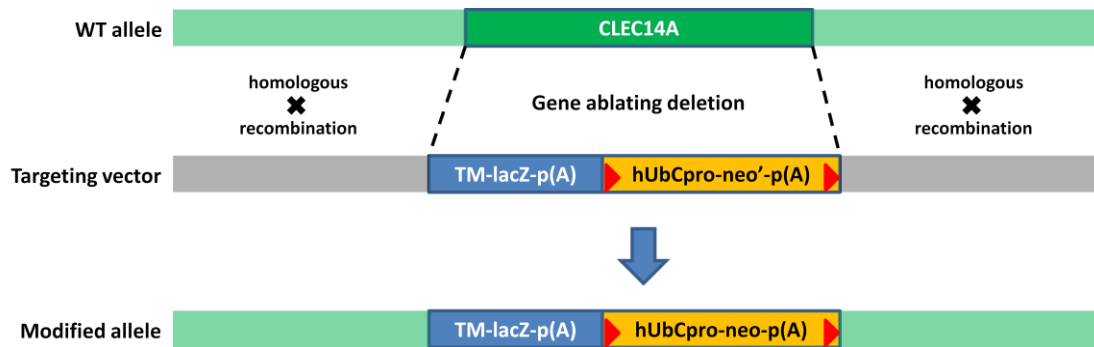


Figure 2.1 Targeting strategy for generation of CLEC14A knockout mice. Top: Wild type CLEC14A allele. Middle: Targeting vector containing a cassette of a lacZ reporter gene, a neomycin resistant gene. 5' and 3' homology arms of 2 kb each end (in gray) were used to target the gene locus. Bottom: Targeted allele after homologous recombination in ES cells.

2.12 Immunogenicity assay

2.12.1 Generation of a standard curve for antibody assay

ELISA plate was coated with papain cleaved human or mouse Robo4 (25 μ l - 0.008 μ l) at 4°C overnight. The wells were blocked with 100 μ l of blocking buffer (3% BSA, PBS) for 1 h at RT. Serial dilutions of primary Robo4 antibody (MR7 against human Robo4 raised from mouse; Abcam antibody against human/mouse Robo4 raised from rabbit) from 1 μ g/ml to 0.008 μ g/ml were applied. After 1 h incubation at RT and 6 washes with wash buffer (0.1 % Tween-20 PBS), peroxidase conjugated anti-mouse IgG or anti-rabbit IgG antibody was diluted 1/10000 in the blocking buffer and 100 μ l was applied to each well followed by a 1 h incubation at RT. After 6 washes with wash buffer, 100 μ l of substrate contained OPD (o-phenylenediamine dihydrochloride) at 0.4 mg/ml in 0.05 M phosphate citrate buffer containing 0.03 % sodium perborate was applied to each well. The reaction was stopped by adding 50 μ l of 3M HCl. The ELISA

plate was read at 490 nm (0.1 s) absorbance on an ELISA plate reader.

2.12.2 Investigation of Robo4 antibody in human and mouse serum

An ELISA plate was coated with 5 μ l per well of papain cleaved human or mouse Robo4 protein stock overnight at 4°C. After 1 h blocking with 3% BSA PBS, 5 μ l of serum from man or mouse were diluted in 45 μ l of PBS and applied to the antigen coated plate. After 6 washes, peroxidase conjugated anti-human IgG or anti-mouse IgG antibody was applied as the secondary. For characterizing antibody isotypes from mouse serum, peroxidase conjugated anti-mouse IgG1, 2a, 2b and 3 and IgM secondary antibody (Southern Biotech, Cambridge, UK) was applied. The rest of the procedure was as previously described.

2.13 Mouse immunization

2.13.1 Immunization with Robo4 protein and Freund's adjuvant in mice

FPLC purified mouse Robo4 protein or commercial human-Fc protein control was subcutaneously injected into C57BL/6 mice with 2 weekly intervals. Two groups of mice received 50 μ g of mouse Robo4-Fc protein or human Fc protein respectively with complete Freund's for the first injection and incomplete Freund's afterwards. 20 μ l of serum from each mouse was collected before each injection. The level of Robo4 specific antibody was tested by ELISA assay using papain cleaved mouse Robo4 as

the coating protein. Organs including brain, heart, lung, liver, kidney and spleen from both groups were collected and fixed in 4% formalin. The tissues were then paraffin embedded and sectioned following H&E staining. The pictures from the stained sections were acquired using a Leica DM IL microscope and USB 2.0 2M Xli camera. Larger scale experiments were performed for further *in vivo* angiogenesis assays.

2.13.2 Immunization with Robo4-CGG conjugate in CGG primed mice

Purified mouse Robo4-Fc protein was cross-linked to CGG (Chicken γ globulin) using glutaraldehyde as previously described [154]. In brief, 2 μ l of glutaraldehyde 25% stock (Sigma, Gillingham, UK) was added to 1 ml of reaction mix containing 1 mg of mouse Robo4-Fc protein and 1 mg of CGG in PBS (pH 7.5 - 8). The human Fc protein alone was also CGG crosslinked following an identical procedure. The reaction mix was incubated at RT for 10 min. The reaction was quenched by adding 100 μ l of 1 M Tris-HCl (pH 8) and left at RT for 15 min. Before injecting into mice, the mix was dialysed (10,000 MWCO) with PBS overnight.

50 μ g of Robo4-CGG or Fc-CGG conjugate was subcutaneously injected into 5-week CGG primed mice. Simultaneously, each mouse received 10^6 Lewis lung carcinoma cell subcutaneously as describe above.

2.14 Bioinformatics websites and programs

Websites

Universal ProbeLibrary Assay Design Center:

<https://www.roche-applied-science.com>

siDESIGNTM center:

<http://www.dharmacon.com/sidesign>

NCBI:

<http://ncbi.nlm.nih.gov/>

Pubmed:

<http://www.ncbi.nlm.nih.gov/sites/entrez/>

SVMtm Transmembrane Domain Predictor:

<http://bioinformatics.org.au/>

TMHMM Server v. 2.0:

<http://www.cbs.dtu.dk/services/TMHMM/>

Bioinformatics and Molecular Analysis Section:

<http://www-bimas.cit.nih.gov/index.shtml>

NEBcutter V2.0:

<http://tools.neb.com/NEBcutter2/index.php>

UCSC Genome Bioinformatics Site:

<http://genome.ucsc.edu/>

SMART:

<http://smart.embl-heidelberg.de/>

Knock out mouse project:

<http://www.komp.org/>

Programs:

AdobePhotoshopCS4

ImageJ

ChromasPro

Rotor-Gene RG-3000

2.15 Statistical methods

Excel was used to generate graphs and perform statistical analysis. The parametric Student t-test and Two-way analysis of variance test (ANOVA) with Dunnett's Multiple comparison post-hoc test were used to compare the means of two and among more than two independent groups respectively. A minimum 95% confidence interval was used in all statistical tests. All error bars depict the standard error of the mean (SEM).

P value	Summary
< 0.001	***
to 0.01	**
0.01 to 0.05	*
>0.05	Non significant (ns)

Chapter three

Validation of potential TEMs

3.1 Introduction

Bioinformatics predicted several putative TEMs [78]. cDNA libraries were used to predict putative TEMs essentially by various methods involving *in silico* subtraction of libraries. The predicted TEM candidates needed validation by profiling their expression in human tissues. An ideal TEM should fulfill the following criteria:

1. Expression in endothelial cells
2. Expression on tumour vessels
3. Absent or low expression in healthy adult tissues.

In this chapter, three putative TEMs: CLEC14A, GBP4 and IKBKE are respectively validated as a TEM on a human cancer array and healthy adult tissues by various techniques, including quantitative real-time PCR, immunohistochemistry and immunofluorescence.

3.2 CLEC14A is predominantly expressed in endothelial cells

To confirm the endothelial specificity of CLEC14A, real-time PCR using CLEC14A primers was performed across a range of primary cell isolates including HUVEC, HDMEC (human dermal microvascular endothelial cells), MRC5 (fibroblasts), HASMC (human aortic smooth muscle cells), PBMC (peripheral blood mononuclear cells), hepatocytes and HBE (human bronchial epithelium). Flotillin 2 was employed as the house keeping gene to which CLEC14A expression was normalized [155]. The $\Delta\Delta C_t$ method was used to calculate the fold change.

As shown in **Figure 3.1**, CLEC14A was predominantly expressed in endothelial cells with some expression in MRC5 fibroblasts. We note, however, that MRC5 is a diploid cell line derived from fetal lung tissue [156] and not a primary cell isolate. Aside from MRC5, CLEC14A expression is essentially absent in other primary cell types.

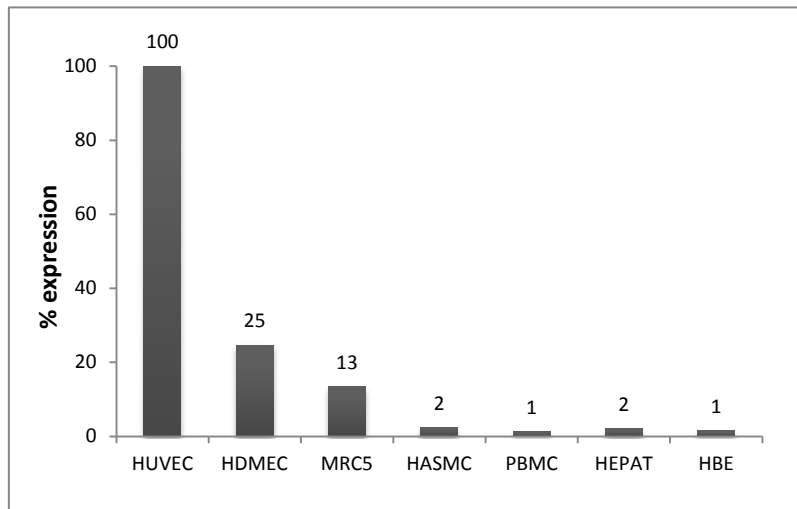


Figure 3.1 Expression analysis of CLEC14A in primary cell isolates by real-time PCR. HUVEC: human umbilical vein endothelial cells; HDMEC: human dermal microvascular endothelial cells; MRC5: MRC5 fibroblasts; HASMC: human aortic smooth muscle cells; PBMC: peripheral blood mononuclear cells; HEPAT: hepatocytes; HBE: human bronchial epithelium. The experiment was repeated three times with similar results.

3.3 CLEC14A siRNA knockdown in HUVEC

Two CLEC14A specific duplexes were transfected into HUVECs at a concentration of 10 nM. Scrambled negative control siRNA duplex, with no homology to known human DNA sequences, was used as control. Mock control with no siRNA but transfection reagent alone was also used to show that the transfection process alone had no effect on cell behavior.

The efficiency of the knockdown was evaluated by western blotting of cell lysate. The predicted molecular weight of CLEC14A is 51.6 kDa. As CLEC14A is heavily glycosylated (one highly conserved N- and nine poorly conserved O-glycosylation sites), the band at around 100 kDa is presumably the glycosylated form of the full length CLEC14A (**Figure 3.2**). No band was detected at 51.6 kDa. The level of tubulin expression was used as the protein loading control. Antisera failed to detect CLEC14A in knockdown cells but clear bands were seen in mock and scrambled siRNA controls. Thus, the specificity of the commercial CLEC14A antisera used later in immunocytochemistry and immunofluorescence staining was confirmed.

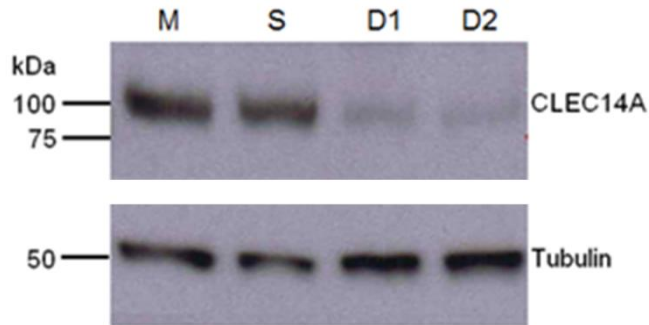


Figure 3.2 Western blot of CLEC14A siRNA knock-down in HUVEC. Western blot of CLEC14A knockdown in HUVECs shows that both siRNA duplexes were effective. Tubulin was used as the protein loading control. M: Mock, S: Scrambled; D1: Duplex1, D2: Duplex2.

3.4 CLEC14A is expressed on vessels in tumours but not those in healthy tissue

To investigate CLEC14A expression, we performed double immunofluorescence staining with CLEC14A antibody and the human endothelial marker *Ulex* lectin. Commercial polyclonal antibody to the extracellular domain of CLEC14A was used to define its expression pattern. FITC conjugated anti-sheep antisera was used to visualize CLEC14A expression in green. *Ulex* is a lectin that specifically binds to the alpha-L-fucose containing glycoproteins present on the surface of human endothelial cells [119]. Rhodamine conjugated *Ulex* was used to visualize the endothelium in red. Co-staining was performed on human tissue arrays which had 12 different types of carcinoma and matching adjacent healthy tissue and 10 samples of each. A confocal microscope was used to acquire the fluorescent images. Fluorescence detected within the vessel lumen was the autofluorescence of erythrocytes leaking through to the red and green channels.

Widespread expression of CLEC14A co-localized with *Ulex* on tumour vessels (**Figure 3.3 a-c**). In contrast we failed to detect CLEC14A on vessels in most of the adjacent healthy tissues. The result of the multiple tissue array staining has been summarized in **Figure 3.4**. Some adjacent healthy tissues showed positive CLEC14A antibody staining that may be due to its proximity to the tumour.

To determine whether CLEC14A is truly absent from healthy tissue, the co-staining was performed on non-tumour related clinical samples derived from various organs. As shown in **Figure 3.5a-b**, CLEC14A was undetectable in healthy bladder, breast, liver, ovary, brain, colon, lung and kidney. Taken together, the expression profile confirmed CLEC14A as a tumour endothelial marker (TEM).

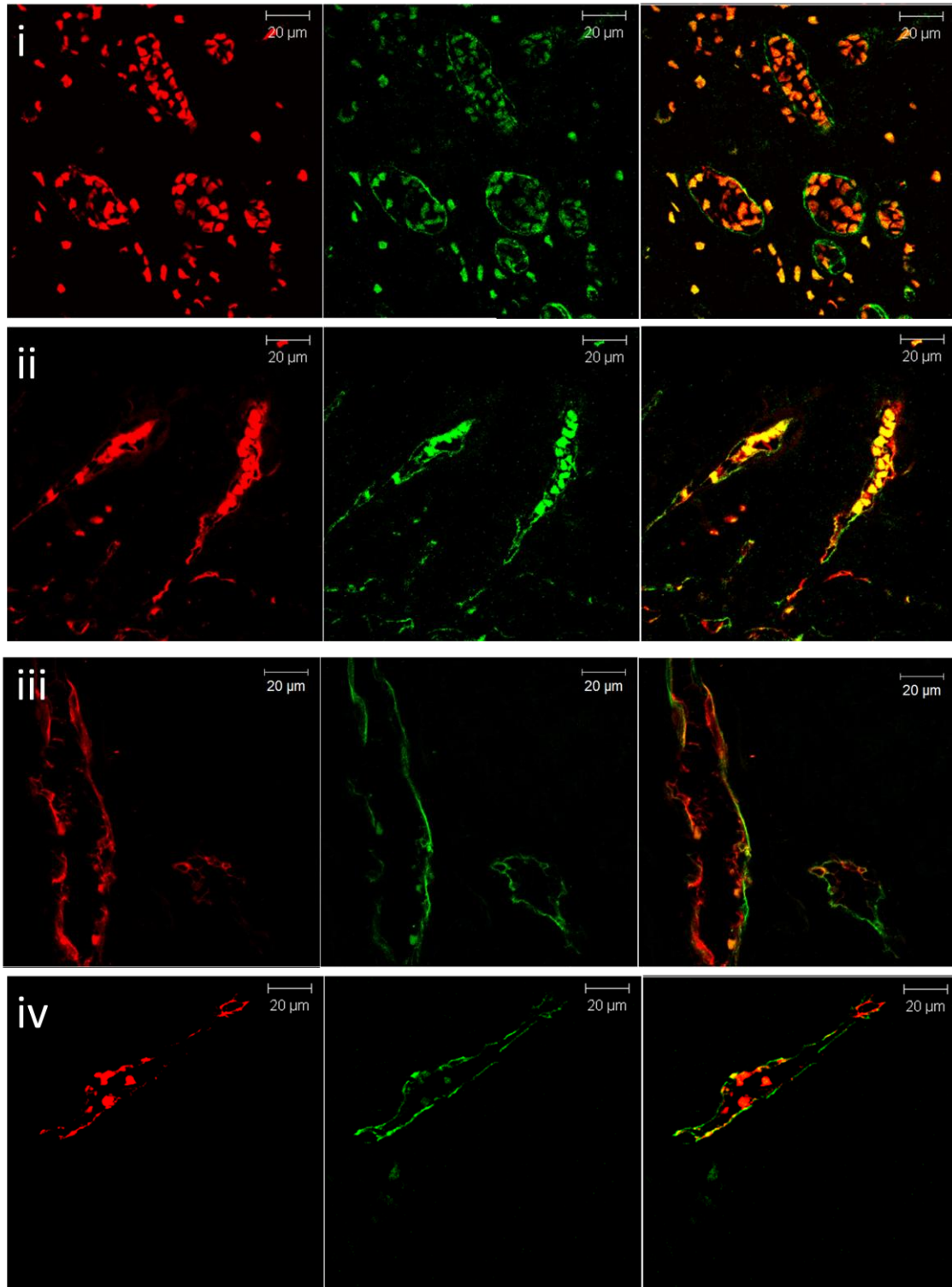


Figure 3.3a Confocal microscopic images (63X) of a human cancer tissue array stained with CLEC14A antibody. Endothelial cells were stained with rhodamine-conjugated *Ulex europaeus* lectin (Red). CLEC14A antibody was labeled with a FITC conjugated secondary antibody (Green). (i) oesophageal carcinoma (ii) thyroid carcinoma (iii) breast carcinoma (iv) lung carcinoma

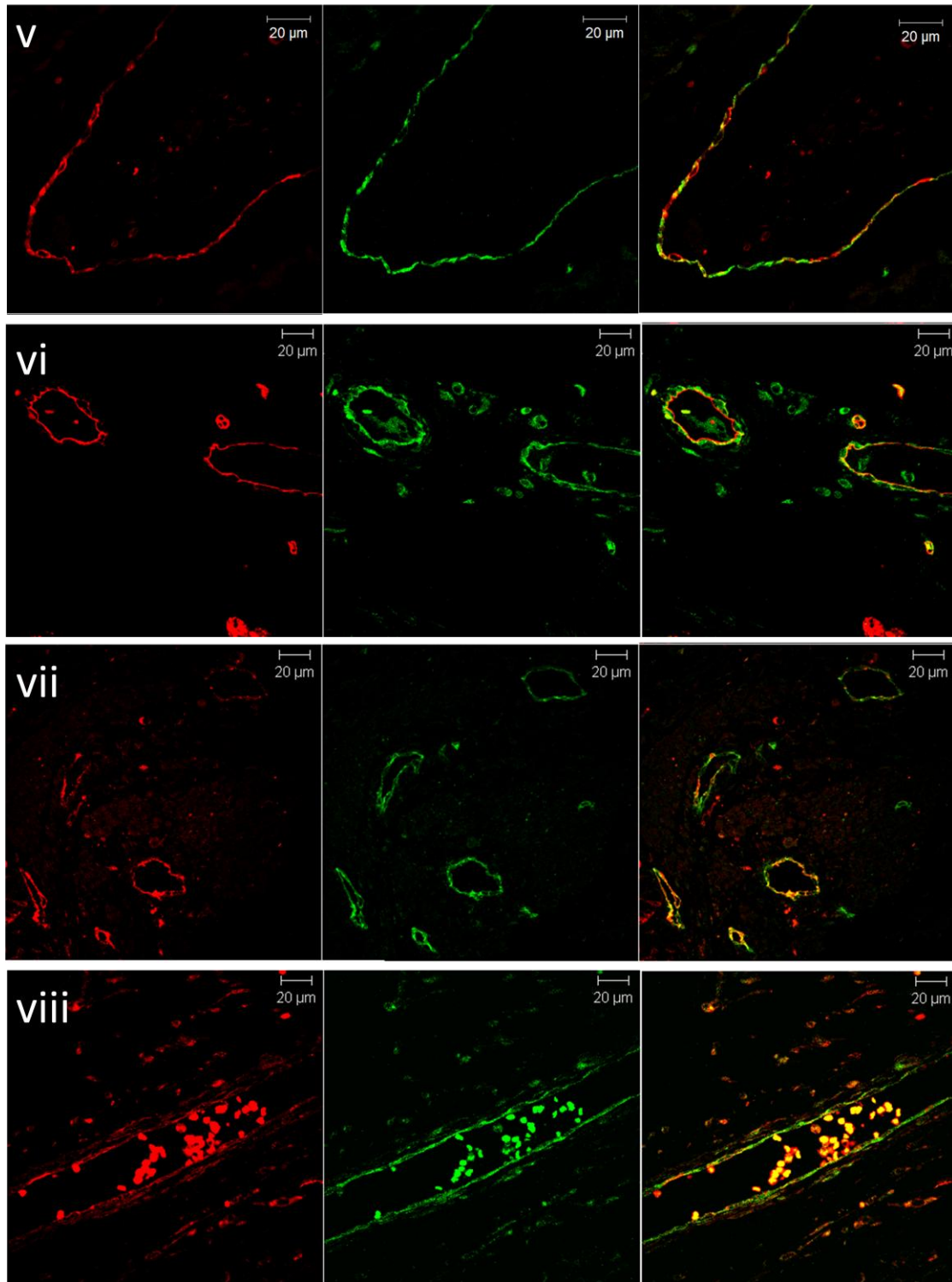


Figure 3.3b Confocal microscopic images (63X) of a human cancer tissue array stained with CLEC14A antibody. Endothelial cells were stained with rhodamine-conjugated *Ulex europaeus* lectin (Red). CLEC14A antibody was labeled with a FITC conjugated secondary antibody (Green). (v) liver carcinoma (vi) stomach carcinoma (vii) pancreatic carcinoma (viii) kidney carcinoma

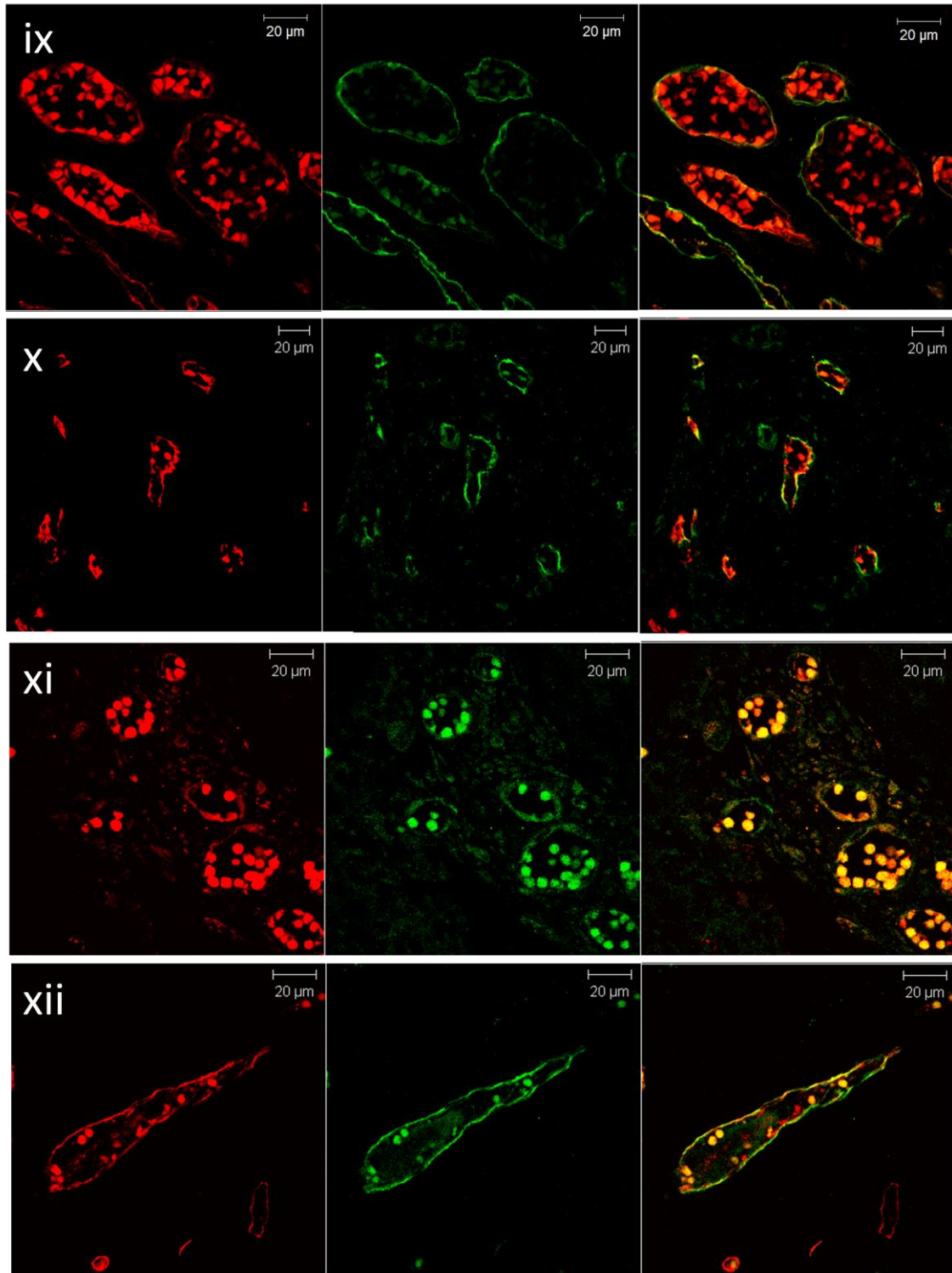


Figure 3.3c Confocal microscopic images (63X) of a human cancer tissue array stained with CLEC14A antibody. Endothelial cells were stained with rhodamine-conjugated *Ulex europaeus* lectin (Red). CLEC14A antibody was labeled with a FITC conjugated secondary antibody (Green). (ix) bladder carcinoma (x) ovary carcinoma (xi) rectal carcinoma (xii) prostate carcinoma

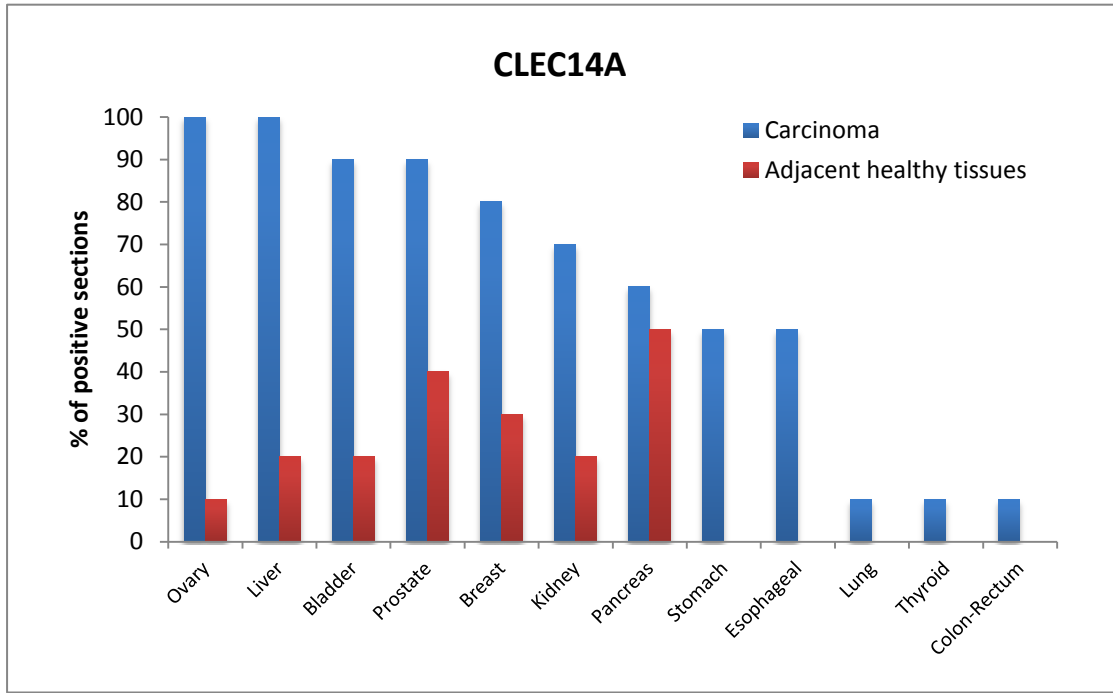


Figure 3.4 Summary of CLEC14A expression in cancer and matched adjacent healthy tissue arrays.

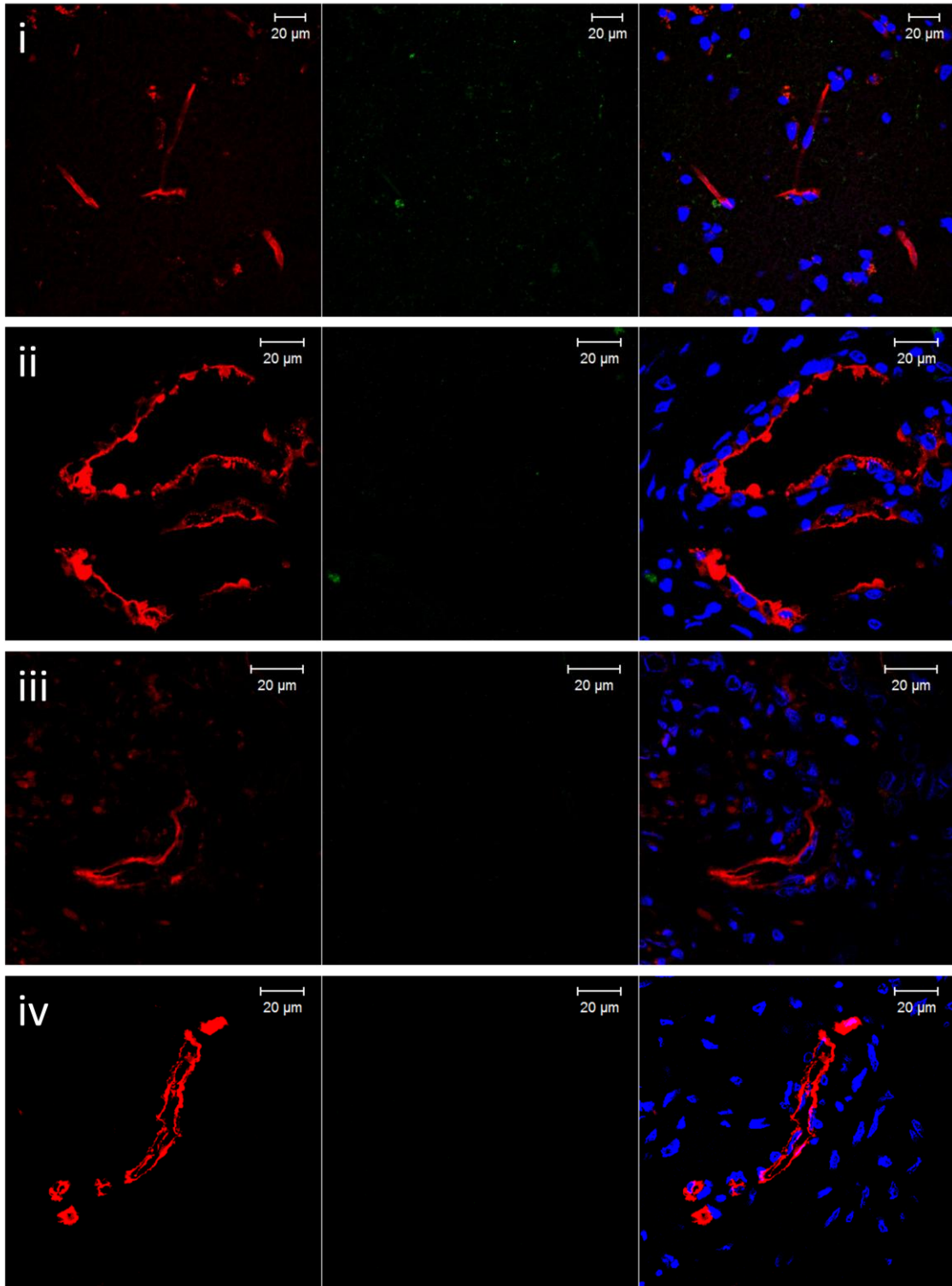


Figure 3.5a Confocal microscopic images (63X) of healthy tissues stained with CLEC14A antibody. Endothelial cells were stained with rhodamine-conjugated *Ulex europaeus* lectin (Red). CLEC14A antibody was labeled with a FITC conjugated secondary antibody (Green). Nuclei were stained with DAPI (Blue). (i) brain (ii) breast (iii) lung (iv) liver.

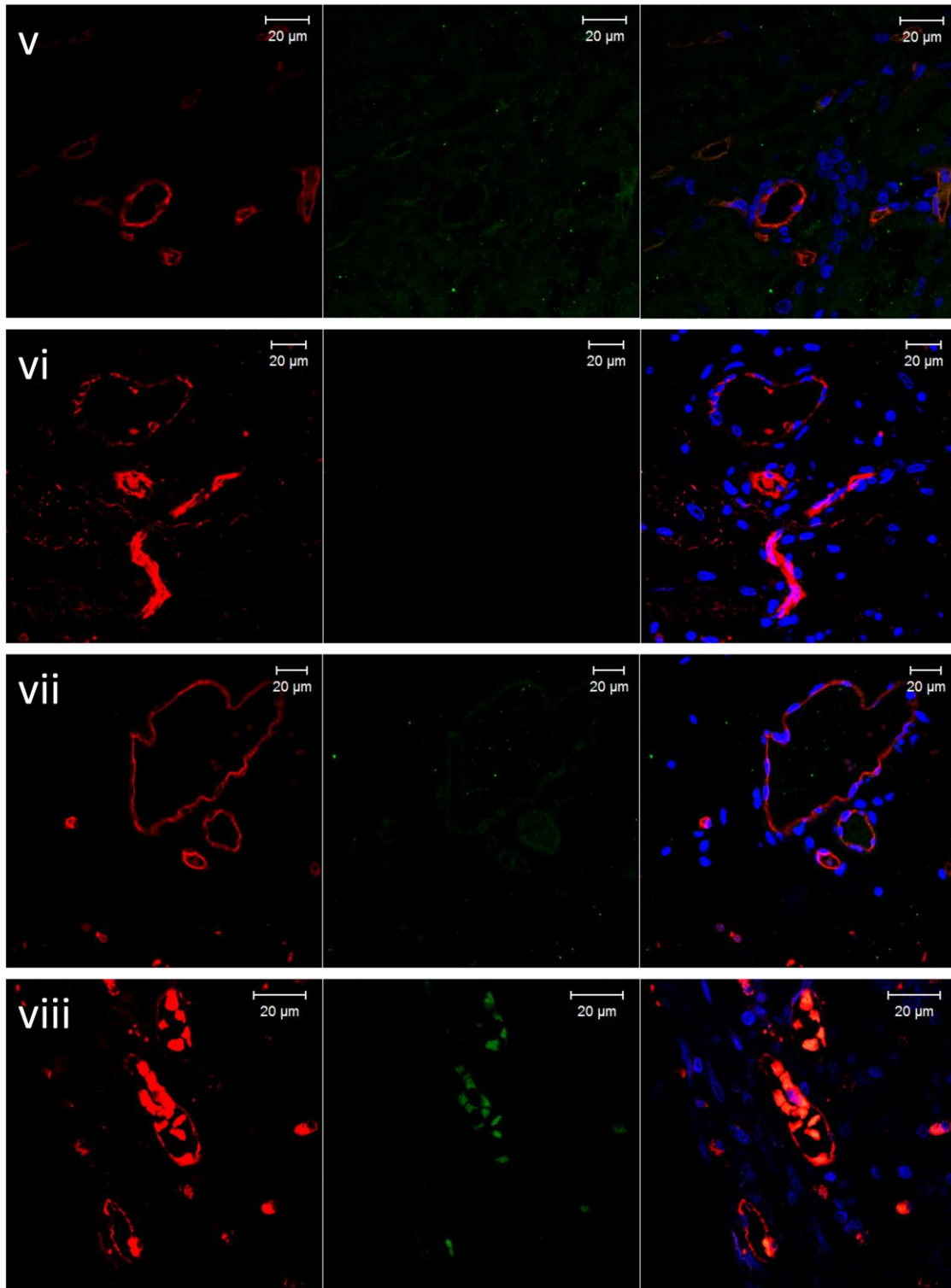


Figure 3.5b Confocal microscopic images (63X) of healthy tissues with CLEC14A antibody. Endothelial cells were stained with rhodamine-conjugated *Ulex europaeus* lectin (Red). CLEC14A antibody was labeled with a FITC conjugated secondary antibody (Green). Nuclei were stained with DAPI (Blue). (v) kidney (vi) bladder (vii) colon (viii) ovary.

3.5 Confirmation of CLEC14A as a tumour endothelial marker by immunohistochemistry

To further confirm that CLEC14A is differentially expressed between healthy and tumour tissues, immunohistochemistry staining was performed on a hepatocellular carcinoma tissue using the same commercial polyclonal antisera to CLEC14A. In a liver cancer section, the tumour tissue was delineated from the adjacent healthy tissue by a fibrotic capsule, strong CLEC14A staining on the vessels was observed in the tumour area but not in the healthy tissues (**Figure 3.6, top**). Higher magnification of the images of vessels in tumour and adjacent healthy tissues are shown in **Figure 3.6, bottom**. Comparison of CLEC14A expression between healthy and tumour tissues derived from other organs was then performed using the same technique. As shown in **Figure 3.6**, CLEC14A was strongly present on tumour vessels in prostate, breast, kidney and thyroid but absent in vessels of corresponding healthy tissue.

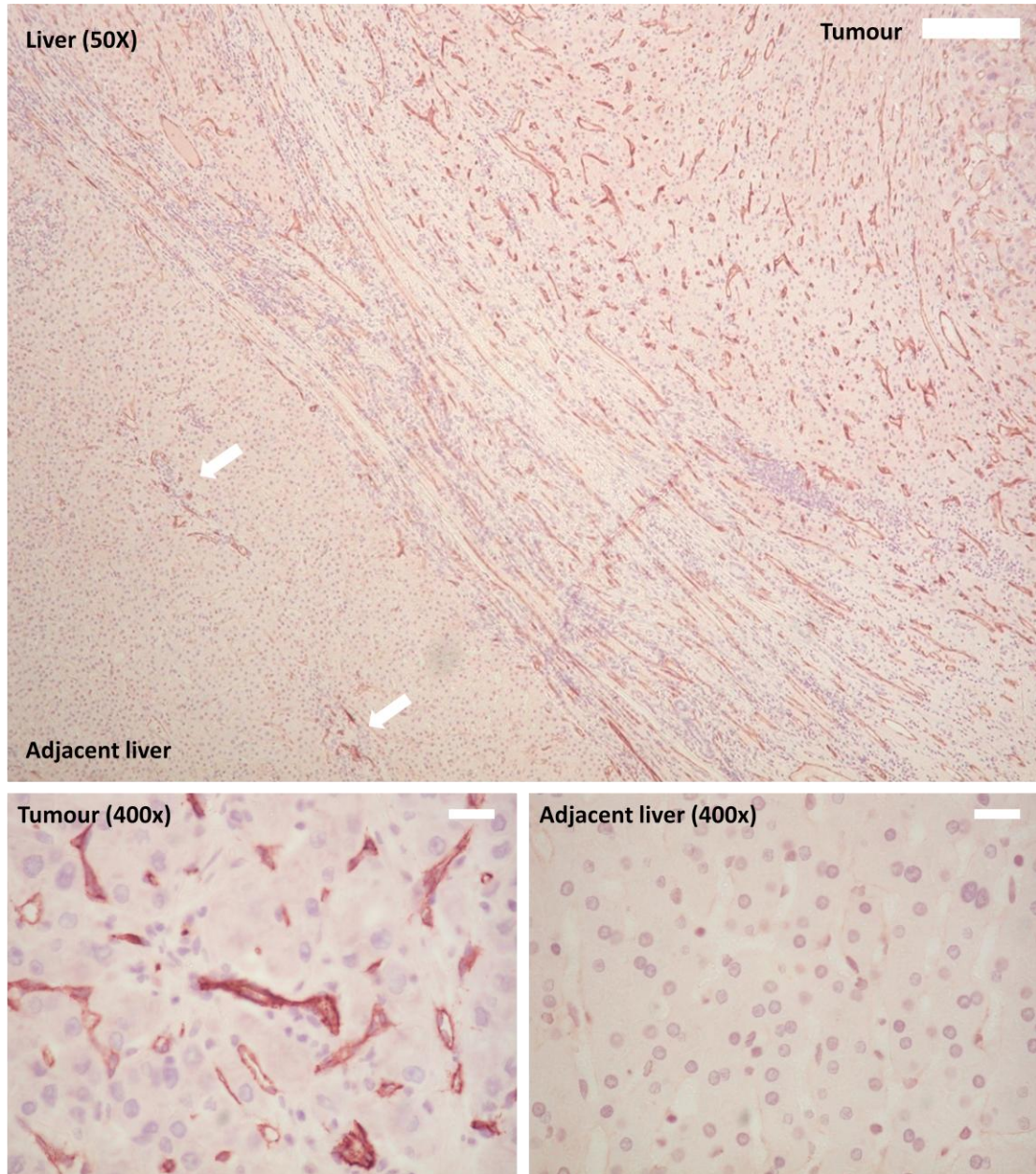


Figure 3.6 Immunostaining of human liver showing adjacent healthy liver and hepatocellular carcinoma in the same section. White arrows indicate invasion of the nearby carcinoma into the healthy tissue. Scale bar = 200 mm (top). Intense staining of vessels in hepatocellular carcinoma while lack of immunostaining of vessels in healthy liver tissue was observed (bottom). Scale bars = 25 mm. (Data provided by Gary Reynolds)

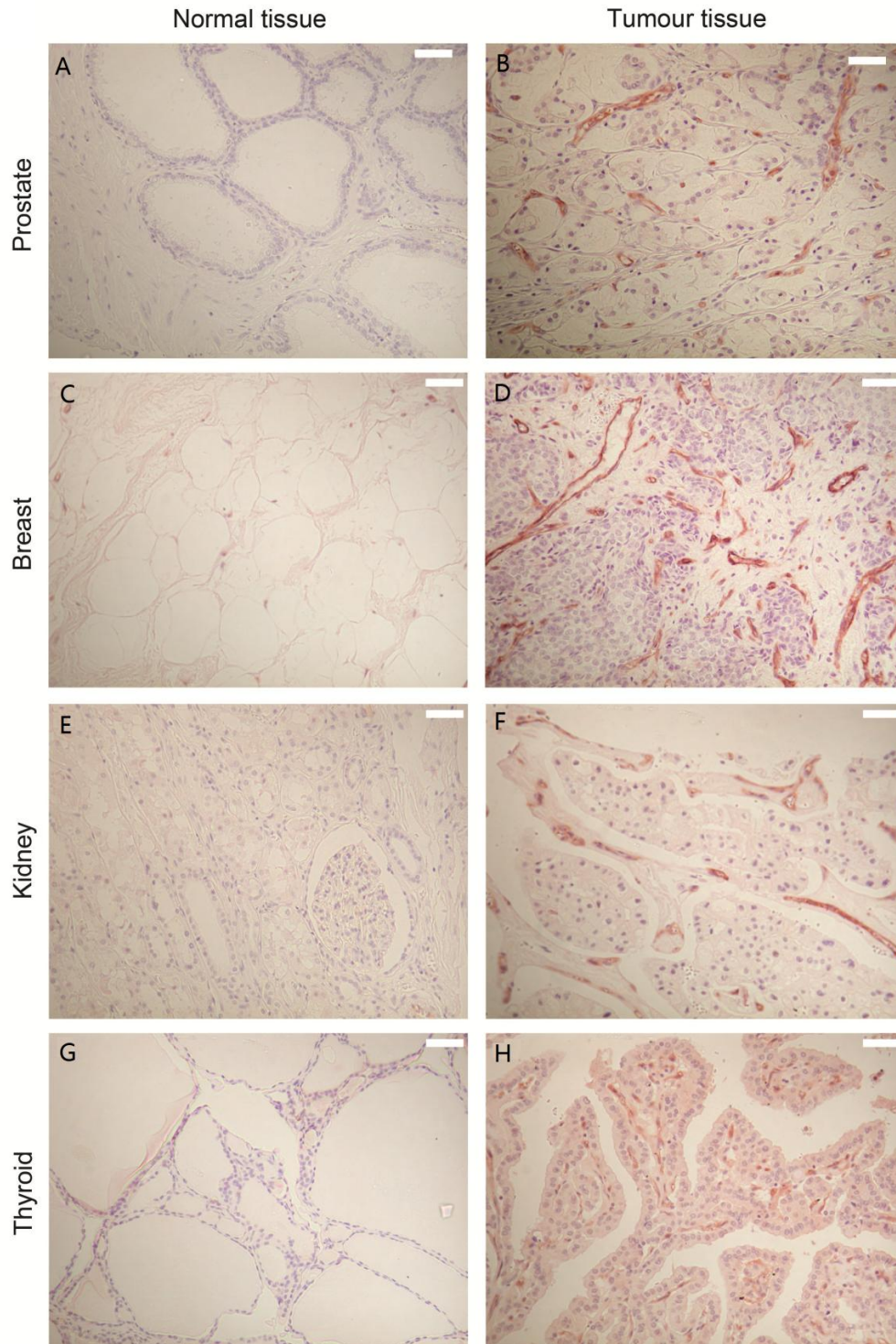


Figure 3.7 Comparison of CLEC14A immunostaining of healthy and tumor tissue. (A-B) prostate, (C-D) breast, (E-F) kidney and (G-H) thyroid. Scale bars = 100 mm. (Data provided by Gary Reynolds)

3.6 GBP4 is highly expressed on tumour vessels and on vessels in some adjacent tissue

To determine whether there is a differential expression pattern of GBP4 in cancer and healthy tissues, we performed immunofluorescence staining on human tissue arrays using a polyclonal antisera to GBP4. The specificity of the antibody was verified by siRNA knockdown of GBP4 in HUVECs (**Figure 3.8**). The efficiency of knockdown was confirmed by Western blotting of cell lysate. GBP4 antibody detected a clear band at 74 kDa which is consistent with the predicted molecular weight of GBP4 (74 kDa).

FITC conjugated secondary antibody was used to demonstrate GBP4 expression. *Ulex* was used to visualize the blood vessels. Tissue arrays were used as previously described. The results demonstrated that GBP4 displayed a differential expression pattern across a wide range of cancer tissues (**Figure 3.9a-c**). GBP4 expression was restricted to the endothelium in thyroid, pancreas, kidney, bladder, ovarian and colon carcinoma while in the liver and prostate carcinoma, it is present in both endothelium and tumour cells. The percentage of positive sections was summarized in **Figure 3.10**. With the exception of stomach where there were more GBP4 positive tissues in the adjacent healthy than that in the cancer tissues, the overall percentage of GBP4 positive tissues in tumour was greater than that in the healthy tissues.

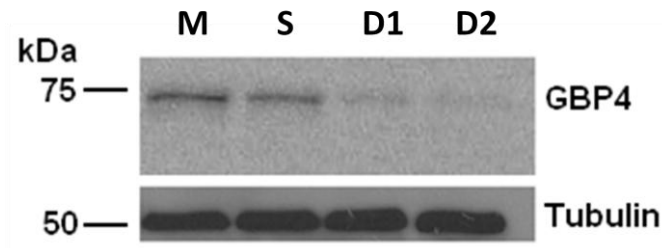


Figure 3.8 Western blot on HUVEC of GBP4 siRNA knock-down. Western blot of HUVECs with GBP4 knockdown using the commercial GBP4 antibody shows that both siRNA duplexes worked efficiently. The level of tubulin expression was used as the protein loading control. M: Mock, S: Scrambled; D1: Duplex1, D2: Duplex2.

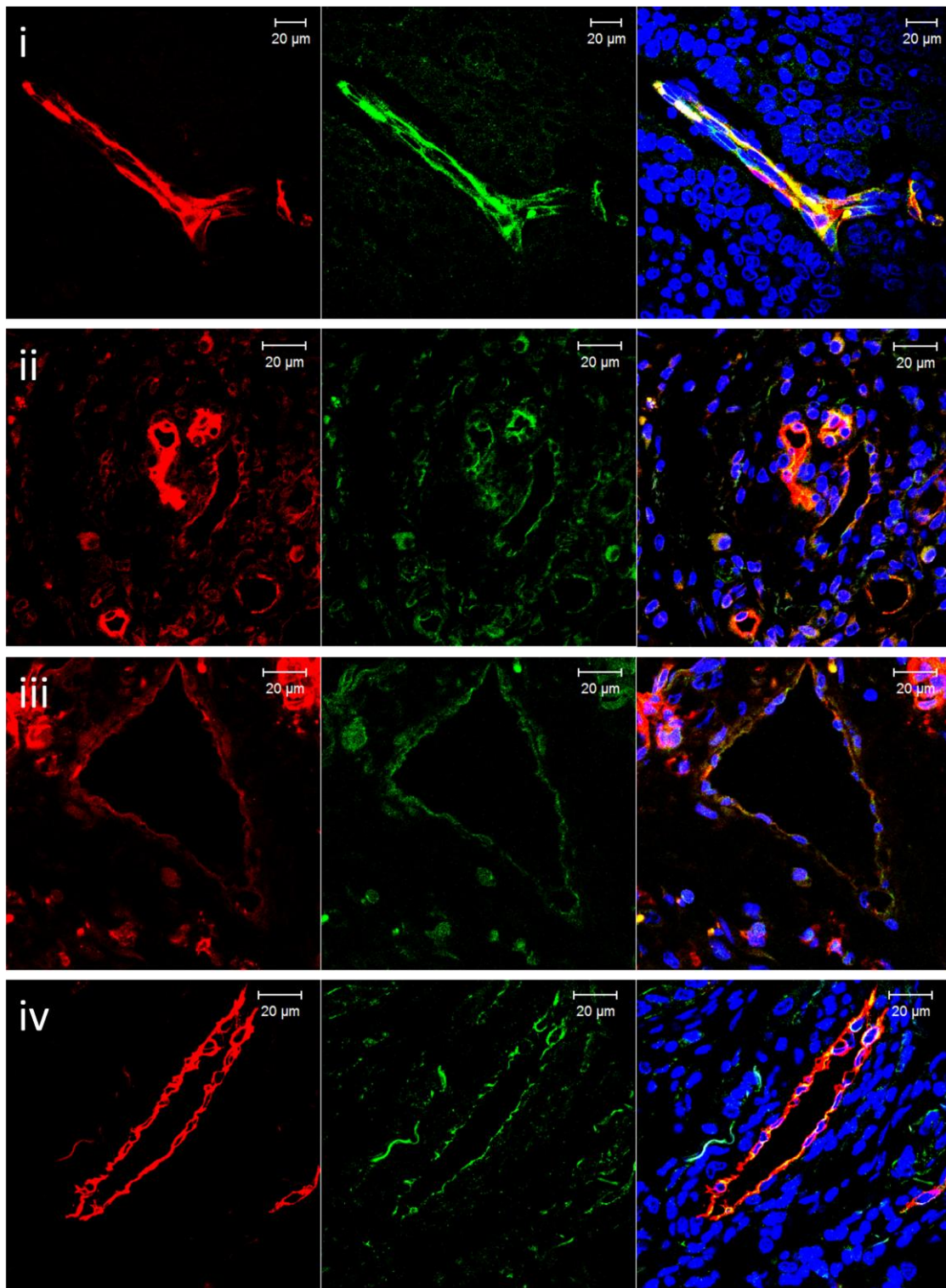


Figure 3.9a Confocal microscopic images (63X) of a human cancer array with GBP4 antibody. Endothelial cells were stained with rhodamine-conjugated *Ulex europaeus* lectin (Red). GBP4 antibody was labeled with a FITC conjugated secondary antibody (Green). Nuclei were stained with DAPI (Blue). (i) oesophageal carcinoma (ii) thyroid carcinoma (iii) breast carcinoma (iv) lung carcinoma

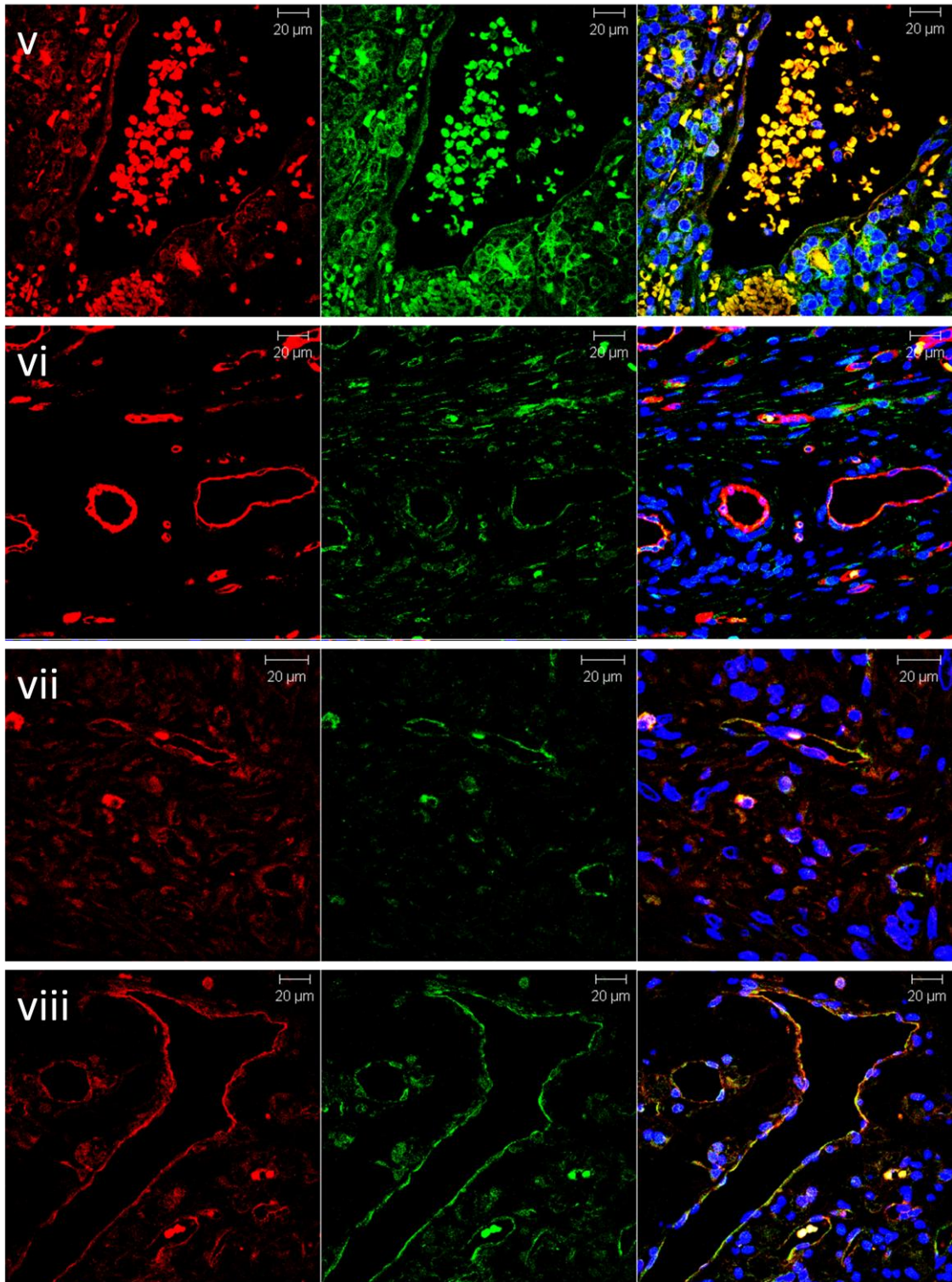


Figure 3.9b Confocal microscopic images (63X) of a human cancer array with GBP4 antibody. Endothelial cells were stained with rhodamine-conjugated *Ulex europaeus* lectin (Red). GBP4 antibody was labeled with a FITC conjugated secondary antibody (Green). Nuclei were stained with DAPI (Blue). (v) liver carcinoma (vi) stomach carcinoma (vii) pancreas carcinoma (viii) kidney carcinoma

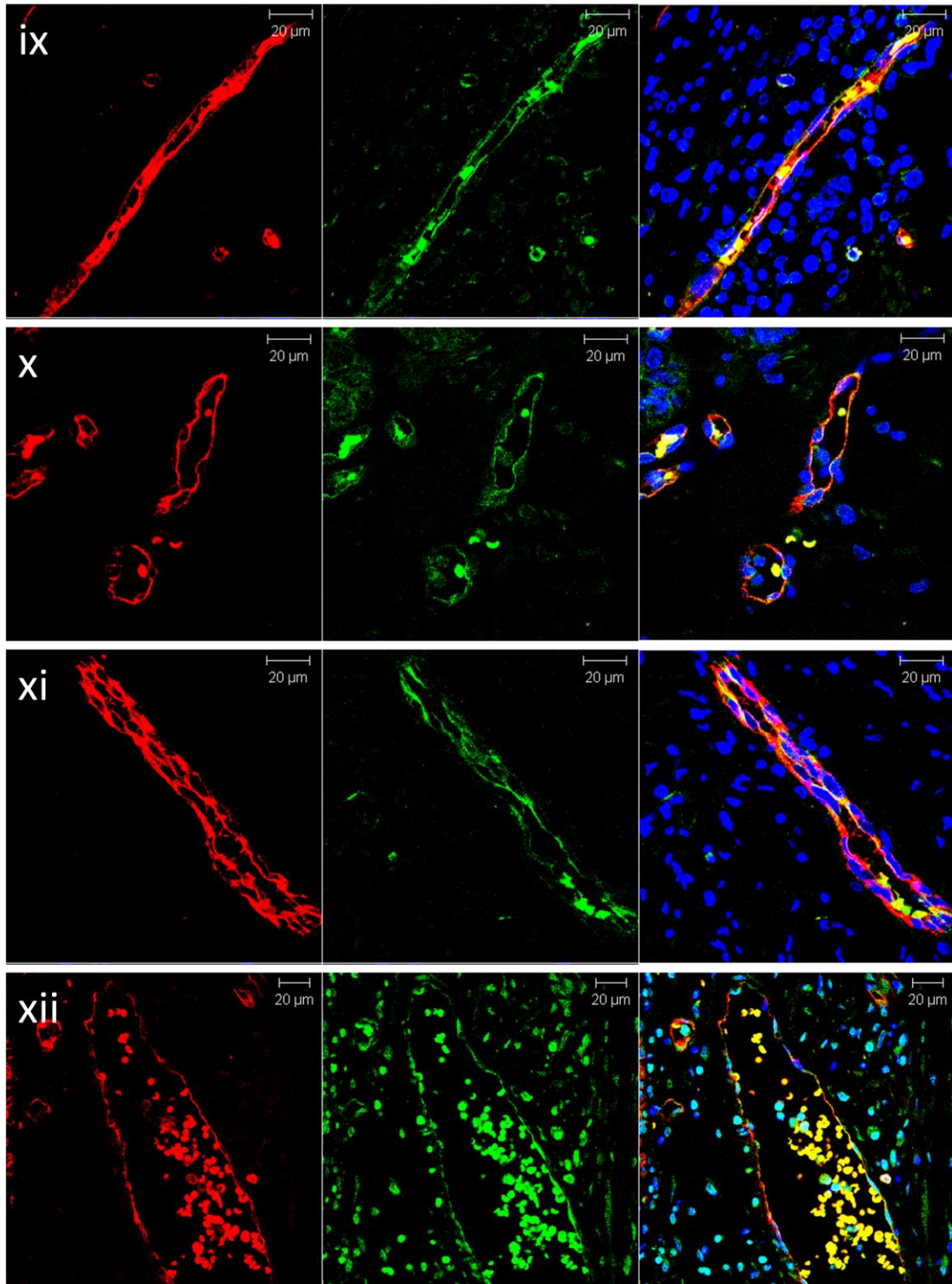


Figure 3.9c Confocal microscopy images (63X) of a human cancer array with GBP4 antibody. Endothelial cells were stained with rhodamine-conjugated *Ulex europaeus* lectin (Red). GBP4 antibody was labeled with a FITC conjugated secondary antibody (Green). Nuclei were stained with DAPI (Blue). (ix) bladder carcinoma (x) ovary carcinoma (xi) colon carcinoma (xii) prostate carcinoma

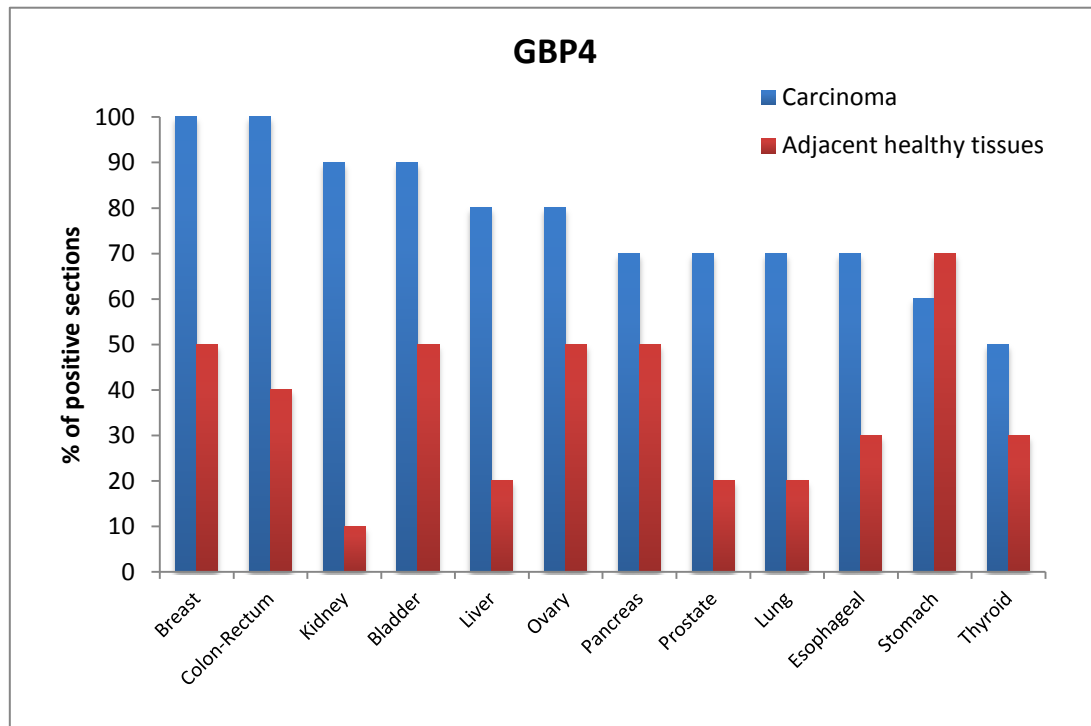


Figure 3.10 Summary of GBP4 expression in cancer and matched adjacent healthy tissue arrays

3.7 GBP4 is absent from vessels in healthy tissue

In order to determine whether GBP4 is present in the non-cancer related healthy tissues, we performed a screen on tissues derived from healthy donors.

Immunofluorescence was performed on a wide range of healthy tissues using the same GBP4 antibody. As shown in **Figure 3.11a-b**, the expression of GBP4 was absent or essentially low in all healthy tissues include brain, breast, lung, liver, kidney, bladder, colon and prostate.

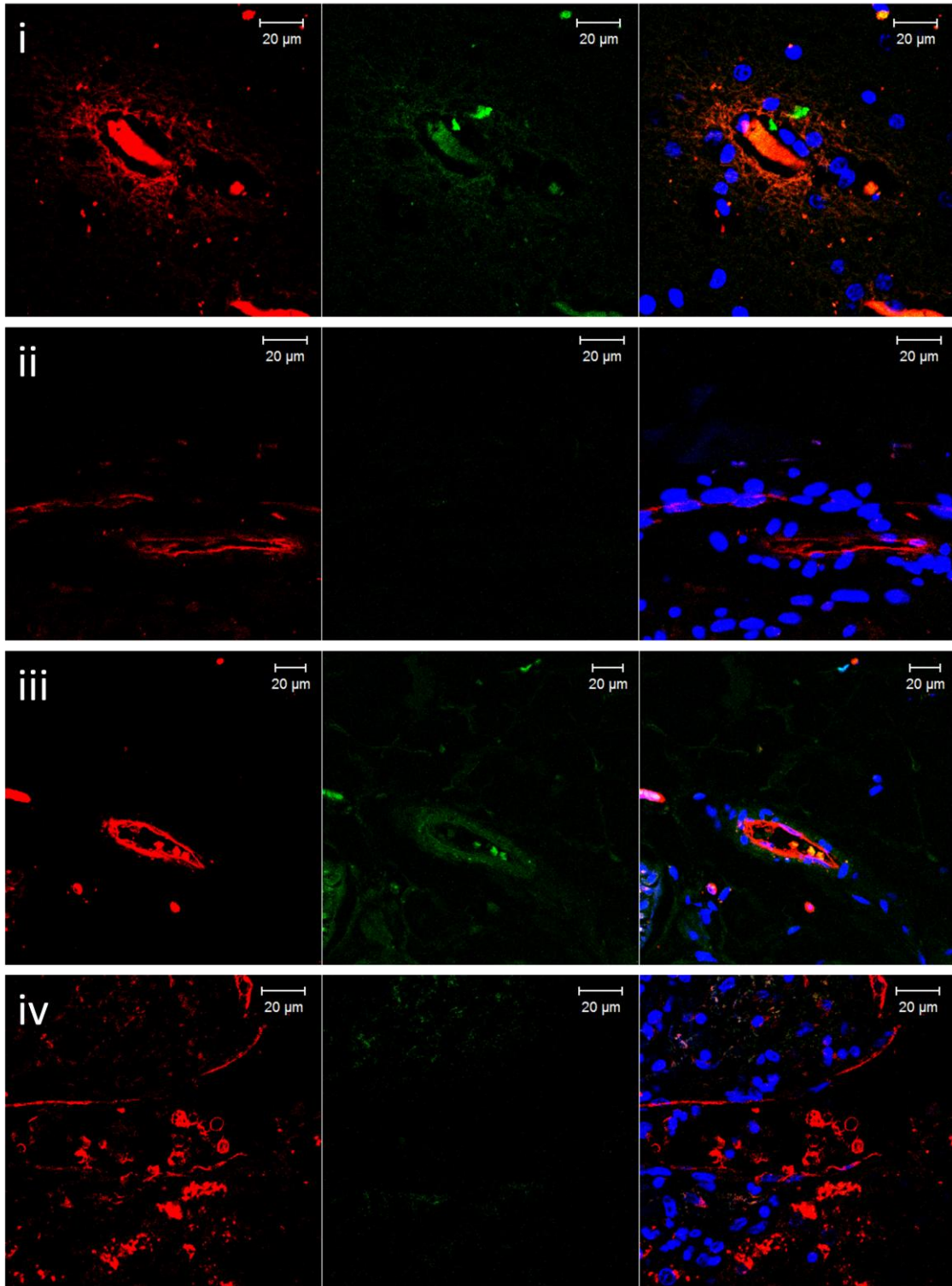


Figure 3.11a Confocal microscopy images (63X) of healthy tissues with GBP4 antibody. Endothelial cells were stained with rhodamine-conjugated *Ulex europaeus* lectin (Red). GBP4 antibody was labeled with a FITC conjugated secondary antibody (Green). Nuclei were stained with DAPI (Blue). (i) brain (ii) breast (iii) lung (iv) liver

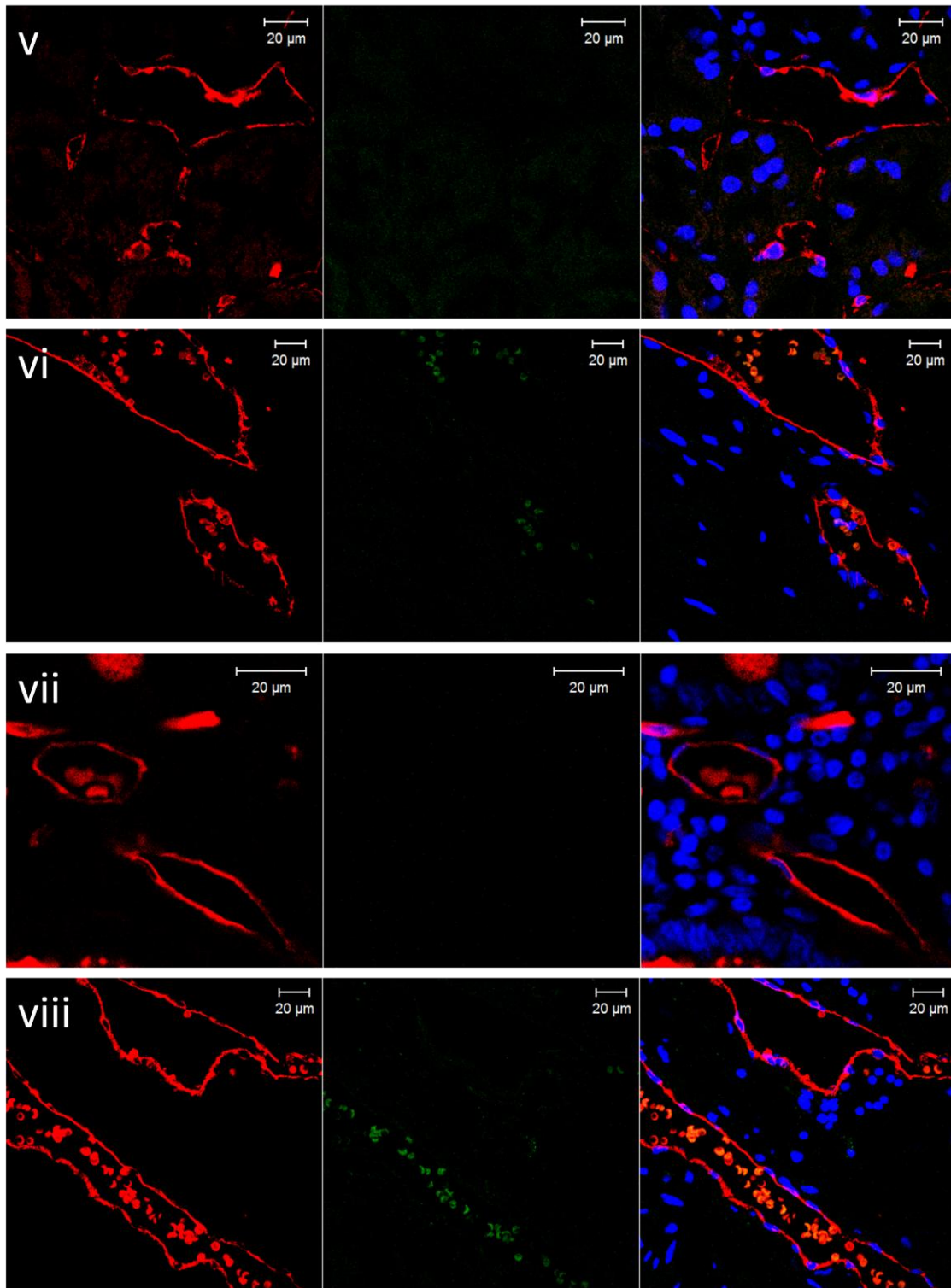


Figure 3.11b Confocal microscopy images (63X) of healthy tissues with GBP4 antibody. Endothelial cells were stained with rhodamine-conjugated *Ulex europaeus* lectin (Red). GBP4 antibody was labeled with a FITC conjugated secondary antibody (Green). Nuclei were stained with DAPI (Blue). (v) kidney (vi) bladder (vii) colon (viii) prostate

3.8 Validation of an IKBKE antibody by siRNA knockdown

Two IKBKE specific siRNA duplexes were transfected into HUVECs at a concentration of 10 nM. The efficiency of the knockdown was evaluated by western blotting of the cell lysate. Consistent with predicted molecular weight, IKBKE appeared at 75 kDa, which was weakly detectable in the siRNA knockdown lysates. The expression level of tubulin control remained the same (**Figure 3.12**). This experiment not only confirmed the efficiency of both siRNA duplexes but also validated the specificity of the commercial IKBKE antibody, which permitted expression profiling of clinical tissue.



Figure 3.12 SiRNA knock-down of IKBKE in HUVEC. Western blot of HUVECs with IKBKE knockdown shows that both siRNA duplexes worked efficiently. The level of tubulin expression was used as the protein loading control.

3.9 Immunofluorescence of IKBKE on tissue samples

To determine whether IKBKE is present in healthy tissues, a preliminary screen of IKBKE expression on multiple healthy samples was performed using the commercial IKBKE antibody (green). Rhodamine conjugated *Ulex* (red) was used as the positive control for endothelium.

The tissue screen showed that IKBKE has a widespread expression and is seen in most healthy tissues being particularly high in the ovary and in tissues involved in the immune system including lymph nodes and spleen. It is also present in vessel surrounding cells in healthy liver, colon and bladder. The expression of IKBKE is relatively rare in brain and heart (**Figure 3.13a-c**). The initial screen suggests that IKBKE is not a TEM due to its expression pattern in the healthy tissues.

We also performed immunofluorescence staining to investigate IKBKE expression in tumour sections including breast, rectal, bladder and endometrial carcinoma. The results showed that IKBKE is also expressed in the tumour cells. However IKBKE expression was found in endothelial cells from breast, bladder and endometrial carcinoma tissues when it was absent from the endothelium in healthy tissues (**Figure 3.14**).

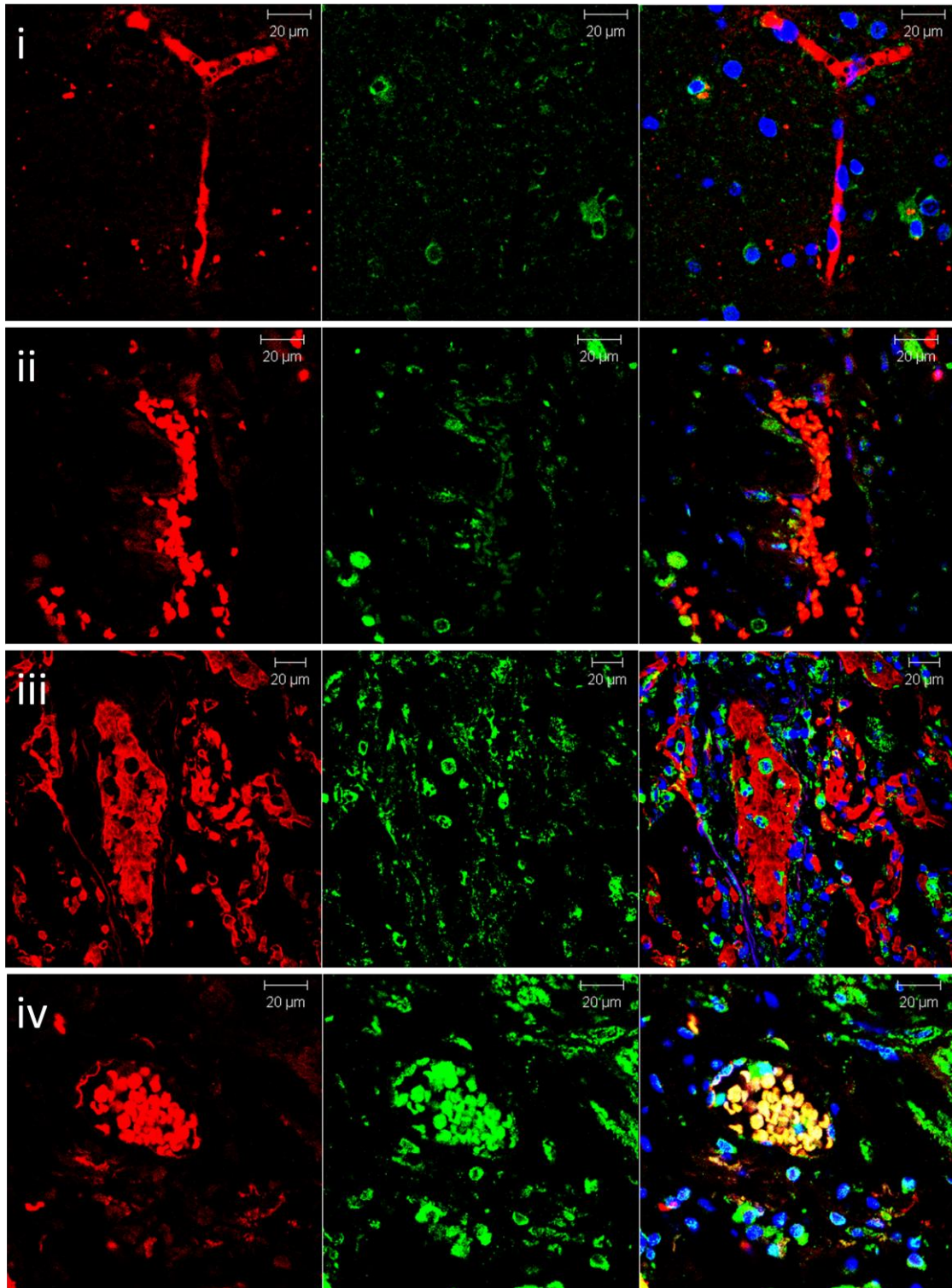


Figure 3.13a Confocal microscopy images (63X) of healthy tissues with IKBKE antibody. Endothelial cells were stained with rhodamine-conjugated *Ulex europaeus* lectin (Red). IKBKE antibody was labeled with a FITC conjugated secondary antibody (Green). Nuclei were stained with DAPI (Blue). (i) brain (ii) heart (iii) lung (iv) stomach.

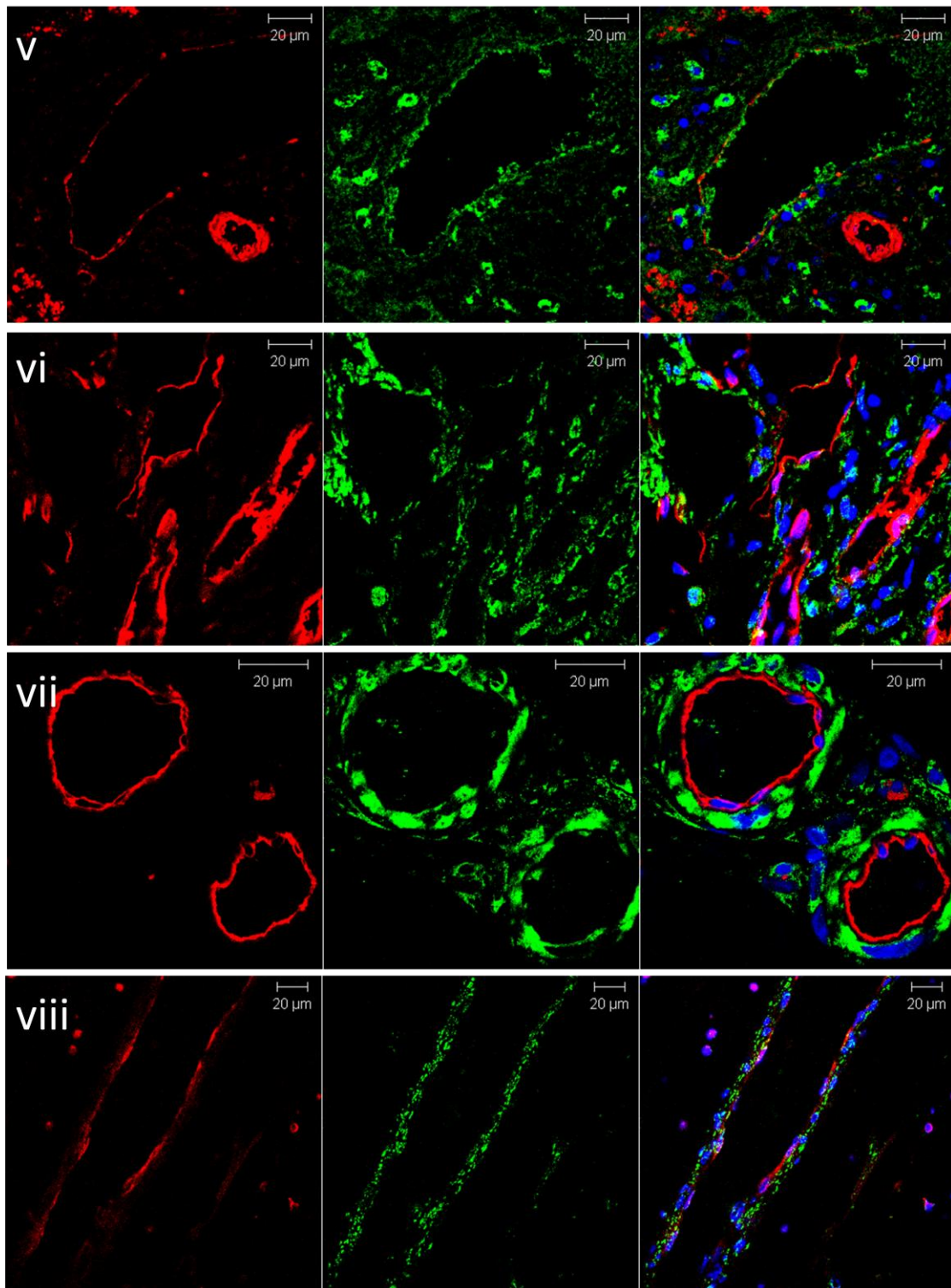


Figure 3.13b Confocal microscopy images (63X) of healthy tissues with IKBKE antibody. Endothelial cells were stained with rhodamine-conjugated *Ulex europaeus* lectin (Red). IKBKE antibody was labeled with a FITC conjugated secondary antibody (Green). Nuclei were stained with DAPI (Blue). (v) liver (vi) kidney (vii) colon (viii) bladder.

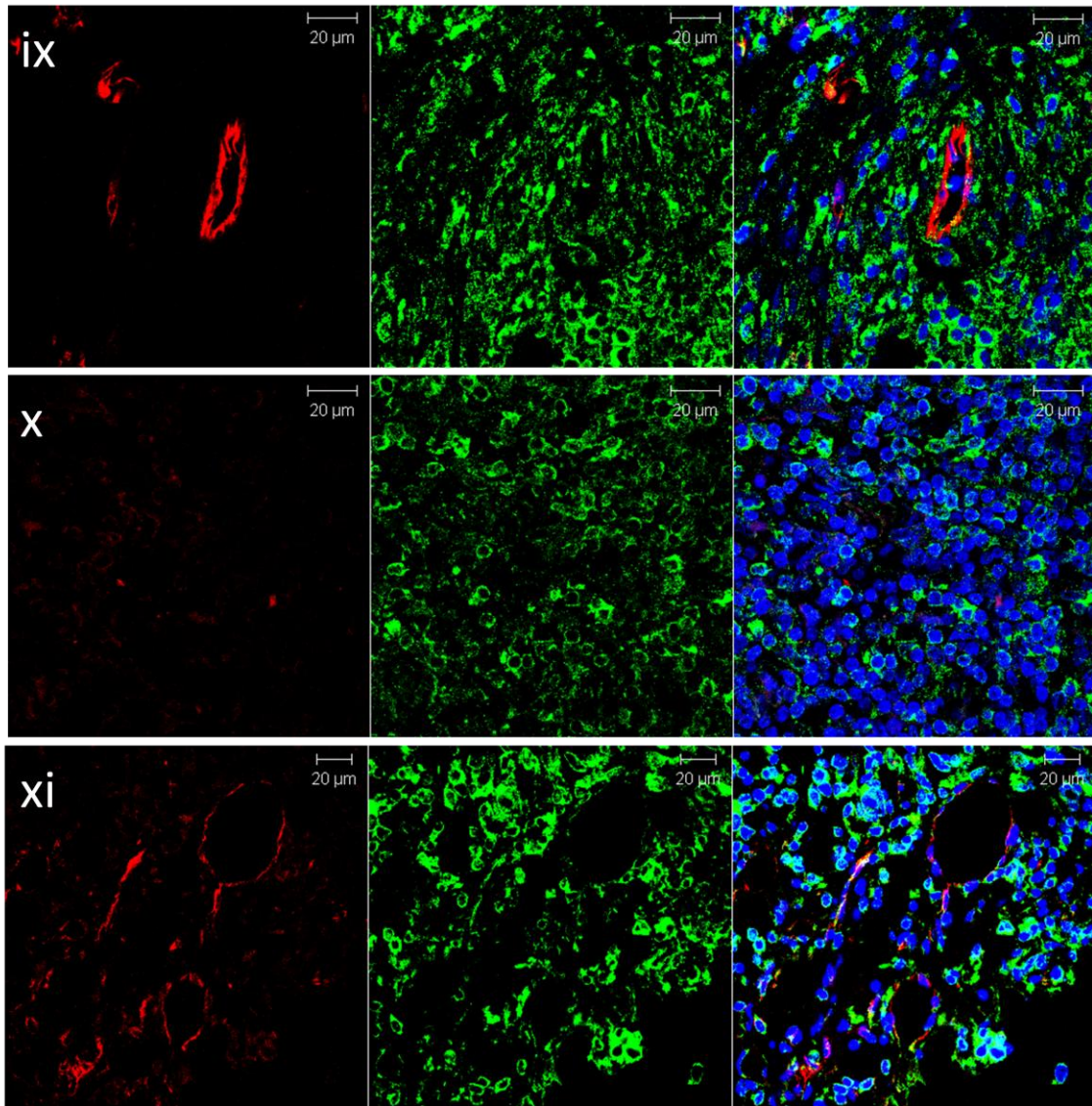


Figure 3.13c Confocal microscopy images (63X) of healthy tissues with IKBKE antibody. Endothelial cells were stained with rhodamine-conjugated *Ulex europaeus* lectin (Red). IKBKE antibody was labeled with a FITC conjugated secondary antibody (Green). Nuclei were stained with DAPI (Blue). (ix) lymph node (x) spleen (xi) ovary.

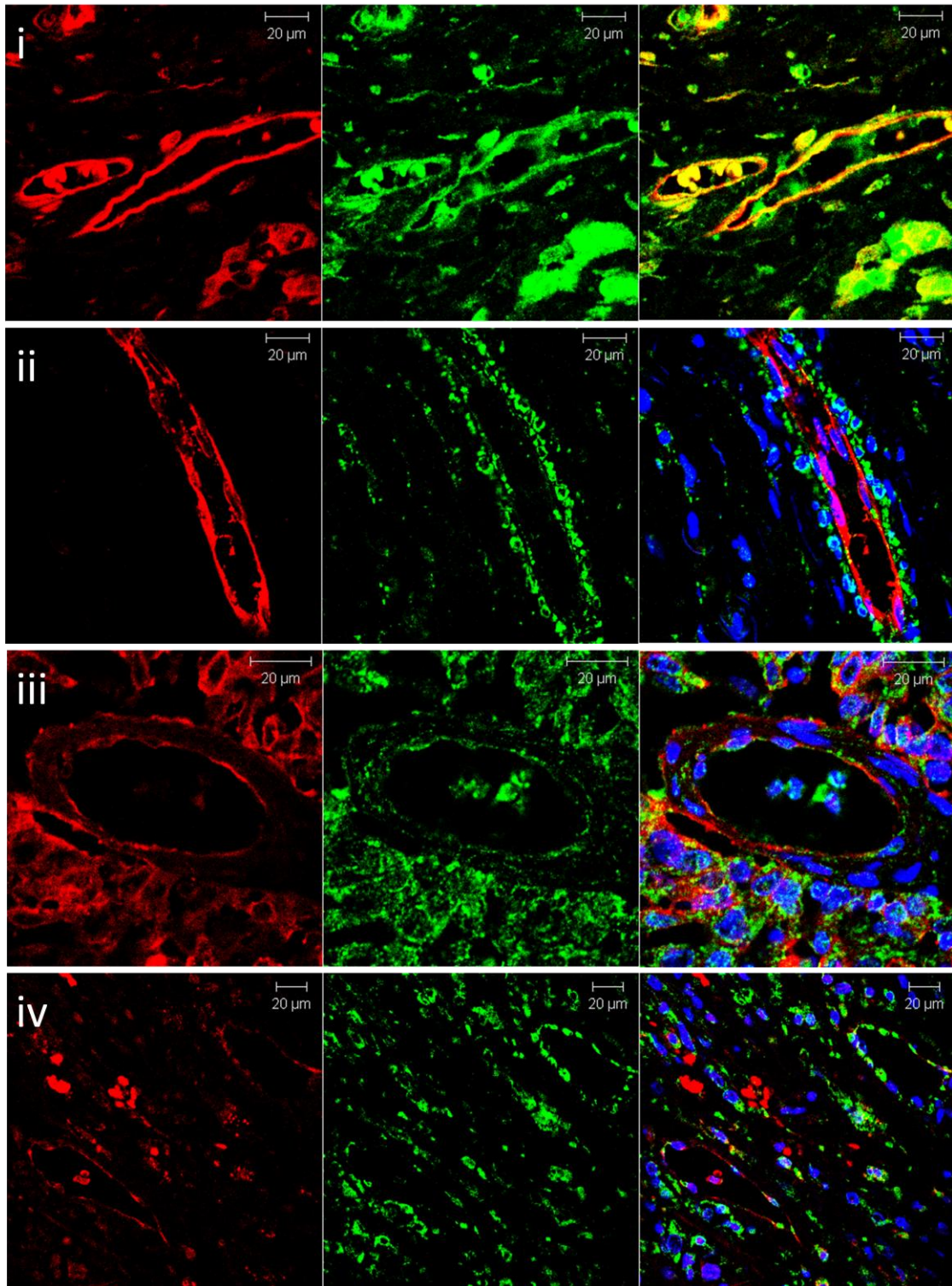


Figure 3.14 Confocal microscopy images (63X) of cancer tissues with IKBKE antibody. Endothelial cells were stained with rhodamine-conjugated *Ulex europaeus* lectin (Red). IKBKE antibody was labeled with a FITC conjugated secondary antibody (Green). Nuclei were stained with DAPI (Blue). (i) breast carcinoma (ii) rectal carcinoma (iii) bladder carcinoma (iv) endometrial carcinoma.

3.10 Conclusions

Three putative TEM's were validated using various techniques. CLEC14A was predominantly found in endothelial cells by qPCR analysis of primary cell isolates. Immunofluorescence and immunohistochemical staining of human cancer tissue arrays using CLEC14A antisera revealed a differential expression pattern in the tumour compared to healthy tissue. Across a wide range of common cancers, CLEC14A was strongly expressed on vessels in ovarian cancer (100%), liver cancer (100%), bladder cancer (90%), prostate cancer (90%), breast cancer (80%) and kidney cancer (70%) but completely absent from all non-cancer related healthy tissues. This data identifies CLEC14A as a novel TEM. Similar validation approaches performed on GBP4 showed a tumour-vessel preferential expression in most common cancers. There was some expression in adjacent healthy tissue but GBP4 was completely undetectable in non-cancer related healthy tissue, indicating potential as a tumour vascular target. IKBKE has been ruled out as a TEM in this study, based on its widespread expression in healthy human tissues. Nevertheless, it is worth noting that IKBKE is found on the endothelium in breast and bladder cancer.

Chapter four

Functional characterization of CLEC14A

4.1 Introduction

Validation of putative TEM expression in human cancer and healthy tissue confirmed CLEC14A as a novel TEM. Past evidence suggested that endothelial specific genes are often functionally involved in endothelial biology and angiogenesis [103, 157]. This chapter explores the function of CLEC14A in endothelial biology, particularly its role in endothelial cell migration, which is a critical step engaged in tumour angiogenesis [16].

In vitro angiogenesis assays are important tools for understanding the molecular mechanisms and identifying new regulators of the angiogenesis cascade [158]. The most widely used *in vitro* assays involve working with cultured endothelial cells, in most cases HUVEC, in systems mimicking each step of the angiogenesis process such as migration, proliferation and tube formation. The scratch wound assay is a well established approach to investigate endothelial cell migration *in vitro*. The assay involves making a ‘wound’ in a confluent cell monolayer and subsequently monitoring the closure of the wound by migrating cells at different time points. This method has been widely used with siRNA knockdown technology to investigate the function of genes in cell migration [159].

The possibility of using CLEC14A antibodies to block endothelial migration is also investigated in this chapter. To further characterize CLEC14A’s role in physiological angiogenesis and tumour angiogenesis, CLEC14A knockout mice were generated.

4.2 CLEC14A knockdown inhibits endothelial cell migration

To investigate whether CLEC14A plays a role in endothelial cell migration, a scratch wound assay was performed on HUVEC after CLEC14A knockdown by siRNA. Reagent only (Mock) and negative duplex (Scrambled) were employed as controls. The effect of CLEC14A knockdown on closure of a scratch wound in a confluent HUVEC monolayer was measured at 0, 6 and 12 hours after injury. At the end of the assay, cells were collected to confirm the knockdown of CLEC14A lasted to the end of the assay.

Figure 4.1a shows representative images of the wound area at each time point for mock, scrambled, D1 and D2 treated cells. Cells treated with mock or control siRNA had fully closed the wound at 12 hours while 50 - 60% of the wound area remained open in the CLEC14A knockdown cells (**Figure 4.1b**). Western blot analysis was performed on the cell lysates at the end of the scratch wound assay (**Figure 4.1c**). This confirmed that CLEC14A was knocked down during the assay. The results suggest that CLEC14A may play a role in endothelial cell migration.

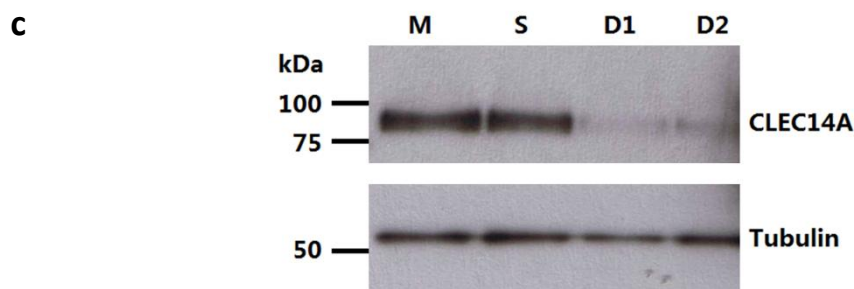
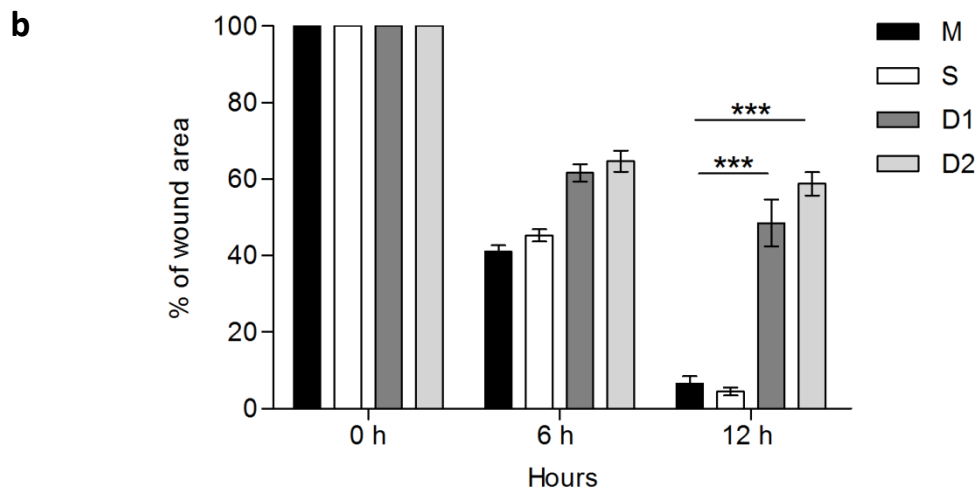
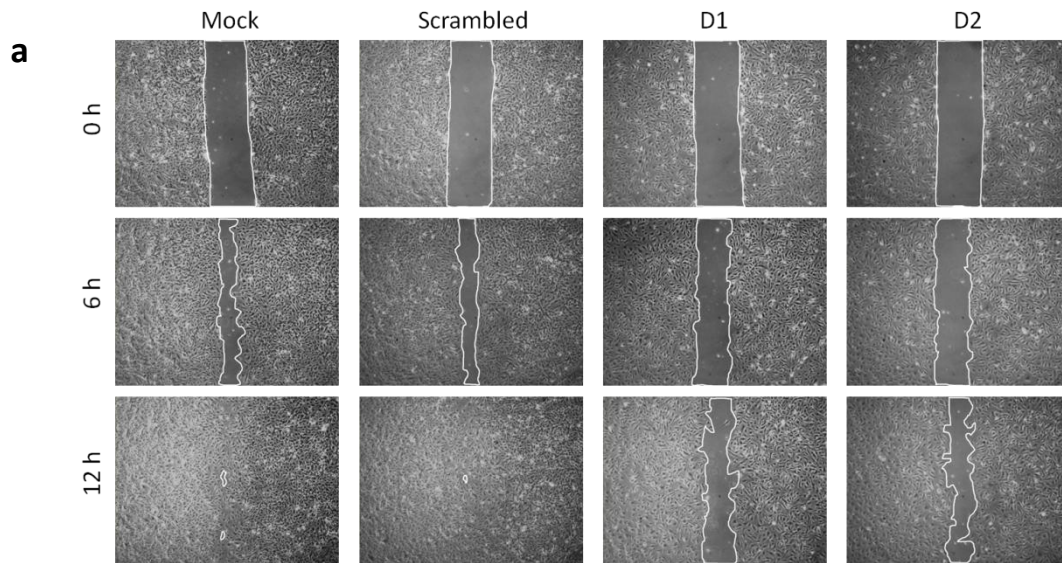


Figure 4.1 siRNA knockdown of CLEC14A inhibits endothelial cell migration. Scratch wound healing assay in a HUVEC monolayer transfected with mock, scrambled, CLEC14A siRNA duplex 1 or duplex 2. **(a)** Images at 0, 12 and 24 hour time points were acquired after wounding. The open wound area was highlighted and quantified using ImageJ software. **(b)** Values represent the means from three independent experiments. Error bars depict the standard error of the mean (Two-way ANOVA, $P < 0.001$). **(c)** CLEC14A knockdown was confirmed by western blotting the cell lysates at the end of the assay.

4.3 Polyclonal antisera to CLEC14A inhibits endothelial cell migration

To investigate whether commercial CLEC14A polyclonal antisera had an effect on endothelial cell migration, antisera at 5, 10 or 20 $\mu\text{g/ml}$ was added to HUVEC cells immediately after wounding. The closure of the wound area of each treatment was then recorded at 0, 12 and 24 hours.

Figure 4.2a shows the delay in wound closure in cells treated with 5, 10 or 20 $\mu\text{g/ml}$ of CLEC14A antibody compared with the untreated cells. Quantification of the remaining area relative to the initial wound showed that 14% of the wound area remained open after 24 hour when HUVECs were treated with 10 or 20 $\mu\text{g/ml}$ of anti-CLEC14A antisera. Controls had almost closed (**Figure 4.2b**). This result suggests that there may be an epitope in CLEC14A that mediates the cell motility that is blocked by polyclonal antibody. If so, it could be possible to generate a monoclonal antibody to CLEC14A that specifically inhibits endothelial cell migration.

The effect of antisera on HUVEC tube formation was examined in the Matrigel assay by colleagues. The formation of the tube-like structures was impaired when cells were treated with 10 $\mu\text{g/ml}$ [109]. This suggests a role for CLEC14A in the process of tube formation.

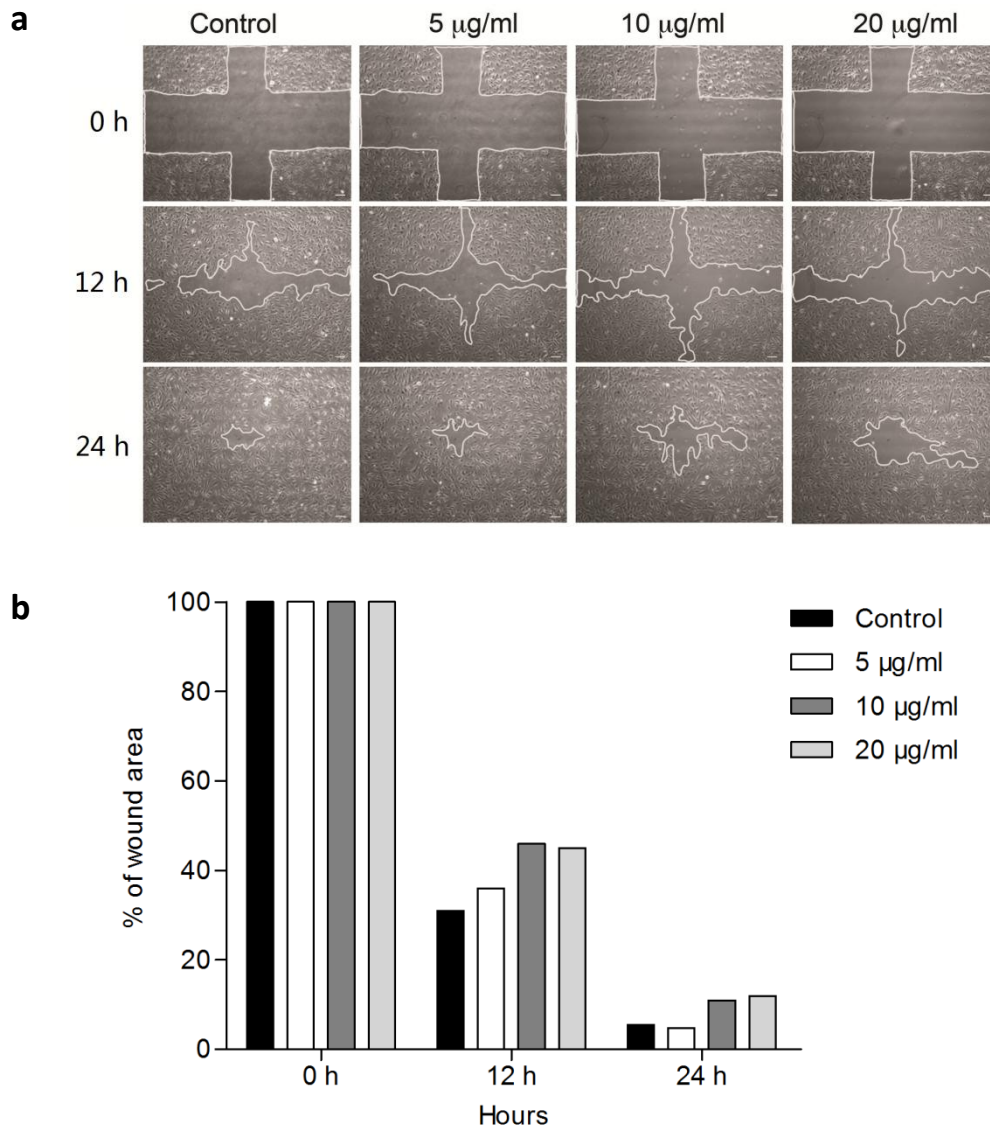


Figure 4.2 CLEC14A polyclonal antisera inhibits cell migration. Scratch wound healing assay in HUVECs, showing a retardation of wound closure in the presence of 5, 10 and 20 µg/ml of CLEC14A polyclonal antisera. Pictures were taken at 0, 12 and 22 h post wounding. (n = 2). Due to the cost of the antisera, replication of this data was prohibited.

4.4 Production of human and mouse CLEC14A protein using lentivirus

Given the inhibitory effects on endothelial migration and tube formation by the commercial CLEC14A polyclonal antiesra, a monoclonal antibody to both human and mouse CLEC14A that has the same function would be of therapeutic interest. Pure CLEC14A protein was required for mouse immunization. Mouse CLEC14A protein was used to immunize mice while the human protein was for the screening.

To express these proteins, the extracellular domain of human or mouse CLEC14A-Fc was inserted into a lentivector (pWPI) which contains a separate GFP expressed from an IRES site. GFP facilitated FACs sorting of the infected cells. The lentivector was transfected with an envelope plasmid and a packaging plasmid into 293T cells for viral production. The supernatant containing the virus was then added to fresh 293T cells following a FACs sorting procedure for a positive selection of GFP expressing cells. A pure population of 293T cells stably expressing human or mouse CLEC14A-Fc was obtained. The recombinant protein was secreted into low serum media and purified by pH gradient (pH 7 to pH 3) elution from a protein A column. Each eluted protein fraction was collected and quantified on a Nanodrop machine at 280 nm (**Figure 4.3a**). The purity of the protein was confirmed by coomassie staining (**Figure 4.3b**). Since the extracellular domain of mouse CLEC14A was predicted to be 85 kDa and human Fc tag was 25 kDa, the band running at 110 kDa is recombinant mouse CLEC14A-Fc protein. The recombinant human CLEC14A-Fc protein was also

purified following the same procedure. To further confirm the purified product, western blot analysis was performed using in house rabbit anti human and mouse CLEC14A antisera and a commercial anti human Fc antibody (**Figure 4.4**).

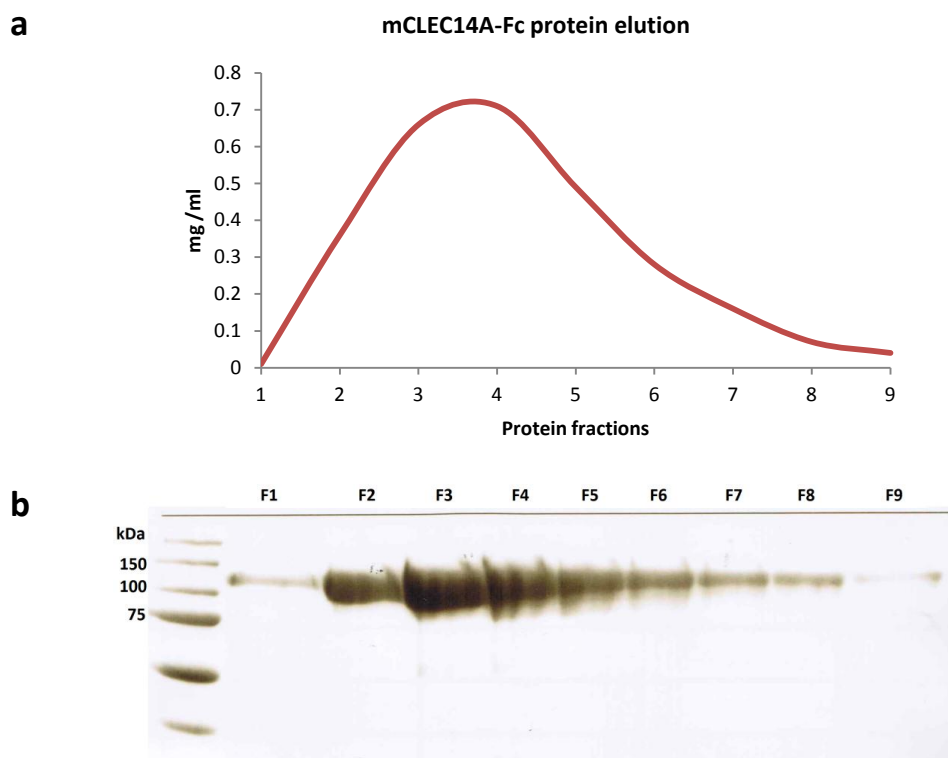


Figure 4.3 Purification of mouse CLEC14A-Fc protein. (a) Elution of protein was performed by pH gradient and the concentration of each fraction was quantified by Nanodrop at 280 nm. (b) The purity of each fraction was confirmed by running the samples on a SDS PAGE followed by coomassie staining.

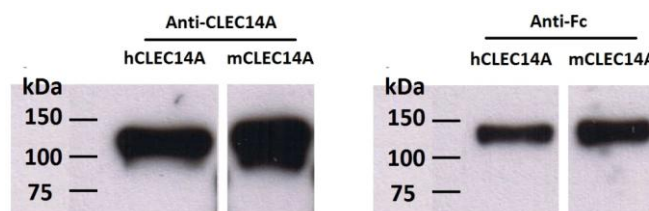


Figure 4.4 Western blot of purified human and mouse CLEC14A-Fc protein. The purified protein fractions were pooled and run on a SDS gel following a western blot against in house rabbit anti mouse CLEC14A antisera. The purified CLEC14A protein was detected between 100 kDa and 150 kDa.

4.5 Generation of monoclonal antibodies to both human and mouse CLEC14A

Monoclonal antibodies to CLEC14A were generated by Serotec (Oxford, UK). The aim was to produce monoclonal antibodies that recognize both human and mouse CLEC14A-Fc, which can then be used in functional assays with human or mouse endothelial cells. Purified mouse CLEC14A-Fc protein was used in the immunization. Human and mouse CLEC14-Fc protein and a commercial purified human Fc fragment were used in the screening process to identify the monoclonal antibodies that recognize both human and mouse CLEC14A and not the human Fc tag. Five monoclonal antibodies were identified following affinity purification (**Table 1**).

Code	Concentration	Isotype	Buffer
CRT1	5.2 mg/ml	IgG1	PBS
CRT2	5.8 mg/ml	IgG1	PBS
CRT3	6.1 mg/ml	IgG1	PBS
CRT4	7.7 mg/ml	IgG1	PBS
CRT5	6.7 mg/ml	IgG1	PBS

Table 1 Monoclonal antibodies to human and mouse CLEC14A.

4.6 Papain cleavage of CLEC14A-Fc protein and Fc fragment depletion

To confirm reactivity of the monoclonal antibodies to human and mouse CLEC14A and not the Fc tag, an ELISA assay with CLEC14A minus the Fc tag was required. The protease papain has been used to cleave the Fc region of antibodies to release a Fab fragment and was used to cleave the Fc tag off recombinant CLEC14A-Fc protein (**Figure 4.5**).

Optimization of the papain digestion reaction was performed on Fc tagged Robo4 protein described in **Chapter five, 5.1**. Using this protocol, papain reaction mix was added to human or mouse CLEC14A-Fc protein followed by an Fc fragment depletion using protein G beads. Digestion was followed by western blotting for CLEC14A or Fc.

Multiple bands were seen in both papain cleaved human and mouse CLEC14A **Figure 4.5 (left)**. CLEC14A minus Fc is seen at 80 kDa. Other bands at 60 and 37 kDa were further breakdown products. Western blot for Fc showed it had all been removed by the beads (**Figure 4.5, right**). As the purpose of this experiment is to release the Fc tag from CLEC14A, the mixture of CLEC14A protein fractions should not affect the downstream ELISA screening assay.

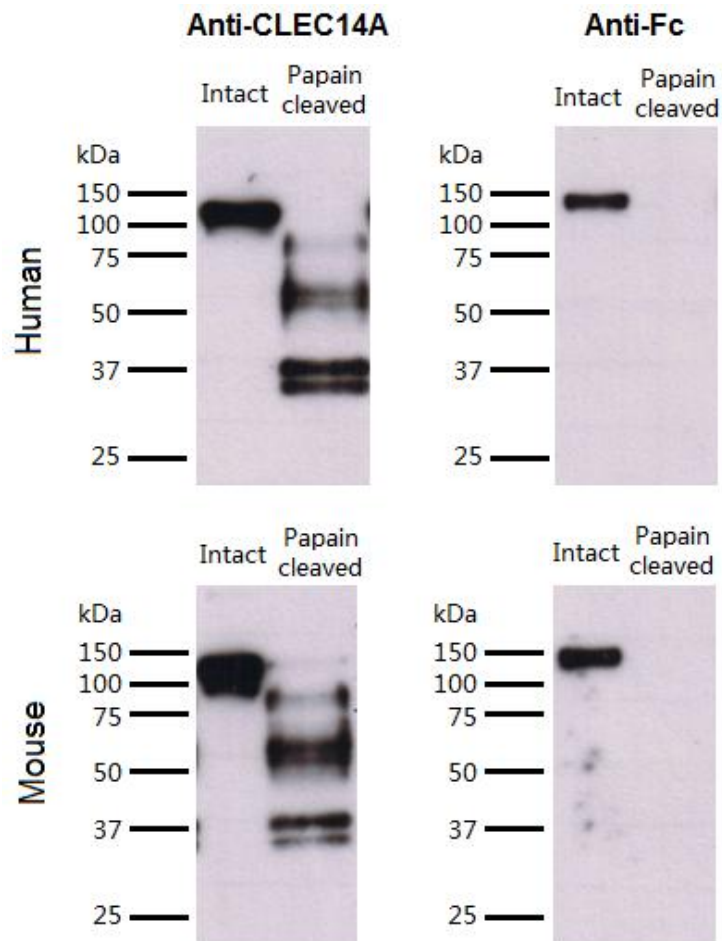


Figure 4.5 Papain cleavage of human/mouse CLEC14A-Fc following Fc fragment depletion. Recombinant human and mouse CLEC14-Fc protein were digested in a papain reaction. The cleaved Fc fragments were depleted by protein G beads. The final protein stocks were run on an SDS gel followed by a western blot using homemade rabbit anti mouse CLEC14A antibody (left) or a commercial anti human Fc antibody (right).

4.7 Evaluation of the CLEC14A monoclonal antibodies

An ELISA assay was designed to evaluate the specificity of the CLEC14A monoclonal antibodies. Human or mouse CLEC14A protein was coated onto ELISA plates. CLEC14A monoclonal antibodies were diluted 1 in 500 (10 µg/ml) and added to the coated wells. Homemade rabbit antisera to both mouse and human CLEC14A was used as the positive control for the coated antigens. PBS or rabbit pre-bleed was used as negative controls for the monoclonal antibodies and anti sera respectively.

As shown in **Figure 4.6**, all monoclonal antibodies recognized both human and mouse CLEC14A. In general, higher absorbance was observed for human CLEC14A coated wells compared to wells coated with the mouse CLEC14A protein. This was probably due to the variable concentrations of the two coating antigens. There is also a possibility that the monoclonal antibodies had higher affinity to human CLEC14A than mouse CLEC14A. This data confirms that these monoclonal antibodies recognize both human and mouse CLEC14A.

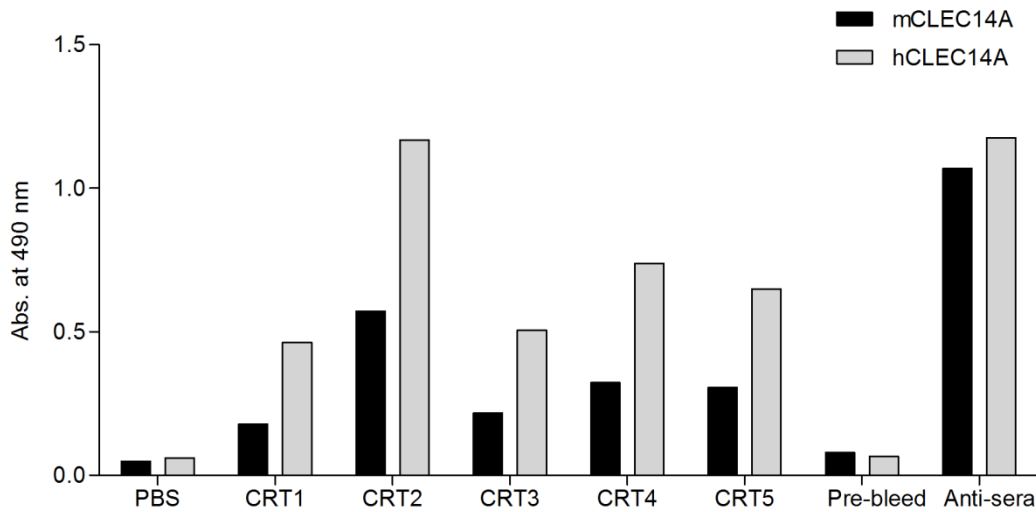


Figure 4.6 Confirmation of the specificity of monoclonal antibodies to human and mouse CLEC14A protein. An ELISA assay was performed in human or mouse CLEC14A protein coated wells by applying each CLEC14A monoclonal antibody into the assay. PBS and rabbit pre-bleed was used as the negative control for the monoclonal antibodies and the positive anti-sera.

4.8 Monoclonal antibody to CLEC14A inhibits endothelial cell migration

Given the inhibitory effect of the commercial CLEC14A antisera on endothelial migration, a monoclonal antibody which can functionally block endothelial cell motility holds therapeutic potential. The five CLEC14A monoclonal antibodies were screened to determine whether they inhibited endothelial cell migration using a HUVEC scratch wound assay.

1 µg/ml or 10 µg/ml of each monoclonal antibody was added to the assay. PBS containing 0.09% sodium azide was used as control treatment. Wound areas for each condition were captured at 0, 4 and 12 hours after injury. Among these five monoclonal antibodies, only CRT3 showed a significant delay of the wound closure in a dosage dependent manner ($P < 0.05$). Other monoclonal antibodies failed to show any effect in this assay.

Images of the effect on wound closure by CRT3 monoclonal antibody are shown in **Figure 4.7a**. After 12 hours, 25% and 15% of the original wound remained open when cells were treated with 10 µg/ml and 1 µg/ml of CRT3 respectively compared to the control (**Figure 4.7b**). Although the inhibitory effect was not dramatic, a statistical significance was observed in a dosage dependent manner. The cross reactivity between human and mouse would also allow future assessments of this particular CLEC14A monoclonal antibody in other HUVEC based *in vitro* assays or *in vivo*

angiogenesis models in mice.

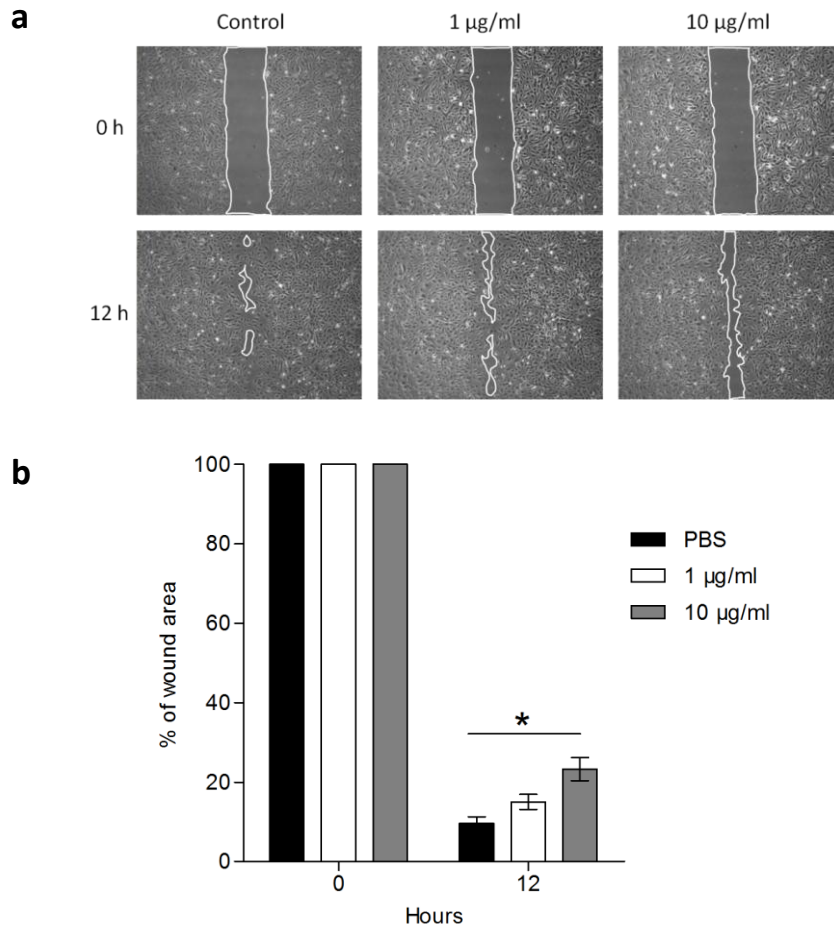


Figure 4.7 A monoclonal antibody to CLEC14A inhibits endothelial cell migration. Scratch wound healing assay in HUVECs, showing a retardation of wound closure in the presence of 1 and 10 µg/ml of CLEC14A monoclonal antibody (CRT3). Images were taken at 0 and 12 h post wounding. Values represent the means from three independent experiments. Error bars depict the standard error of the mean (Two-way ANOVA, $P < 0.05$).

4.9 Overexpression of CLEC14A in HUVEC using a lentiviral system

Given that CLEC14A knockdown and antisera treatment inhibited endothelial cell migration, we further explored how overexpression of this protein would affect endothelial cell motility. The lentiviral expression system was used to achieve stable overexpression of CLEC14A in HUVECs.

Full length human CLEC14A was constructed into a lentivector (pWPI) which contains independent GFP driven by an IRES site. Production of the virus from 293T cells was performed as described previously. HUVECs were then transduced with this lentivirus following a positive FACs sorting procedure for GFP to obtain a pure population of CLEC14A overexpressing HUVECs. Western blot was performed on the HUVEC lysates to confirm the overexpression (**Figure 4.8**). Tubulin staining confirmed equal protein loading.

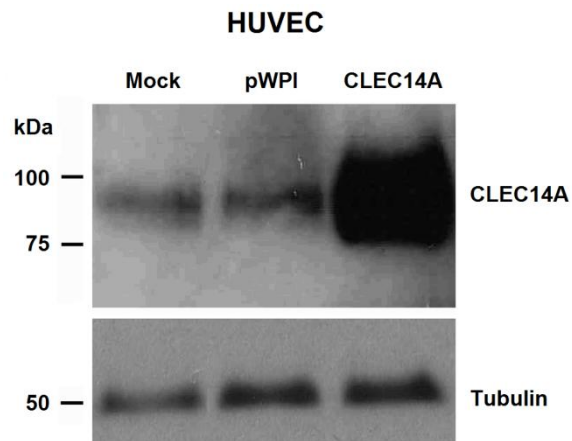


Figure 4.8 Western blot of CLEC14A transfected cells. HUVECs were transduced with lentivector containing full length human CLEC14A and IRES linked GFP. Cells were FACS sorted and then analyzed by Western blot against CLEC14A antibody. Tubulin, at 50 kDa, was employed as the loading control for the lysates.

4.10 Overexpression of CLEC14A inhibits HUVEC migration

To assess whether overexpression of CLEC14A has an effect on endothelial cell migration, FACs sorted HUVECs overexpressing CLEC14A were used in a scratch wound assay. The uninfected or solely GFP infected HUVECs were used as negative controls. Images of the wound area were captured at 0, 4, 8 and 12 hour and the open wound area was quantified using ImageJ software.

A significant delay in the wound closure was observed in the CLEC14A overexpressing cells compared to the control cells (**Figure 4.9**). Thus, overexpression of CLEC14A phenocopied the effect caused by CLEC14A knockdown. Migration is clearly sensitive to the precise level of CLEC14A in the cell.

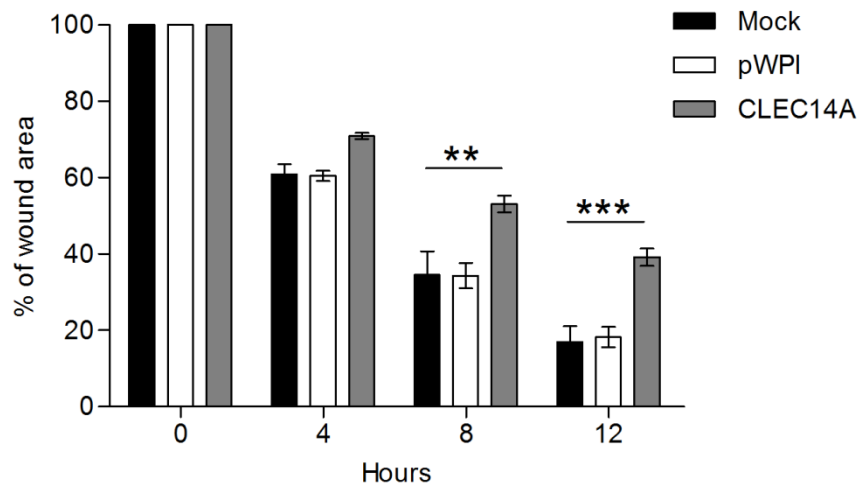
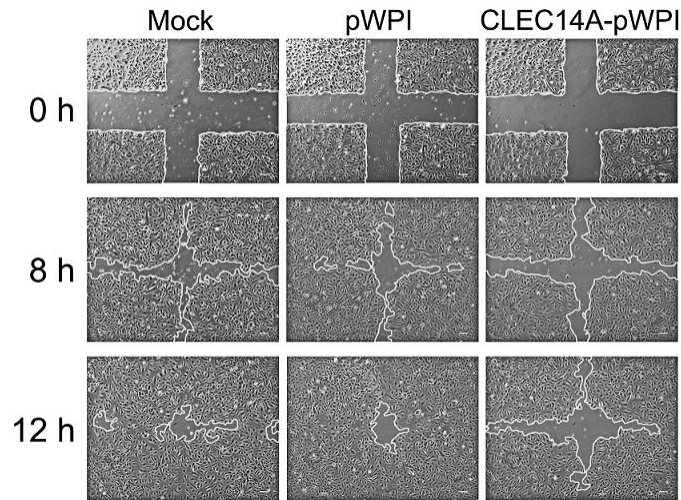


Figure 4.9 Overexpression of CLEC14A inhibits cell migration. Scratch wound healing assay in HUVECs, showing a retardation of wound closure in the CLEC14A overexpressing cells. Images were taken at 0, 4, 8 and 12 hours post wounding. Values represent the means from three independent experiments. Error bars depict the standard error of the mean (Two-way ANOVA, $P < 0.001$ at 8 h, $P < 0.001$ at 12 h).

4.11 Generation of germline transmission mice carrying a CLEC14A knockout allele

In vitro functional assays have shown that CLEC14A plays a role in endothelial cell migration and tube formation. The inhibitory effect of CLEC14A monoclonal antibodies on endothelial cell migration indicates a possible therapeutic potential for anti-vascular or anti-angiogenesis treatment. It is important to determine the function of CLEC14A *in vivo* to further understand its role in development and physiological and pathological angiogenesis.

Targeted vector transfected embryonic stem cells [160] were purchased and injected into the inner cell mass of blastocysts which was then implanted into pseudopregnant C57BL/6 mice. 22 Chimeric mice were born and mated to Albino mice for germline transmission screening. Chimera No.15 showed germline transmission by offspring color recognition (**Figure 4.10**). Chimera No.15 was then used to generate heterozygous offspring on a C57BL/6 background.



Figure 4.10 Chimera No.15 was identified carrying CLEC14A KO in the germline cells.

4.12 Generation of CLEC14A knockout mice

Chimera No.15 was crossed with wild type C57BL/6 mice to generate heterozygous mice. Three pairs of CLEC14A heterozygous crossings were set up to generate complete knockout offspring. Two sets of primers were optimized to genotype the genomic DNA isolated from ear clips of the offspring (**Figure 4.11**). The resulting offspring were born in the expected Mendelian ratios (**Table 2**)

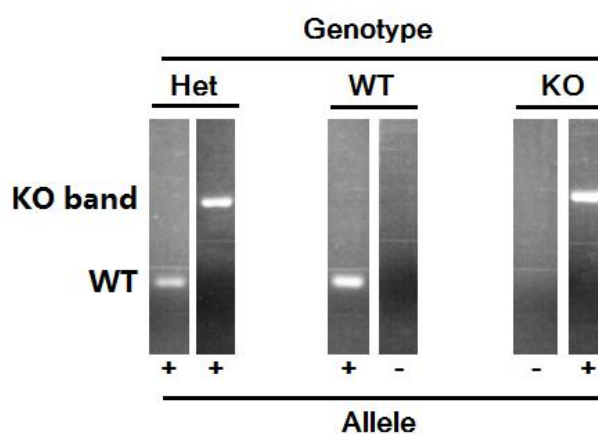


Figure 4.11 PCR on wild type and crossed arm of target vector and CLEC14A in wild type, CLEC14A heterozygous and KO mice. Ear clips were collected for genomic DNA isolation. Genotyping was performed using an internal CLEC14A primer set and a crossed neomycin and downstream arm of CLEC14A primer set which generated a 200 bp and 404 bp fragment respectively.

Genotype	Mice generated	Mendelian genetics prediction
+/+	24%, 18	25%, 18.75
+/-	48%, 36	50%, 37.5
-/-	28%, 21	25%, 18.75

Table 2 Number of offspring of each genotype from CLEC14A heterozygous parents. The ratio of each group was in line with the Mendelian genetics prediction (n = 75).

4.13 Confirmation of CLEC14A knockout in mice at the protein level

Organs including brain, heart, lung, liver, spleen, kidney and colon from wild type and CLEC14A KO mice were snap-frozen in liquid nitrogen. Each organ was lysed and analyzed by western blot using rabbit anti mouse CLEC14A anti sera. A band detected at 30 kDa was due to non specific binding of the anti serum and it was used as the loading control. As shown in **Figure 4.13**, CLEC14A runs between 75 and 100 kDa. This was detected in lung and weakly in kidney from the wild type C57BL/6 mice while the protein was completely absent in the CLEC14A KO mice. Endothelial specific genes are most easily detected in the lung where 30% of the cells are endothelial compared to the 1 – 3% in most tissues. No obvious developmental defect was observed in all CLEC14A KO mice. These mice are fertile and remain healthy throughout their adult life.

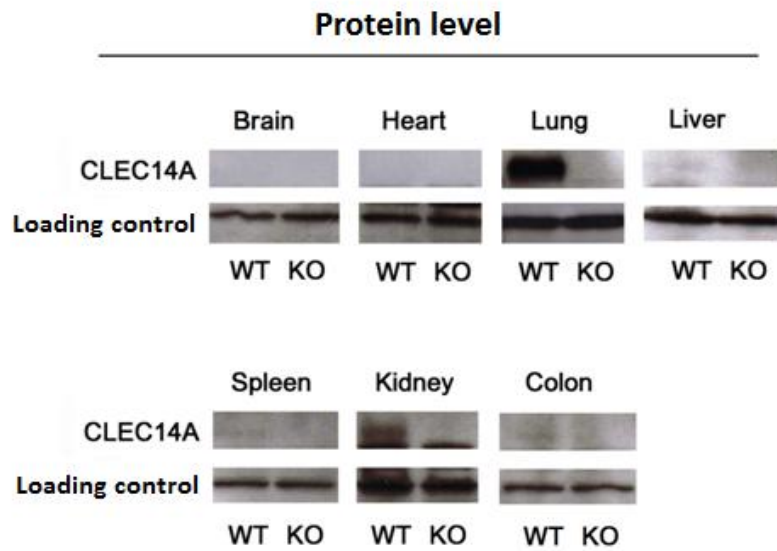


Figure 4.12 Confirmation of CLEC14A KO at the protein level. Organs including brain, heart, lung, liver, spleen, kidney and colon were collected from wild type and CLEC14A KO mice. Each organ was lysed in protein lysis buffer. The lysates were run on an SDS gel following a western blot probed with homemade rabbit anti mouse CLEC14A antisera

4.14 Conclusions

To begin to understand the role of CLEC14A in endothelial biology and angiogenesis, this chapter describes a preliminary functional characterization. Endothelial cell migration was the focus of the study. Silencing of CLEC14A in HUVEC using siRNA technology showed an inhibitory effect on endothelial migration, suggesting a pro-angiogenic role of CLEC14A. Unexpectedly, overexpression of CLEC14A in endothelial cells resulted in the same effect, indicating that a fine tuning of CLEC14A expression is critical for endothelial cell function. Furthermore, an identical inhibitory effect on migration was observed when HUVEC were treated with polyclonal CLEC14A antisera, which prompted the idea of generating monoclonal antibodies that may also be inhibitory to endothelial migration. Five monoclonal antibodies to CLEC14A were produced and indeed one of them (CRT3) phenocopied the polyclonal antisera. To address the *in vivo* role of CLEC14A, a knockout mouse was generated. CLEC14A KO mice are fertile, showing no developmental defect and remained healthy throughout their lifetime. Others in the group have investigated tumour growth in CLEC14A KO mice. Regulation of CLEC14A expression in tumour vessels was also investigated. The outcomes will be discussed in the last chapter.

Chapter five

Identification of TEMs in lung cancer

5.1 Introduction

Lung cancer remains difficult to treat largely due to the lack of a well-defined target. Here we attempt to identify novel TEMs in lung cancer using 2nd generation sequencing technology.

To profile the differential gene expression between normal and tumour lung vasculature, endothelial cells need to be isolated from whole tissue. To this end, two independent approaches were investigated (**Figure 5.1**).

Laser microdissection was specially designed for acquiring a pure cell population from heterogeneous tissue samples. The advantage of this approach was that it can precisely dissect and collect the desired tissue at a cellular level. The technology was chosen to dissect endothelial cells from blood vessels of frozen lung slides. In addition, such technology is meant to be particularly useful due to its accuracy because endothelium accounts for only a minor proportion of the whole tissue. Laser microdissection normally yields a small amount of RNA allowing downstream work such as qPCR and microarray.

The magnetic bead isolation approach is performed on fresh tissue from surgery. A major benefit of this approach is that the RNA integrity is secured and the yield is greater. Thus, the bead isolation approach not only permits downstream gene profiling work involving microarray but also allows 2nd generation sequencing, with which

laser microdissection is not compatible (**Figure 5.1**).

Although both approaches have been used in isolating endothelium from several tumour types, the attempt to do so in lung cancer has not yet been reported and remained a challenge.

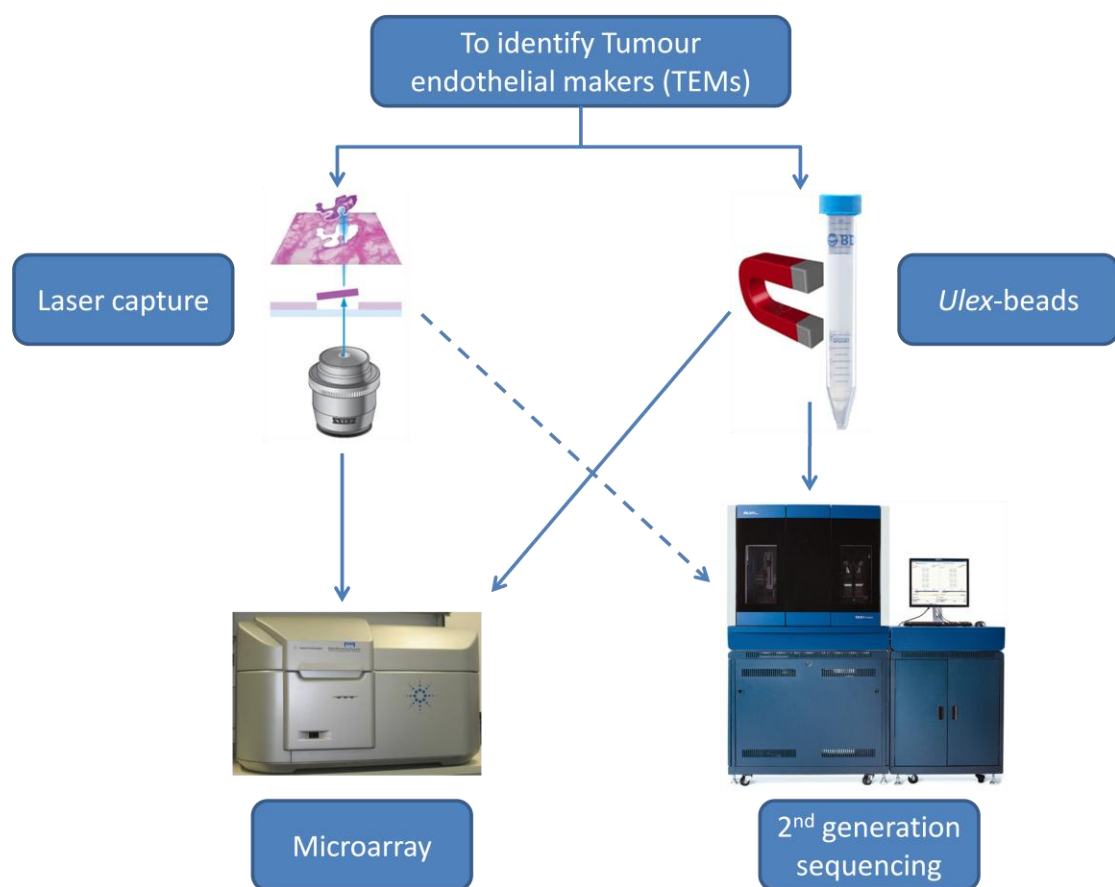


Figure 5.1 Scheme of strategies to identify TEMs in lung cancer. Two strategies were used to enrich the endothelial population from normal and tumour lung tissue. The laser capture microdissection technique was used to isolate vessels from frozen sections for microarray, but not for 2nd generation sequencing due to the limited yield of RNA. The bead isolation performed on fresh lung tissue would permit both microarray and 2nd generation sequencing due to a greater yield of RNA.

5.2 Laser microdissection approach

5.2.1 Comparison of staining methods to visualize vessels and preserve RNA integrity

To obtain quality RNA from endothelium using laser microdissection, there exists a major technical challenge, namely, visualizing the blood vessels while preserving RNA quality. To this end, two staining methods (i) Cresyl violet and (ii) immunohistochemistry for the endothelial marker CD31 were tested on frozen lung tumour sections.

Cresyl violet is a basic dye that stains the negatively charged nucleus and is often used for visualization of malignant cells and revealing basic tissue morphology [161]. Although its rapid staining protocol preserves the RNA quality, whether the cresyl violet method would help visualizing vessels in lung is not clear. CD31 is a well-validated endothelial marker and the monoclonal antibody (JC70, Dako) has been long-known to label endothelium. However the immunostaining procedure involves multiple washing and incubation steps and may result in RNA degradation. Thus RNA integrity number (RIN) derived from the Bioanalyzer was used to assess the quality of RNA extracted from slides stained by both methods. A RIN above 7 was taken as high enough quality to permit downstream applications [162, 163].

Frozen lung tumour slides were stained with cresyl violet or CD31 immunohistochemistry. RNA integrity was then analysed on a Bioanalyzer. As shown

in **Figure 5.2 left**, although the RIN was well preserved (RIN = 8.8), Cresyl violet staining failed to highlight the blood vessels in the tissue, making it impossible to distinguish blood vessels from small bronchial tubes (**Figure 5.2 left, white arrows**). On the other hand, immunohistochemistry of CD31 clearly delineated the endothelium within the tumour however significant degradation of RNA was observed after the staining process (RIN = 5), (**Figure 5.2, right**). This probably arose from multiple incubation and washing steps where the tissue was exposed to aqueous solutions that reactivate endogenous nucleases. Thus, neither method could achieve the vessel visualization and RNA preservation at the same time.

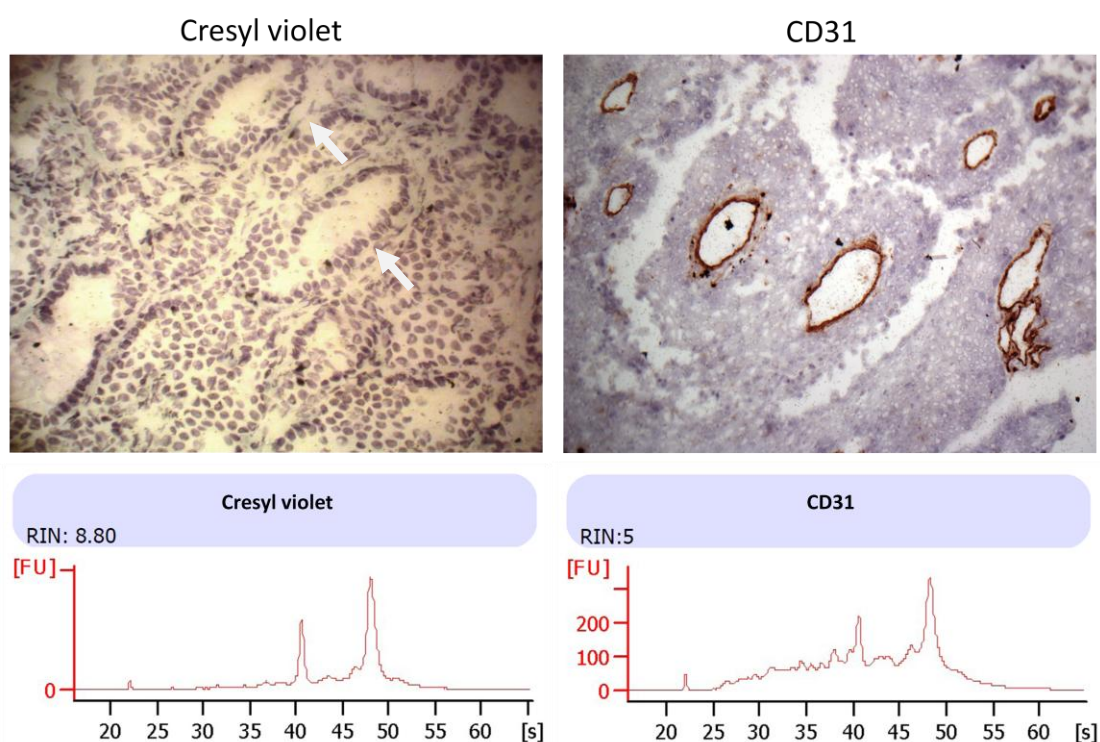


Figure 5.2 Comparison of Cresyl violet and CD31 staining in the use of vessel dissection and RNA preservation. Cresyl violet or CD31 immunohistochemistry staining was performed on frozen lung tumour tissue. After staining, RNA was extracted from the whole tissue section and RNA integrity determined on a Bioanalyzer.

5.2.2 Mapping strategy, the combination of two staining methods

A combined strategy was developed to overcome the drawbacks of each staining method. Firstly, one slide was immune stained with CD31 antibody to highlight the blood vessels and this slide was used as a ‘map’. Secondly, the adjacent two slides derived from either side of the ‘map’ were cresyl violet stained. Cresyl violet staining revealed a basic tissue morphology which facilitated the reorientation according to the ‘map’. Eventually, the vessels that need to be laser dissected were selected on the CD31 stained ‘map’ and the laser microdissection was carried out on adjacent cresyl violet stained slides (**Figure 5.3a**). Total RNA was then isolated from the dissected samples and shown to be of good quality (RIN = 7), (**Figure 5.3b**).

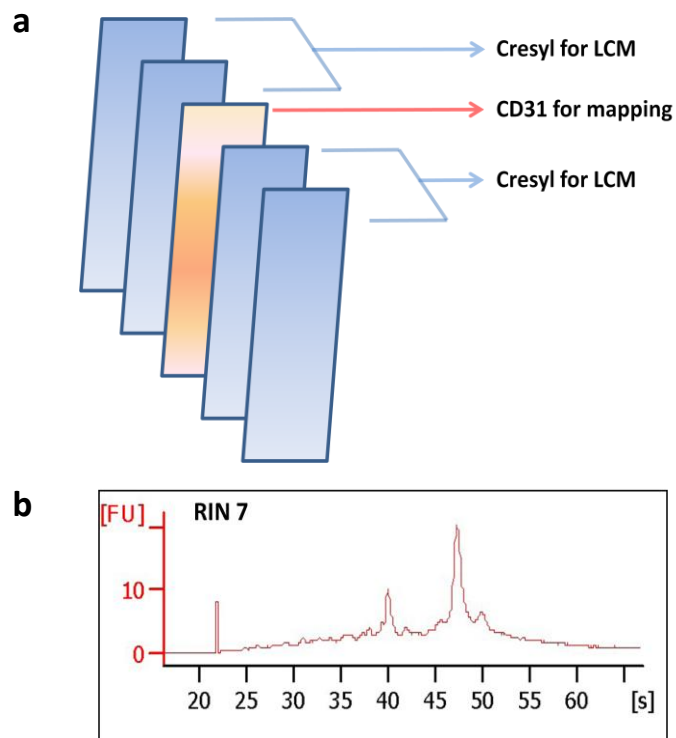


Figure 5.3 Mapping strategy to obtain high quality RNA from laser microdissected samples. (a) A ‘map’ slide was stained with CD31 antibody to visualize blood vessels. The adjacent two slides were cresyl violet stained to display basic morphology and used for laser microdissection. **(b)** The RIN value of laser dissected samples was determined on a Bioanalyzer.

5.2.3 Microarray of laser microdissected samples

Using the mapping strategy, good quality and sufficient RNA was obtained. Two laser microdissected endothelial samples from lung tumour (LCM1 and LCM2) were amplified and labeled using an Agilent Quick-Amp kit. Two RNA samples extracted from fresh lung tissue were included as controls. The specific activity of all samples was above 6, which is considered the minimal requirement for array analysis.

Single color microarray analysis was performed on an Agilent 4x44k chip. The analysis of microarray data was performed using the Quantile normalization method and the gene expression level was normalized to Flotilin 2, a house keeping gene. The expression level of epithelial cell adhesion molecule (EPCAM) which is expressed on most normal epithelial cells and almost all carcinomas was used as a measure of purity. **Figure 5.4a** shows that CD31 and EPCAM were expressed at an equal level in the laser dissected samples indicating considerable epithelial/carcinoma contamination. Despite that an equal amount of labeled cRNA was applied to the microarray. Weaker signals were detected in the laser dissected samples than that in control samples (**Figure 5.4b**).

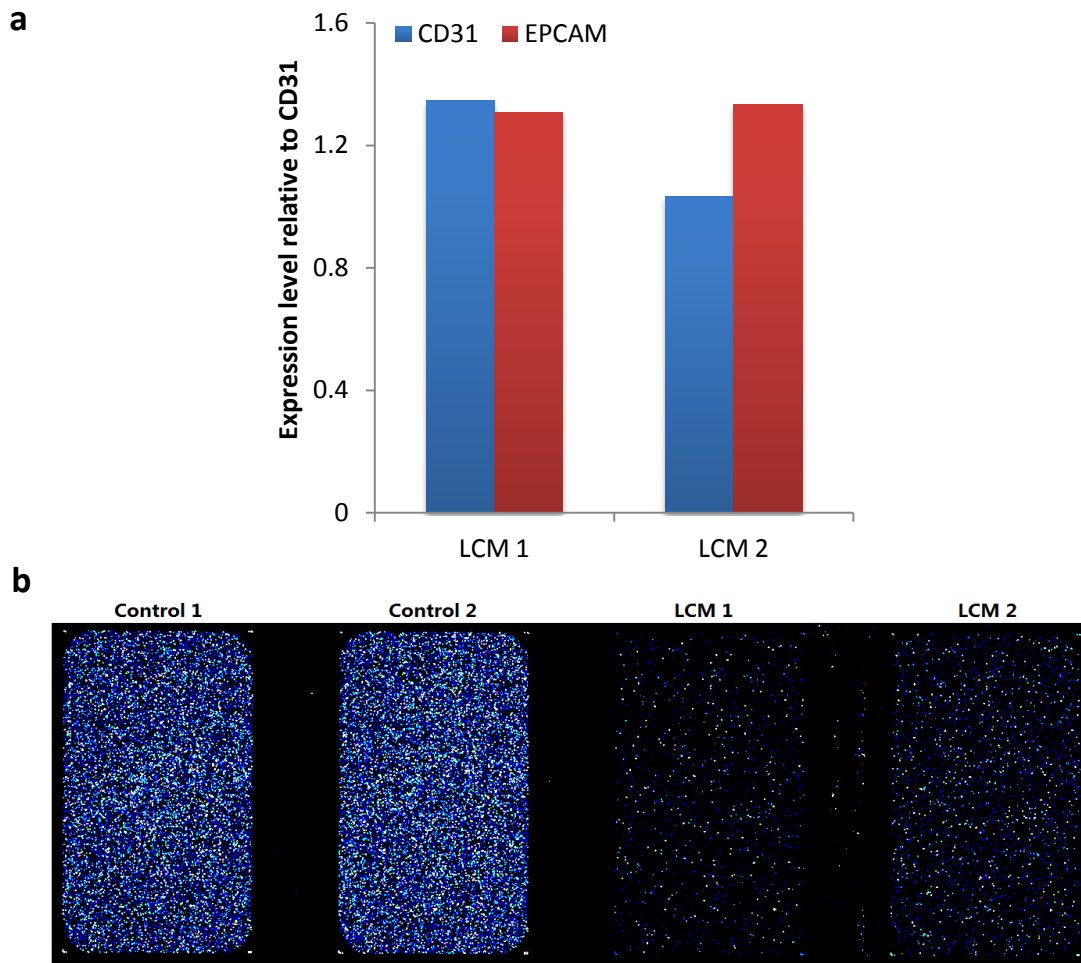


Figure 5.4 Microarray of laser microdissected samples. (a) Comparison of endothelial and epithelial compartments in two laser dissected samples: LCM1 and LCM2; (b) Weak signals were detected in laser microdissected samples compared with control samples.

5.2.4 Potential difficulty of capturing vessels from normal lung tissue by laser microdissection

To make a comparison of gene expression between normal and tumour endothelial cells, laser microdissection also needs to be performed on normal lung tissues. To first understand the morphology and vessel distribution, CD31 immunohistochemistry was performed on normal lung tissue. **Figure 5.5a** shows intense staining throughout the whole lung tissue. This was presumably due to the high endothelium content of normal lung, which adds extra difficulty to identify vessels for laser dissection. To avoid damaging the RNA, the vessel area for laser dissection has to be delineated. It proved unavoidable to exclude mural cells (pericytes and smooth muscle cells) in the dissected materials, due to their proximity to the endothelium (**Figure 5.5b**).

In conclusion, laser microdissection proved unsuitable to isolate endothelial cells, particular those in lung tissue. In parallel, an alternative, *Ulex*-bead isolation approach was investigated for the same purpose.

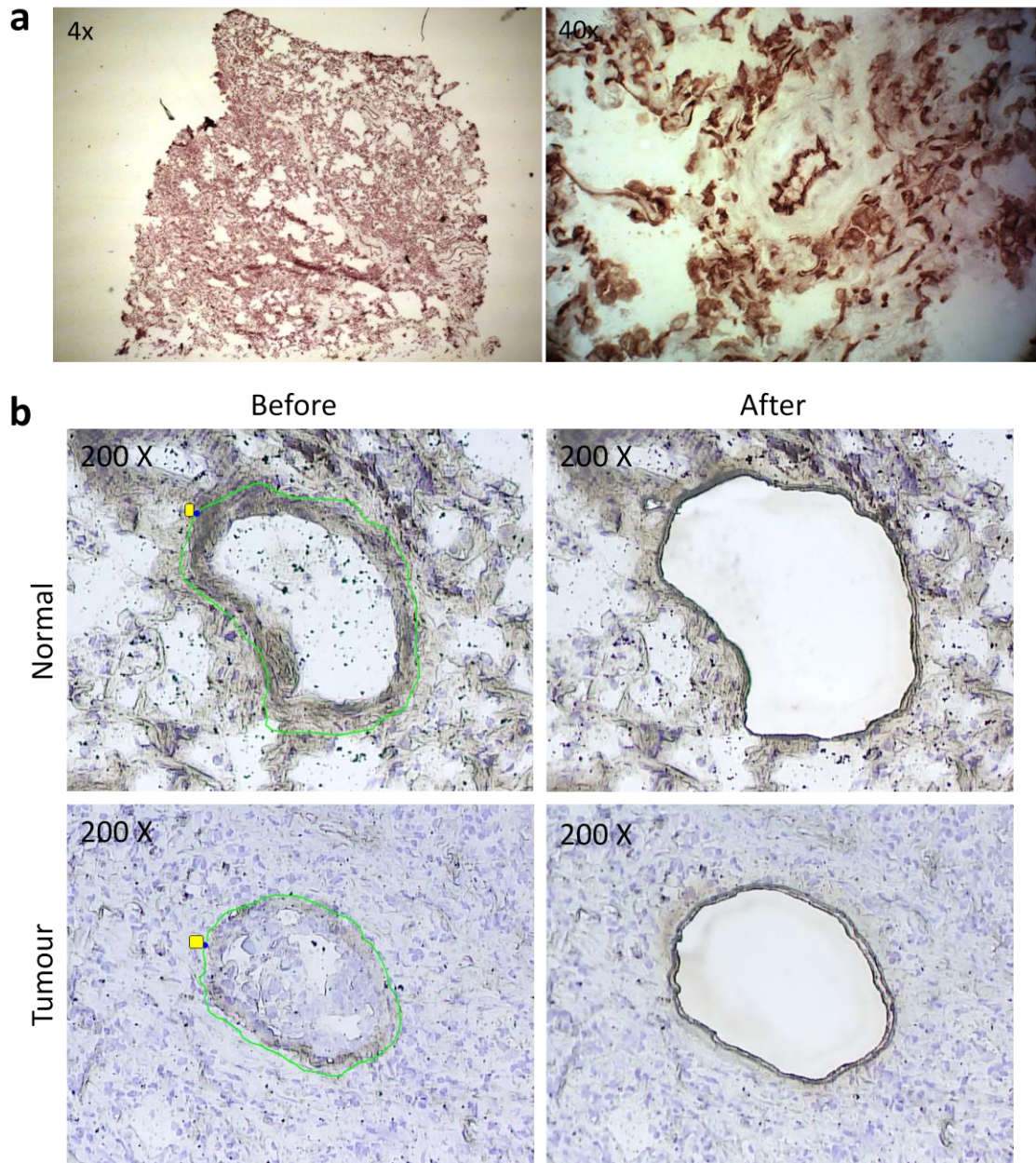


Figure 5.5 Potential difficulties for laser microdissection of normal and tumour lung. (a) Frozen normal lung sections were stained with CD31 monoclonal antibody. Images were captured under a light microscope. (b) Examples of laser microdissection of vessels from cresyl violet stained lung normal and tumour tissue.

5.3 Endothelial isolation using *Ulex* coated beads

Endothelial cells were isolated from fresh healthy and tumour lung tissue using *Ulex*-conjugated beads. To determine the endothelial enrichment, total RNA extracted from endothelial isolates or whole tissue was converted to cDNA. The expression of CD31 in bead isolated samples was compared with that in whole tissue by real-time PCR.

As shown in **Figure 5.6a**, a 15 fold increase of CD31 expression was achieved in the bead isolated samples compared to the whole lung tumour extracts. A 4 fold enrichment of endothelial cells was seen in endothelial cells isolated from normal lung compared to the whole tissue. The different fold increase of CD31 expression between normal and tumour samples was due to the fact that the proportion of endothelial cells is higher in normal (30%) than in tumour (3-5%). Therefore, the endothelial enrichment was expected to be more dramatic in the tumour sample than in the normal tissue. RNA quality of the *Ulex*-bead isolated samples were confirmed to be good (RIN > 7) on a Bioanalyzer (**Figure 5.6b**).

Generally a lower RNA yield was seen from endothelial cells isolated from healthy lung tissue compared with that from tumour. This was possibly due to the endothelial cells in the healthy lung tissue being in a quiescent state. In the tumour, endothelial cells are active and transcription possibly more extensive. To obtain sufficient RNA (5 µg) to perform the deep sequencing, three endothelial isolates of normal lung were

pooled together to make up 4.8 μg while 6.1 μg of RNA was isolated from the endothelium from a single tumour.

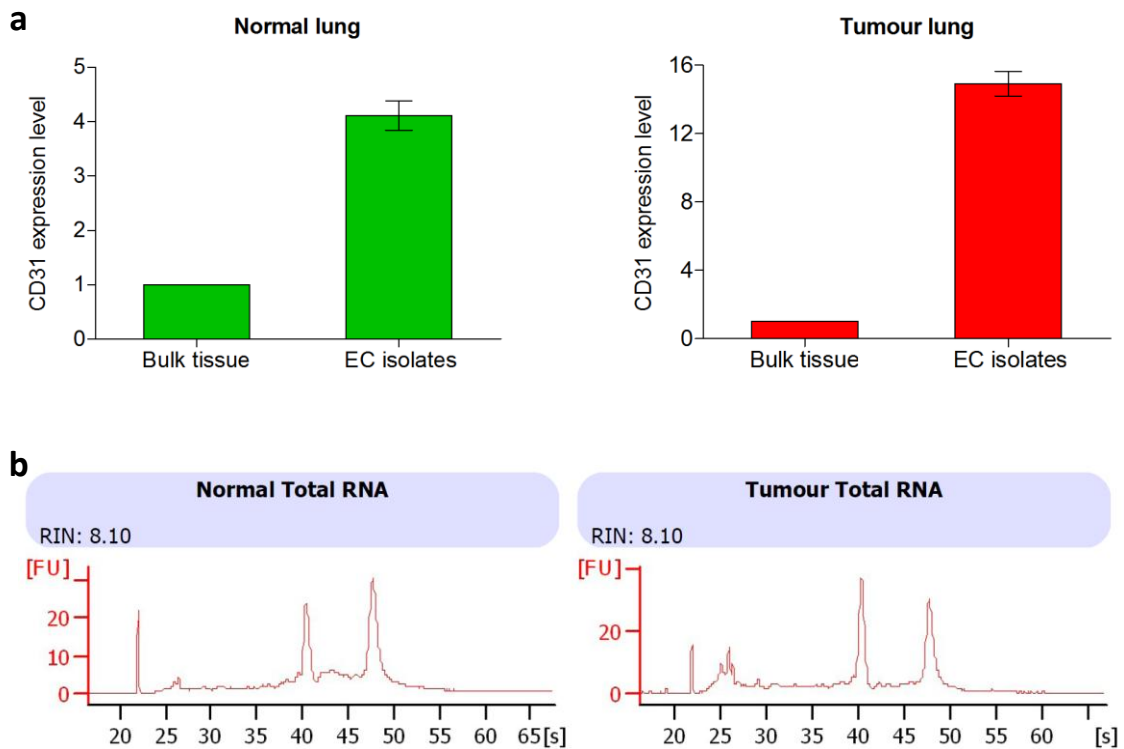


Figure 5.6 Confirmation of endothelial enrichment and RNA integrity of *Ulex*-coated bead isolated endothelial samples. Endothelial cells were isolated from lung normal or tumour tissue using *Ulex* coated beads. **(a)** Real-time PCR using a primer set for CD31 was performed on the bead isolated endothelial cells and bulk tissue. The expression level of CD31 in the bead isolated sample was normalized to that in the bulk tissue. **(b)** RNA was extracted from the bead isolated endothelial cells from normal lung or tumour tissue. The RNA integrity of normal and tumour lung endothelial cells was determined on a Bioanalyzer machine.

5.4 RNA-seq of lung endothelium

RNA-seq using deep sequencing (2nd generation sequencing) is a large scale parallel sequencing method for transcriptome analysis. It utilizes short read sequencing technologies such as the SOLiD 4 platform to sequence millions of reads from a cDNA library prepared from RNA. RNA-seq has the advantage of querying both known and novel transcripts and does not rely on a prior knowledge and annotation. Neither does it suffer from probe cross hybridization of closely similar genes that can occur on a microarray.

As described earlier, RNA of endothelial cells isolated from three normal lung tissues (pooled) and one tumour lung tissue were sequenced as 1 tumour and 1 normal sample on a SOLiD4 sequencer. Bioinformatics analysis of the deep sequencing data confirmed the purity of the endothelium by comparing the expression level of CD31 to EPCAM, CD68, PDGFR2 and CD11b. As shown in **Figure 5.7a**, the level of markers for non-endothelial cell types including epithelium, macrophage, pericytes and leukocytes was absent or at a low level compared to that of CD31.

Angiogenesis occurs with proteolysis of the extracellular matrix followed by endothelial proliferation and migration [164, 165]. MMPs open the path for endothelial migration by remodeling and degrading the extracellular matrix. To test whether known angiogenic associated genes and MMPs were elevated in lung tumour endothelium, a differential gene expression analysis was performed using the DESeq

v1.5 package. The results showed a number of known angiogenic genes and MMPs to be elevated in lung tumour versus healthy tissue endothelium (**Figure 5.7b, c**).

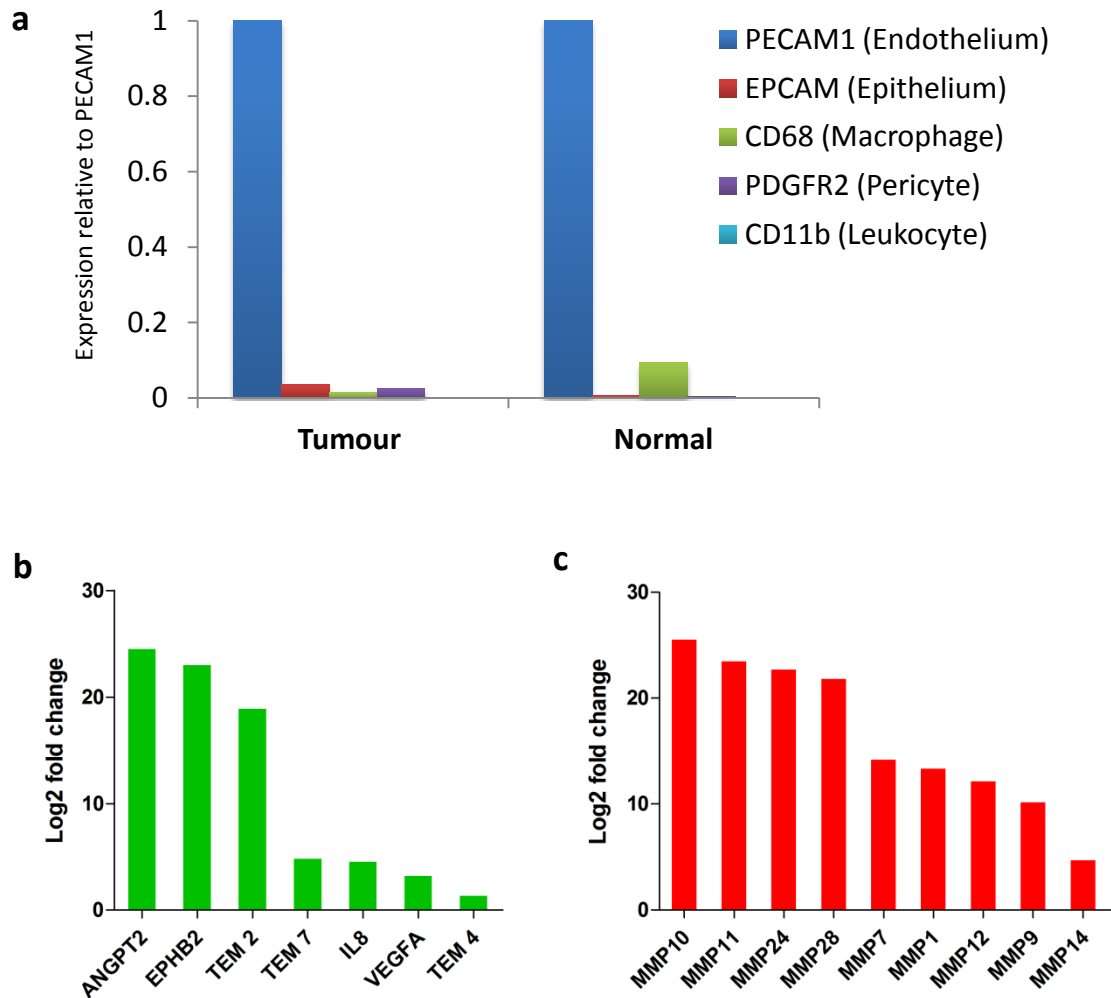


Figure 5.7 RNA-seq confirmation of endothelial enrichment and elevation of MMPs and angiogenic associated genes. (a) According the analysis of RNA-seq data, expression of EPCAM, CD68, PDGFR2 and CD11b in both normal and tumour samples were normalized to that of CD31/PECAM1, confirming the endothelial enrichment by the *Ulex*-bead isolation approach. Differential gene expression analysis revealed a panel of angiogenic genes (b) and MMPs (c) that were elevated in lung tumour endothelium

5.5 Microarray of biological replicates

As described earlier, the large amount of RNA (5 µg) and high cost restricted deep sequencing to one tumour and normal sample. Therefore, to perform differential gene expression analysis that compensates for patient variability, a microarray was experiment was performed on 4 pairs of normal and tumour endothelial isolates from lung on an 8x60k microarray chip (**Figure 5.8a**).

A PCA plot in **Figure 5.8b** shows variation in both tumour and normal samples and between samples of each group. This was to be expected as samples were collected and extracted from different patients and statistically significant genes are those that are consistent across replicate samples. Nevertheless, it is clear that all normal endothelial isolates are more similar to each other than to any tumour endothelium.

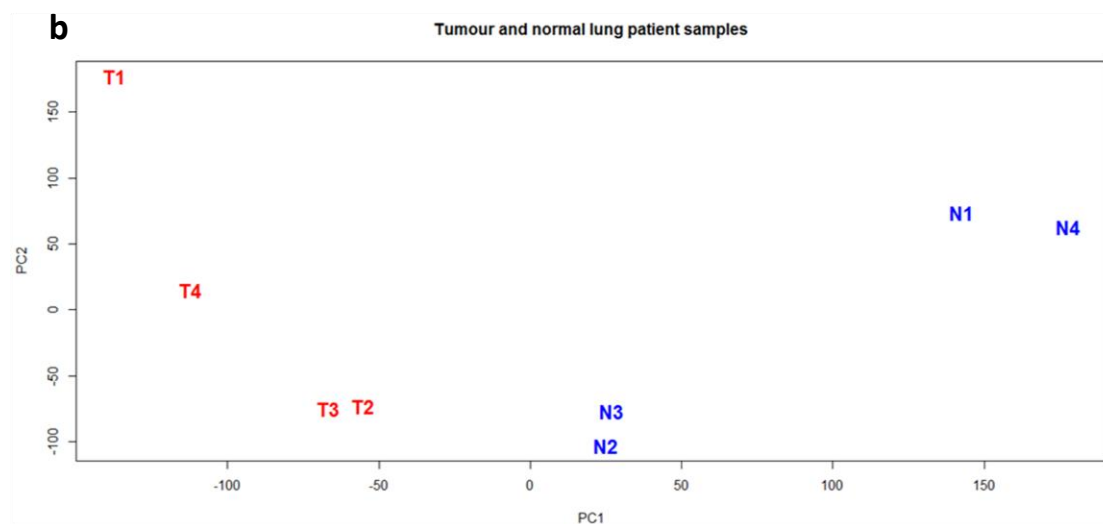
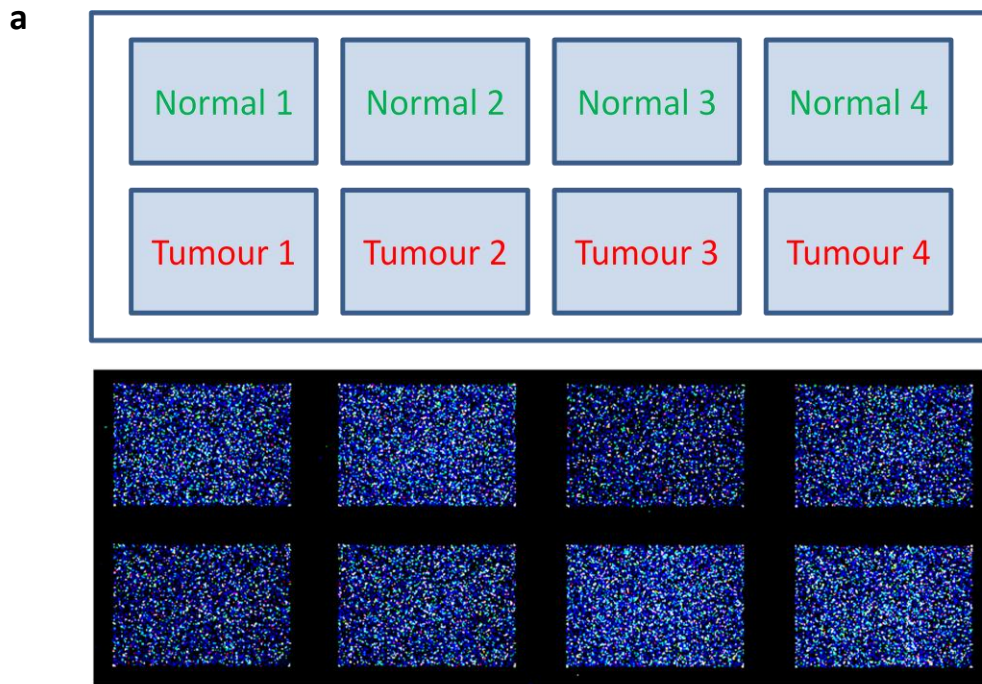
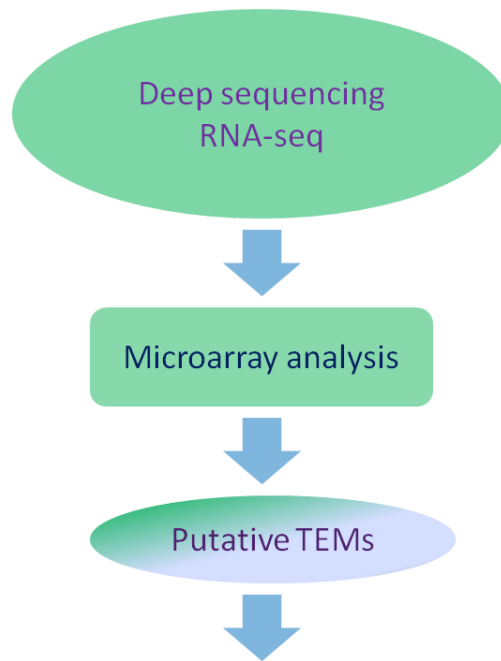


Figure 5.8 Microarray of endothelial isolates from multiple patient samples. (a) 4 pairs of normal and tumour endothelial isolates were analysed by microarray on an 8x60k Agilent microarray chip. **(b)** A PCA plot demonstrates variation between endothelium isolated from normal and tumour samples.

5.6 Identification of lung TEM candidates

For target identification, differentially expressed genes obtained from deep sequencing data were filtered with multiple criteria. 477 genes with log₂ fold change magnitude > 1, a p-value < 0.5 and containing a transmembrane or signal peptide domain was generated.

Differential gene expression analysis was performed on the microarray data using the program Limma and genes were filtered based on the same criterion as RNA-seq. This resulted in 584 genes. The intersection of the microarray and deep sequencing gene pools were assigned lung TEM candidates, consisting of 126 genes. 13 lung TEM candidates were chosen for further validation based on additional criteria including the level of association with endothelial cells, previously published work, intellectual property, sites of expression and relation to known genes with interesting functional properties (**Figure 5.9**).



GeneSymbol	RefSeqAccession	GeneName
ROS1	ENST00000403284	c-ros oncogene 1 , receptor tyrosine kinase
TPBG	NM_006670	trophoblast glycoprotein
LMTK3	NM_001080434	lemur tyrosine kinase 3
PLXDC1	NM_020405	plexin domain containing 1
PROM2	NM_001165978	prominin 2
PCDH7	NM_002589	protocadherin 7
STEAP1	NM_012449	six transmembrane epithelial antigen of the prostate 1
BAMBI	NM_012342	BMP and activin membrane-bound inhibitor homolog)
SLCO1B3	NM_019844	solute carrier organic anion transporter family, member 1B3
TMEM116	NM_138341	transmembrane protein 116
BIRC5	NM_001012271	baculoviral IAP repeat containing 5
GJB2	NM_004004	gap junction protein, beta 2, 26kDa
SYT12	NM_177963	synaptotagmin XII

Figure 5.9 Deep sequencing and microarray for the identification of putative lung TEMs

5.7 Validation of lung TEM candidates in EC isolated from NSCLC patients

To validate putative lung TEMs, primer sets of each candidate were designed. A quantitative real-time PCR was performed on four pairs of normal and tumour endothelial isolates from lung. Flotillin 2 was used as the house keeping gene to which the data was normalized. The double delta Ct method was used to compare expression levels in tumour relative to normal endothelial isolates.

Figure 5.10 demonstrates that all candidates had elevated expression in tumour ECs versus normal ECs, which ranged from a 3 to 60 fold increase.

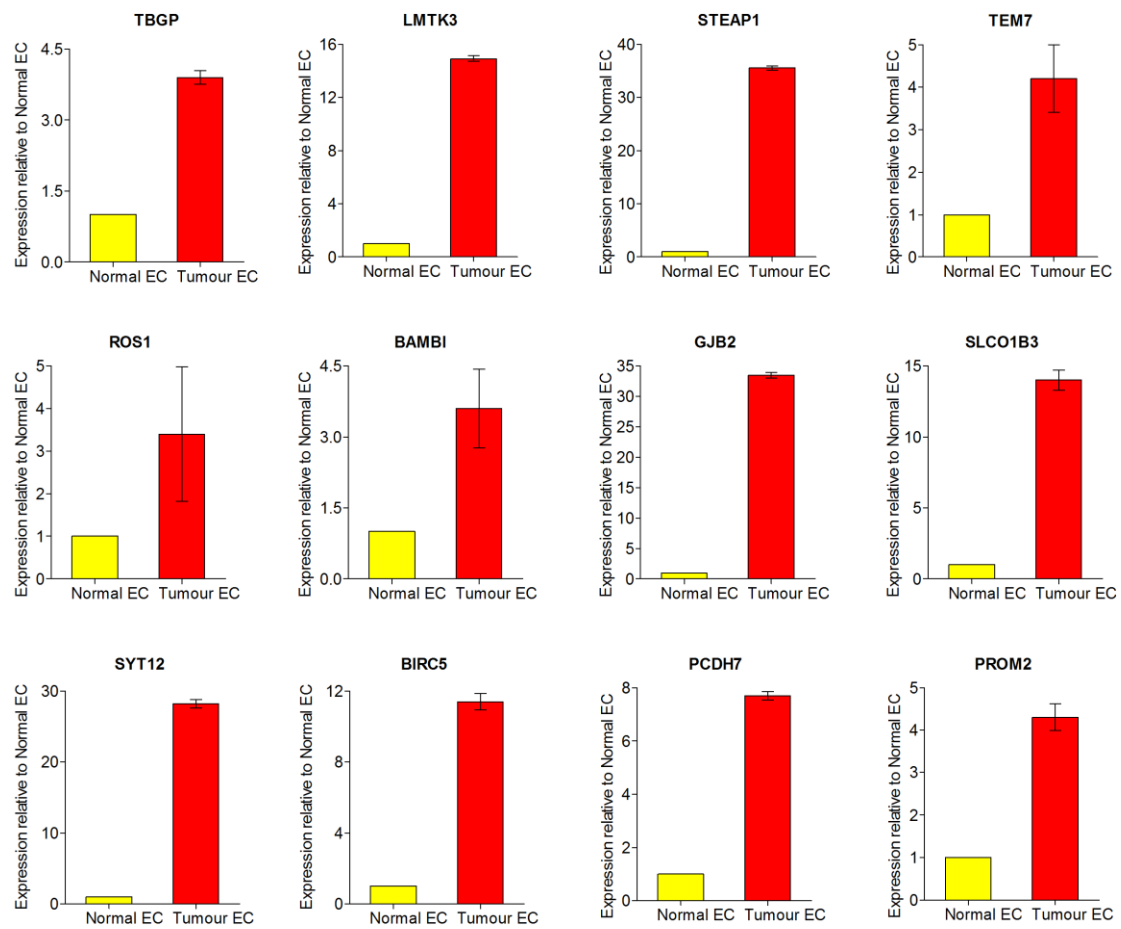


Figure 5.10 Quantitative real-time PCR validation of lung TEM candidates in EC isolated from NSCLC patients

5.8 Expression of TEM candidates in angiogenic tissue and lung cancer

Immunohistochemistry staining was performed on placental and lung tumour tissues using antibodies to the lung TEM candidates. Among the fourteen candidates, the six genes: BIRC5, GJB2, PCDH7, PROM2, ROS1 and STEAP1 showed endothelial expression in placenta which is a site of active angiogenesis (**Figure 5.11**). Lung tumour tissue was also immunostained and **Figure 5.12** shows that these six candidates are indeed expressed on the tumour vessels.

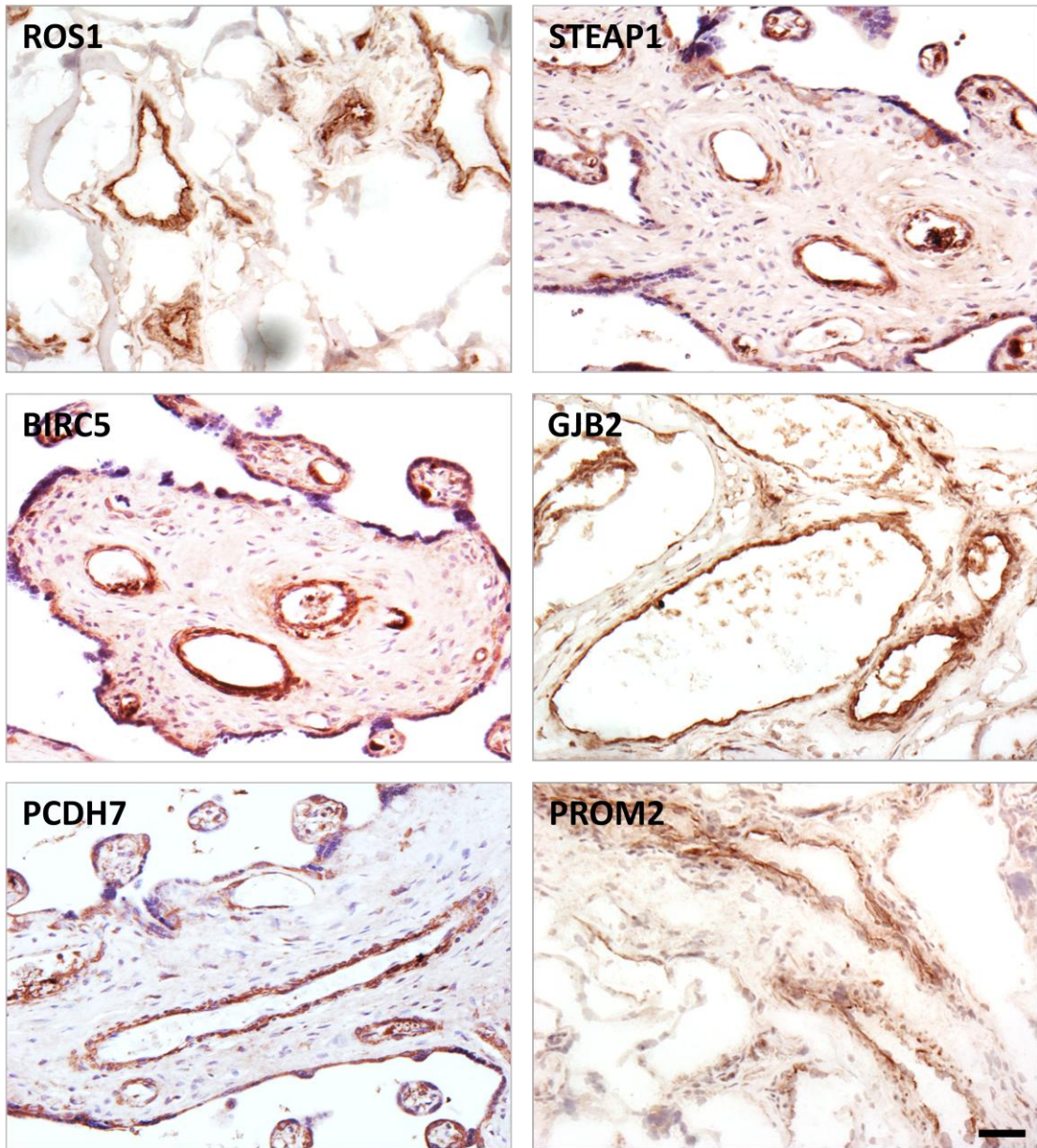


Figure 5.11 Immunohistochemistry of lung TEM candidates on placental tissue.
Scale bar = 25 mm

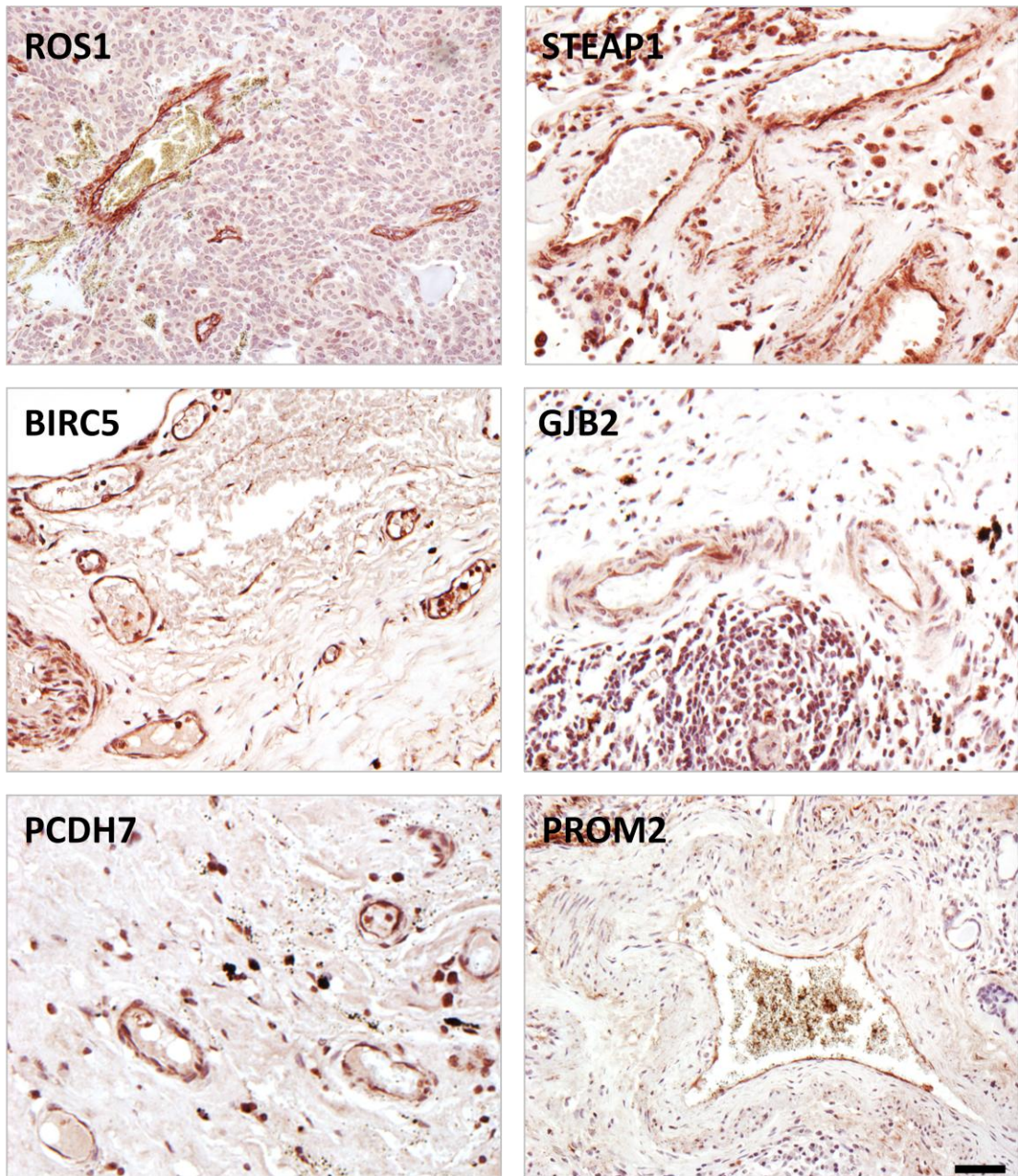


Figure 5.12 Immunohistochemistry of lung TEM candidates on lung cancer tissue. Scale bar = 25 mm

5.9 Conclusions

A major barrier to effective treatments for lung cancer is the lack of well characterized markers or targets. In this chapter we aimed to identify novel lung cancer vascular targets by transcriptional profiling of lung endothelium. Two methodologies were investigated and compared to characterize healthy and cancerous lung endothelium. Laser microdissection technology proved problematic for isolating lung endothelial cells. Beside an inadequate endothelial enrichment, the poor RNA integrity and limited yield restricted downstream work. In contrast, the *Ulex*-bead isolation approach achieved excellent endothelial purity and RNA quality and yield from fresh clinical samples. Using this approach, deep sequencing technology was combined with microarray analysis to profile the transcriptome of endothelial isolates from tumour and healthy lung of multiple cancer patients. Differential gene expression analysis of the two data sets identified 126 TEM candidates. The subsequent qPCR validation on tumour and healthy endothelial isolates from multiple patients produced a short list of 13 genes. Immunohistochemistry staining on placental and lung tumour sections identified six lung vascular targets with strong endothelial expression, namely STEAP1, ROS1, PCDH7, BIRC5, GJB2 and PROM2. Further characterization of these targets is on-going.

Chapter six

Robo4 as a cancer vaccine

6.1 Introduction

TEMs localized at the plasma membrane or secreted into the extracellular matrix are accessible for targeting by antibody, and such antibodies can be either infused or generated *de novo* via vaccination with the TEM. An advantage of active vaccination is the possibility of generating both antibody production *in situ* and cytotoxic T-cell mediated immunity. In experimental mouse models, reduction of tumour growth has been demonstrated after vaccination with a range of endothelial expressed proteins including the vascular endothelial growth factor receptor (VEGFR) -2, Endoglin/CD105, Delta-like 4 (DLL4) and the extra domain-B of fibronectin (reviewed in [166], [67, 146])

Crucially important to the success of the immunotherapy is the selection of the TEM. The TEM should ideally be present throughout the tumour vasculature and show negligible expression on the normal vasculature. An example of such a TEM is Robo4. Expression of Robo4 on the vasculature in tumour but not healthy tissues identifies it as a potential target for immunotherapeutic approaches such as vaccination. Its expression is up-regulated by low shear stress, and it is present on the vessels of a number of tumour types including pancreatic, bladder, lung and prostate cancer [73, 108, 109, 167, 168]. This chapter investigates the effect of Robo4 vaccination on angiogenesis and tumour growth.

6.2 Papain cleavage of human Robo4-Fc

Prior to vaccination to a self-antigen, it is necessary to show that there is no pre-existing immunity. An ELISA assay was designed to investigate whether Robo4 antibodies are present in serum from healthy people and cancer patients. In this assay, the ELISA plate was coated with pure Robo4 protein as the antigen. Robo4 protein was expressed fused to an Fc tag that allowed purification on a protein A column. Unfortunately the Fc tag was recognised by the secondary anti-human IgG antibody and so was first removed by papain digestion.

Pilot experiments showed that although the Fc tag was cleaved off, the papain rapidly digested the remaining Robo4. To optimize the yield of cleaved Robo4, the cleavage reaction mix was sampled at a series of time points over one hour. Samples were resolved on acrylamide gel followed by coomassie staining. As shown in **Figure 6.1**, the top band (intact Robo4-Fc) gradually disappeared across the time points while the cleaved band at 50 kDa (cleaved Robo4) increased during the papain digestion. 40 min was chosen as the optimal reaction time to maximize the yield of cleaved Robo4.

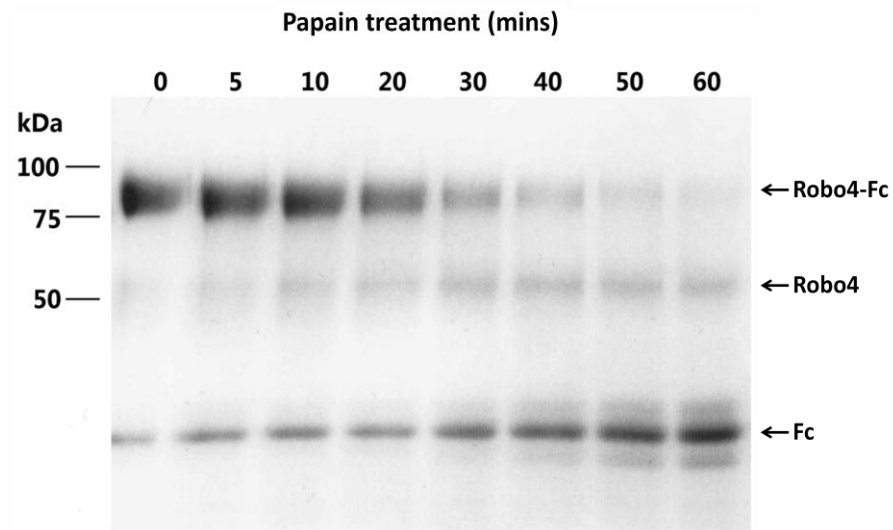


Figure 6.1 Optimization of papain cleavage of recombinant human Robo4-Fc. Intact human Robo4-Fc protein was cleaved in a papain digestion. The reaction mix was sampled at serial time points and run on a SDS PAGE gel following coomassie staining. The band between 75 – 100 kDa is the intact human Robo4-Fc protein while the band at 50 kDa is the cleaved Robo4 without the Fc tag.

6.3 Depletion of Fc fragments after papain digestion of human Robo4-Fc protein

To avoid cross reaction with the secondary anti-human Ig antibody in the ELISA assay, the papain cleaved Fc fragments from recombinant Robo4-Fc protein need to be removed. Protein G beads which have high affinity for human Fc were used to deplete the Fc fragments from the papain digested mix. After the papain reaction was quenched, protein G beads were added and incubated for 1 hour. The beads were then removed and the resulting supernatant contained Robo4 only. This supernatant was collected and analyzed by Western blot. A clean band of human or mouse Robo4 was detected at 50 kDa by the Robo4 antibody while both were absent when re-probed with human IgG antibody (**Figure 6.2**). The results show that, with the optimized protocol, an effective Fc cleavage and depletion was achieved in both human and mouse Robo4-Fc.

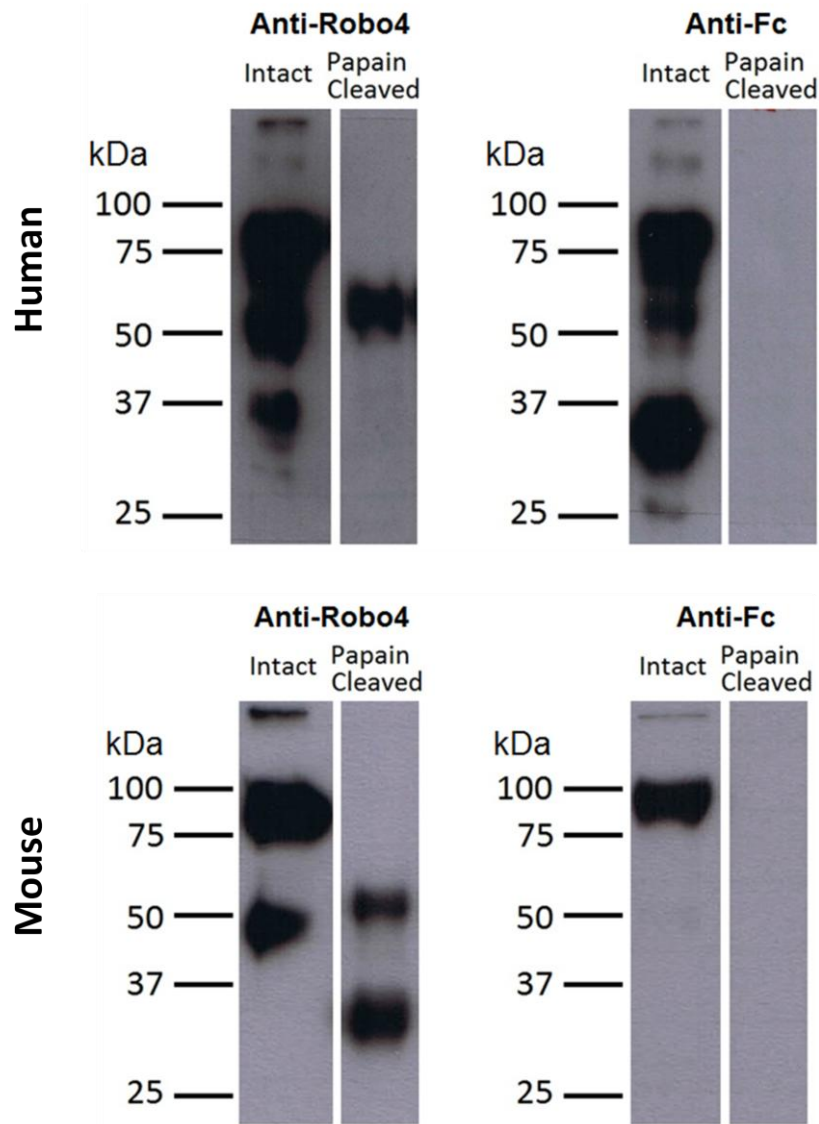


Figure 6.2 Depletion of Fc fragments from papain cleaved human/mouse Robo4-Fc. The depletion of Fc fragments from papain cleaved human/mouse Robo4-Fc was performed using protein G beads. Beads to which the Fc fragments bound were spun down and the supernatant containing Robo4 only was collected and western blotted against human or mouse Robo4 antibody and human Fc antibody respectively. The upper figure is the western blot on papain cleaved human Robo4-Fc using human Robo4 and human Fc antibody. The lower figure is the western blot on papain cleaved mouse Robo4-Fc using mouse Robo4 and human Fc antibody.

6.4 Generation of a standard curve for assay of Robo4 antibodies in serum

We first developed a standard curve for the ELISA in order to measure antibodies in serum. To optimize the amount of coating antigen (papain cleaved Robo4), 5-fold titration of coating antigen and a monoclonal antibody to human Robo4 - MR7 or a polyclonal antisera to mouse Robo4 (1 to 0.008 $\mu\text{g/ml}$ and 25 to 0.2 μl respectively) was applied to the assay. The result shows that the minimum amount of coating antigen (5 μl) used gives a valid read out. The detection limit of the assay was found to be an antibody concentration of 8 ng/ml (**Figure 6.3**).

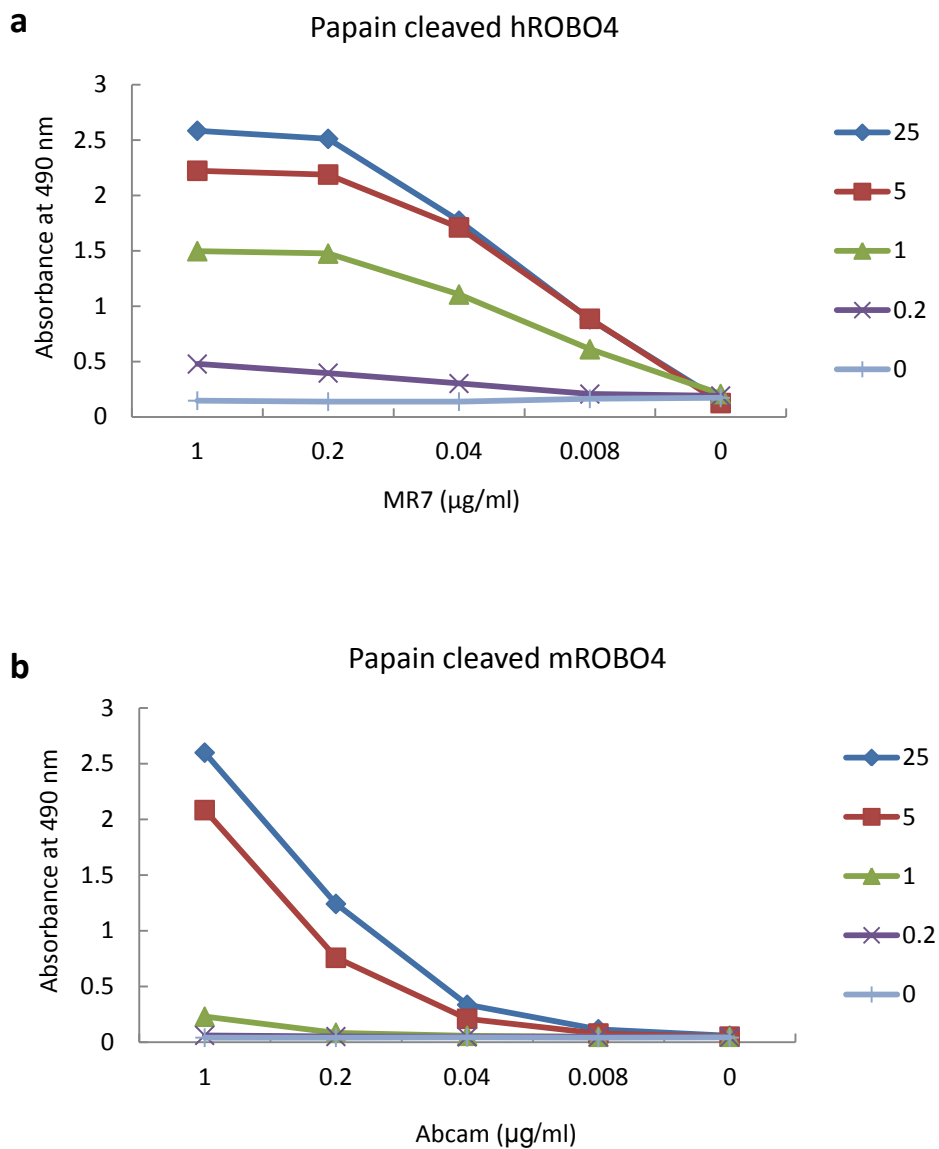


Figure 6.3 Standard curves for the assay of Robo4 antibodies in serum. Recombinant human or mouse Robo4-Fc protein underwent papain cleavage followed by Fc fragment depletion. Titration of papain cleaved Robo4 stock (25 μl ~ 0.2 μl) and antibody (1 μg / ml ~ 0.008 μg / ml) enables generation of a standard curve. **(a)** and **(b)** show the standard curve generated by papain cleaved human and mouse Robo4 respectively.

6.5 Assay for Robo4 antibody in serum from cancer patients and healthy individuals

It is important to determine whether Robo4 antibody is present in the serum from healthy people and cancer patients. This is particularly critical for cancer patients, because overexpression of Robo4 in tumour vessels could potentially induce an immune response.

An ELISA assay was used to determine whether Robo4 antibodies could be detected in the serum of colorectal cancer patients. ELISA wells were coated with Robo4 protein. Serum samples at different dilutions were applied to the plate in a range from neat to a dilution of 1 in 25. Six serum samples from either healthy donors or cancer patients were tested in this assay. Robo4 monoclonal antibody (MR7) was employed as the positive control. As shown in **Figure 6.4**, there was no Robo4 antibody detected in the serum of either patient sera or healthy donors.

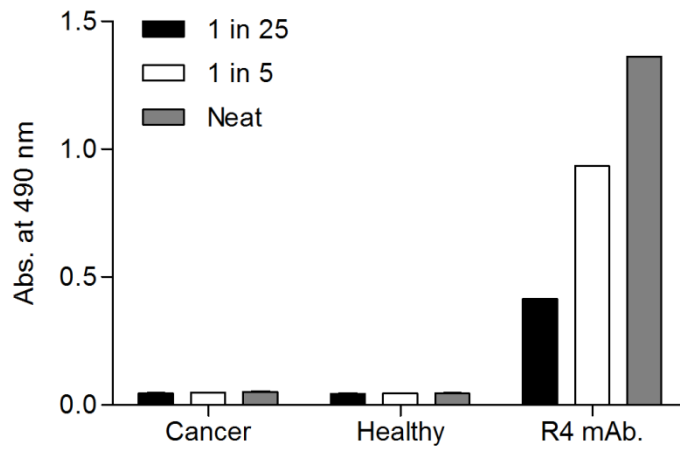


Figure 6.4 Assay of Robo4 antibody levels in serum from cancer patients. An ELISA plate was coated with papain cleaved human Robo4 and the neat serum from 6 healthy donors or cancer patients were applied to each well. A Robo4-specific monoclonal antibody MR7 (R4 mAb) was used as the positive control with 5-fold dilution ranging from 40 to 1.6 ng/ml.

6.6 Expression of mouse Robo4-Fc in 293T cells after calcium phosphate transfection.

To vaccinate mice, pure mouse Robo4 protein was required. Plasmids with the extracellular domain of mouse Robo4 fused to a human Fc tag were obtained from Cancer Research Technology. Mouse Robo4-Fc-pIG was transfected into HEK 293T cells using calcium phosphate. As the recombinant protein was secreted from the cells, the conditioned media was collected and run through a protein A column that has high affinity for the Fc tag. Robo4-Fc loaded column was then eluted with a pH gradient on an FPLC machine. The purity of the protein was verified by western blot and coomassie staining.

Abcam anti-human Robo4 antibody that cross reacts with mouse Robo4 revealed clear bands between 75 kDa ~ 100 kDa (**Figure 6.5a**). The purity of the protein was confirmed by coomassie staining (**Figure 6.5b**).

The aim was to produce sufficient mouse Robo4 protein for mouse immunization. However the expression was lost a few days after transfection and the protein yield was limited. To overcome this, a stable cell line that expresses mouse Robo4 using a lentiviral system was generated.

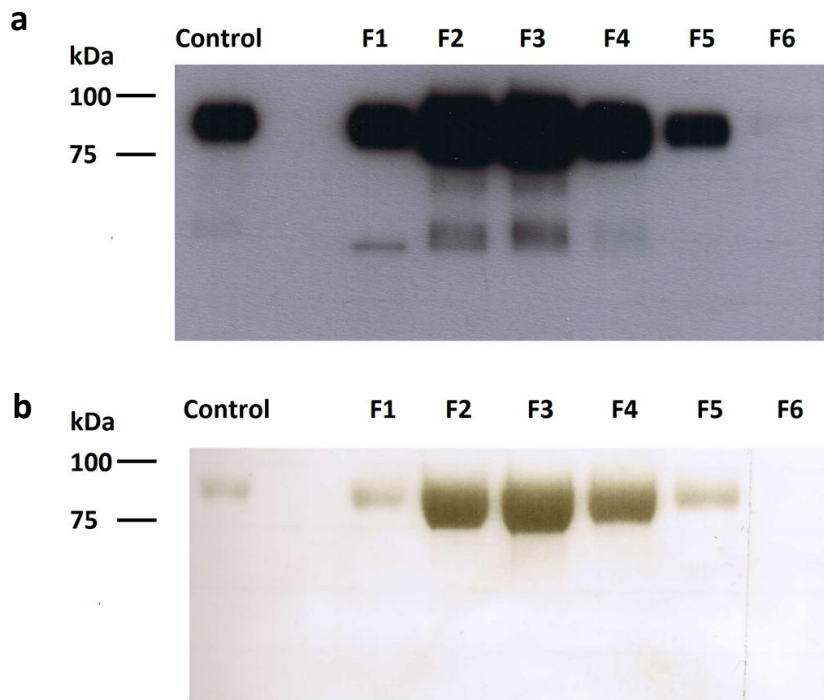


Figure 6.5 Coomassie stain and western blot of Robo4 fractions from FPLC purified mouse Robo4-Fc. **(a)** For western blot, 10 μ l of each fraction was added to 2 μ l of 6x SDS loading buffer and 10 μ l was loaded on to a 10% SDS PAGE gel. Western blot was performed using Abcam antisera which cross reacts with mouse Robo4. **(b)** Coomassie stain was performed on each fraction with 1 μ g of human Robo4-Fc as the positive control. For coomassie stain, 30 μ l of each fraction was added to 6 μ l of 6x SDS loading buffer and 25 μ l was loaded on to a 10% SDS PAGE gel.

6.7 Generation of a stable cell line expressing mouse Robo4 using lentivirus

Lentiviral expression systems are widely used in the transduction of non-dividing cells. These systems provide long term expression of the delivered genes, and we adopted a lentiviral approach to generate a stable cell line that expressed mouse Robo4.

Mouse Robo4-Fc was amplified by PCR from the Robo4 containing pIG vector and sub-cloned into a lentivector: pWPI, which contains a GFP tag after an IRES sequence. Lentivirus was produced by calcium phosphate transfection of 293T cells with the lentivector that contains mouse Robo4-Fc, packaging plasmid (psPAX2) and envelope plasmid (PMD2G). The transduction efficiency of 293T cells (87.62%) 4-days post-transduction is shown. Transduced cells were sorted for GFP by flow cytometer and the percentage of the GFP positive cells (99.39%) is shown in **Figure 6.6a**.

Further experiments were performed to optimize the number of collections from the stable line. Five collections of conditioned media were analyzed by coomassie stain and all of them were confirmed to be mouse Robo4-Fc (**Figure 6.6b**). Quantification allowed comparison of the yield to the calcium phosphate method. The comparison showed that the stable cell line produced 4x the amount of protein (6 mg) compared to the calcium phosphate method (**Table 3**).

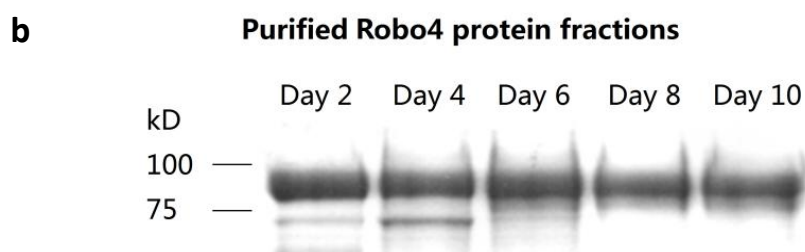
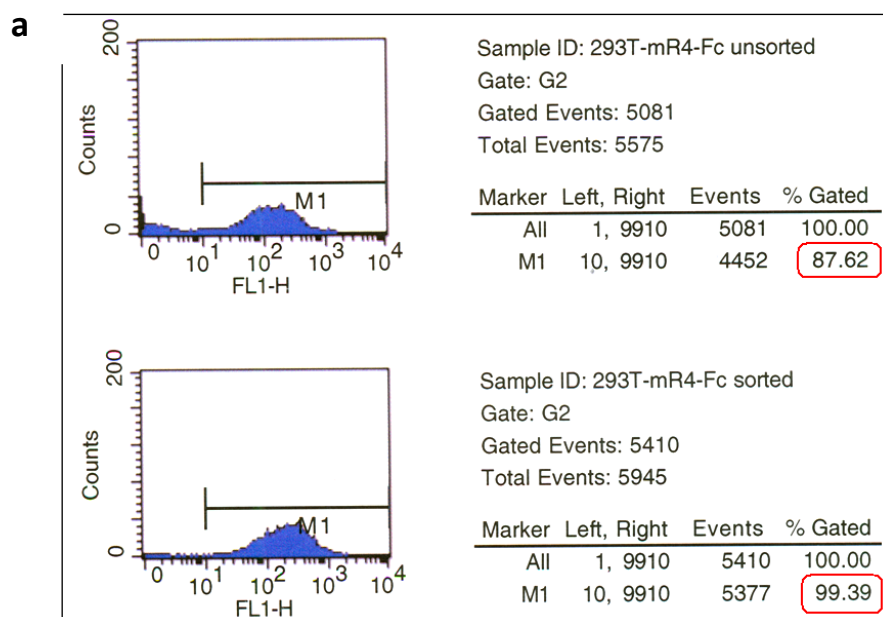


Figure 6.6 Generation of a stable cell line expressing Robo4 and the purification of recombinant Robo4 protein. (a) Generation of a stable cell line that expresses mouse Robo4-Fc by FACS sorting of GFP positive cells (FL1). 293T cells transduced by lentivirus were analyzed before and after FACS sorting. The number highlighted in the red box indicates the transduction efficiency (top profile) and the percentage of GFP⁺ cells after sorting (bottom profile). (b) Coomassie stain for Robo4 from media conditioned by the stable line expressing mouse Robo4-Fc. 10 ml of conditioned media was collected on alternate days for 10 days. Recombinant protein was purified using protein A beads. The protein bound beads were boiled in 50 μ l of 1xSDS loading buffer and 25 μ l was loaded on a 10% SDS PAGE gel.

	Culture size	Volume	Yield	Highest conc. of 1 ml elution
Calcium phosphate	40 dishes	3 L	3 mg	0.8 mg/ml
Lentiviral cell line	20 dishes	1.5 L	6 mg	3 mg/ml

Table 3 Comparison of protein production by calcium phosphate transfection and lentiviral expression systems

6.8 Immunization with Robo4 in mice using protein vaccination

In order to break immune tolerance to Robo4, protein immunization was performed in C57B/6 mice. Freund's complete adjuvant was used to achieve immunization because Robo4 is a self antigen and self antigens often show low immunogenicity. The antibody response was then characterized using the ELISA assay. Papain cleaved mouse Robo4 was used as the coating antigen.

For immunization, six mice received 50 µg of mouse Robo4-Fc protein or Fc control subcutaneously at two-week intervals. Complete Freund's adjuvant was used on day 0 and incomplete Freund's on day 14 (**Figure 6.7a**). Serum was collected on day 0, 14 and 28 and assayed for Robo4 antibodies by ELISA. As shown in **Figure 6.7b**, a robust antibody response against Robo4 was induced by day 28 in the Robo4 vaccinated groups, suggesting that tolerance to Robo4 had been broken by the immunization.

Further characterization of the induced antibodies showed that there were high levels of IgG1, with lower titres of IgG3 and IgG2b (**Figure 6.7c**). Immunization with proteins tends to induce Ig class switching to the IgG1 isotype associated with T helper 2-type immunity [169]. This result confirmed that vaccination stimulated a TH2 response.

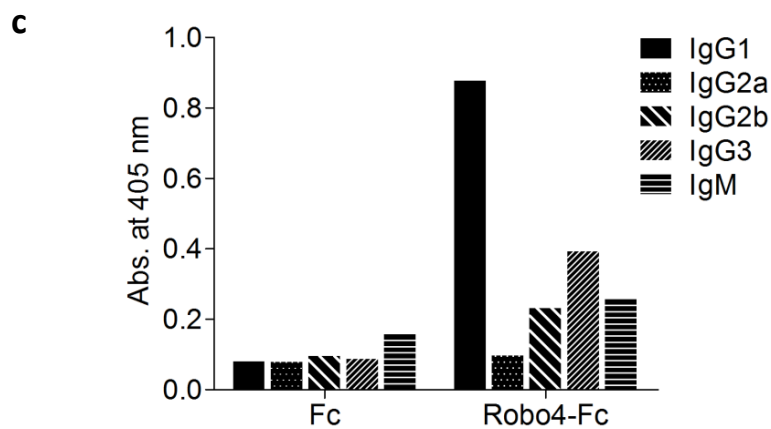
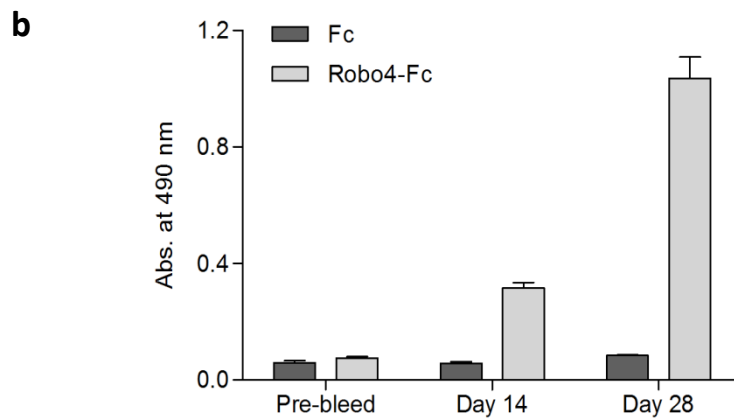
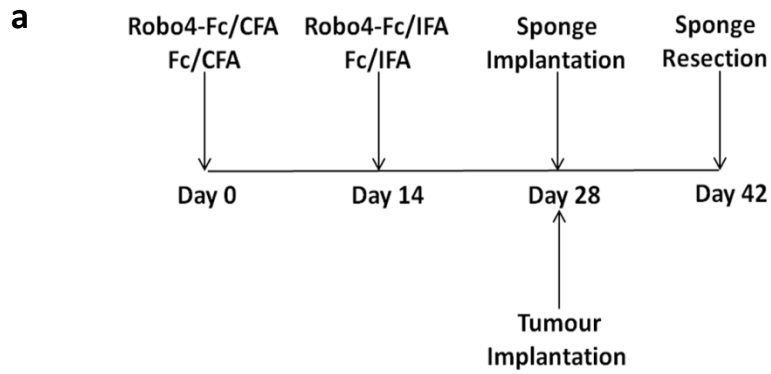


Figure 6.7 Vaccination of mice with mouse Robo4 generates a Robo4-specific IgG response. (a) Protocol for Robo4 vaccination prior to *in vivo* angiogenesis assays and tumour experiments. (b) Vaccination with Robo4-Fc induces Robo4-specific antibody production. Mice (C57B/6) were vaccinated with Fc or mouse Robo4-Fc protein injection according to the protocol in (a). Robo4 antibodies were determined by ELISA at day 14 and day 28. (c) Determination of antibody isotypes in control and Robo4 vaccinated mouse sera. Sera, harvested at day 28 from Fc or Robo4-Fc vaccinated mice, was diluted tenfold and used in an ELISA with secondary antibody specific for mouse IgG1, 2a, 2b, 3 or IgM.

6.9 Sponge implantation assay in Robo4 immunized mice

Subcutaneous implantation of a sponge is a robust technique to study *in vivo* angiogenesis [170, 171]. To investigate whether there is an anti-angiogenic effect in Robo4 vaccinated mice, single sponges were implanted into Robo4 immunized and control mice. bFGF was delivered to the sponge on alternate days. At the end of the experiment, the implanted sponges were resected and fixed in formalin following paraffin embedding and sectioning. Hematoxylin and eosin staining was carried out to reveal the cellular morphology of the sponge implant.

Invasion of the sponge by new vessels and fibrotic tissue was assessed by microscopic imaging. Pictures of whole sponges were captured and the area of invasion was analyzed. A dramatic reduction in invaded fibrotic tissue and blood vessels was observed in sponges from Robo4 vaccinated mice compared to controls. Two representative pictures from Robo4 vaccinated group and controls are shown in **Figure 6.8a**. The invaded area was quantitated using Image J software. The percentage of invaded area was quantitated for each individual sponge and results shown in **Figure 6.8b**. Comparison of the mean values showed, 77.6% of the control sponge was invaded by blood vessels and fibrotic tissue while only 36.2% of the Robo4 vaccinated group was invaded.

The vessel density of each sponge was determined by counting vessel numbers in random fields. **As shown in Figure 6.9a**, there was a significant decrease of vessel

density in sponges from Robo4 vaccinated mice (average 2 vessels per field) compared to those from control mice (average 10 vessels per field).

A noteworthy observation was that when comparing the size of the blood vessels in the invaded area between these two groups, large vessels were observed in sponges from control mice while these were rarely seen in sponges from Robo4 vaccinated mice (**Figure 6.9a**). Quantification of the actual vessel dimension from each group was performed using Image J software (**Figure 6.9c**). A significant decrease in vessel dimensions was seen in Robo4 vaccinated mice (4.5×10^3 pixels) compared to that in control mice (9.3×10^3 pixels).

Taken together, an immune response against Robo4, and most likely Robo4-specific antibodies, elicited by protein vaccination induced a striking anti-angiogenic effect *in vivo*.

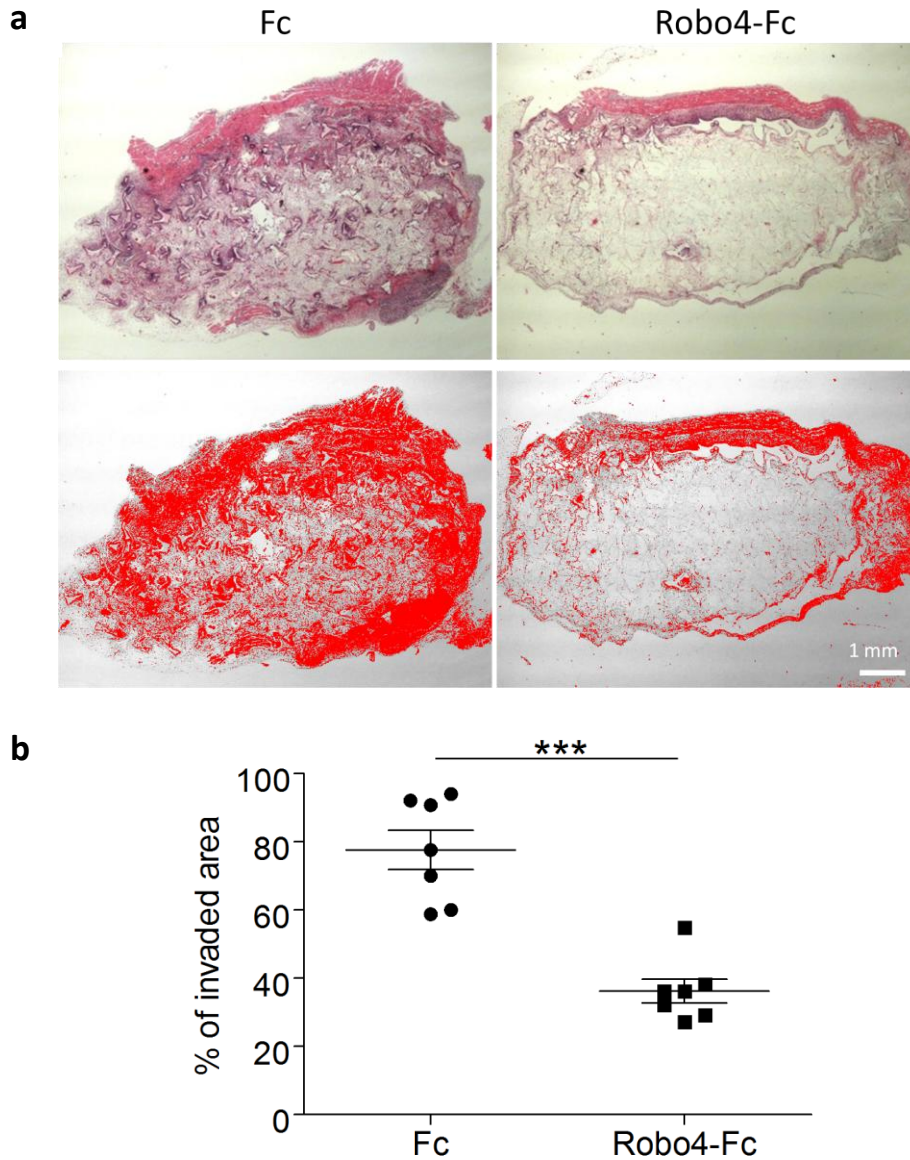


Figure 6.8 Sponge implantation assay in Robo4 vaccinated mice. (a) Sponges were harvested, sectioned, and stained with H&E. The invading blood vessels and fibrotic tissue were visualized under a light microscope (10X); (top). Pictures of the implanted sponges were taken on a light microscope and the invaded areas analysed using Image J software (bottom). Areas in red show the invaded areas which were quantified by the software. (b) The invaded area of each sponge from Robo4 immunized or control mice was quantified using Image J software and the percentage of the invaded area versus the whole sponge was calculated. Invaded area as a percentage of the whole sponge was plotted for a representative section for each mouse. The mean and standard error of the mean (SEM) are shown ($P = 0.0006$, Mann-Whitney test).

6.10 Expression of Robo4 in the vasculature of the Lewis lung carcinoma tumour

Since angiogenesis plays a key role in the growth of solid tumours, the effect of Robo4 vaccination on the growth of subcutaneously implanted mouse tumour cells was examined. Lewis lung carcinoma (LLC) is a highly aggressive cancer cell line derived from the C57Black/6 mouse strain. It is a widely used model for investigating effects on the tumour vasculature [172, 173]. To determine whether an immune response to Robo4 would target the tumour vessels in the LLC mouse model, immunostaining of Robo4 was performed on formalin fixed LLC tumour sections.

Antisera to human Robo4 (Abcam) that cross reacts with mouse Robo4 was used. CD31 antibody was used as a positive control for the vasculature. Staining showed that Robo4 is indeed expressed in the vessels of Lewis lung carcinoma tumour (**Figure 6.10**). The staining pattern is consistent with previous studies [174].

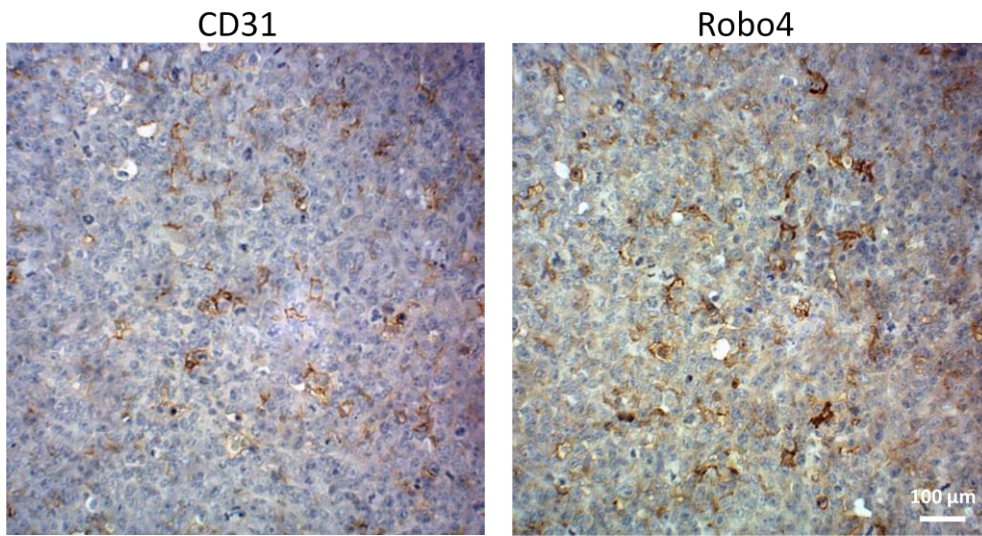


Figure 6.10 Expression of Robo4 in the vasculature of the Lewis lung carcinoma tumour. Immunohistochemistry was performed on Lewis lung carcinoma tumour sections. CD31 or Robo4 antibody was used as the primary antibody. A similar staining pattern was observed in the tumour vasculature for both antibodies (This figure courtesy of Dr. F. Ahmed).

6. 11 Effect of Robo4 vaccination on growth of Lewis lung carcinoma in mice

To determine whether Robo4 vaccination affected tumour growth, a dose of 10^6 LLC cells were implanted into Robo4 vaccinated and control (Fc) mice. The cells were injected subcutaneously on the back of the mice and the growth of tumour was measured three times a week. The tumour volume was calculated according to the formula described previously. A significant delay of tumour growth was seen in the Robo4 vaccinated mice compared with that in control mice (**Figure 6.11**).

In order to elucidate the effect of the Robo4 specific immune response on the tumour vessels, tumour samples from both groups were harvested and fixed for further analysis.

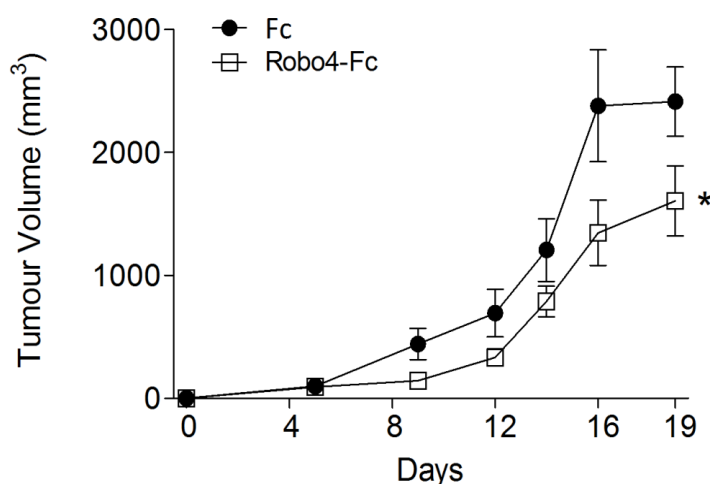


Figure 6.11 Tumour growth in Robo4 vaccinated mice. Each mouse was implanted with 10^6 Lewis lung carcinoma cells subcutaneously and the size of tumour measured three times weekly. Tumour volume was plotted and two-way ANOVA analysis of tumour volume was performed ($P < 0.05$, $n = 6$ per group \pm S.E.M.).

6.12 Increased vascular leakage and neutrophil infiltration in tumours grown in Robo4 vaccinated mice

Fibrinogen deposition has been used as an indicator of increased vascular leakage [175]. To examine whether Robo4 vaccination had an effect on the tumour vasculature, an immunofluorescence staining of fibrinogen was performed on tumour sections from control or Robo4 vaccinated mice. The fibrinogen antibody was labeled with FITC (green). Stained sections were analyzed with a confocal microscope and images were captured of random fields for statistical analysis. The fluorescence of fibrinogen was quantitated using Image J software. Quantification showed there was a significant increase of extravasated fibrinogen in the tumours derived from Robo4 vaccinated mice (**Figure 6.12a**), indicating increased vessel damage. Antibody to the neutrophil marker Gr-1 was used to stain tumour sections derived from control and Robo4 vaccinated mice. Images of random fields were taken on a confocal microscope. As shown in **Figure 6.12b**, increased neutrophil infiltration was observed in tumour tissue derived from Robo4 vaccinated mice confirming increased inflammation in these tumours.

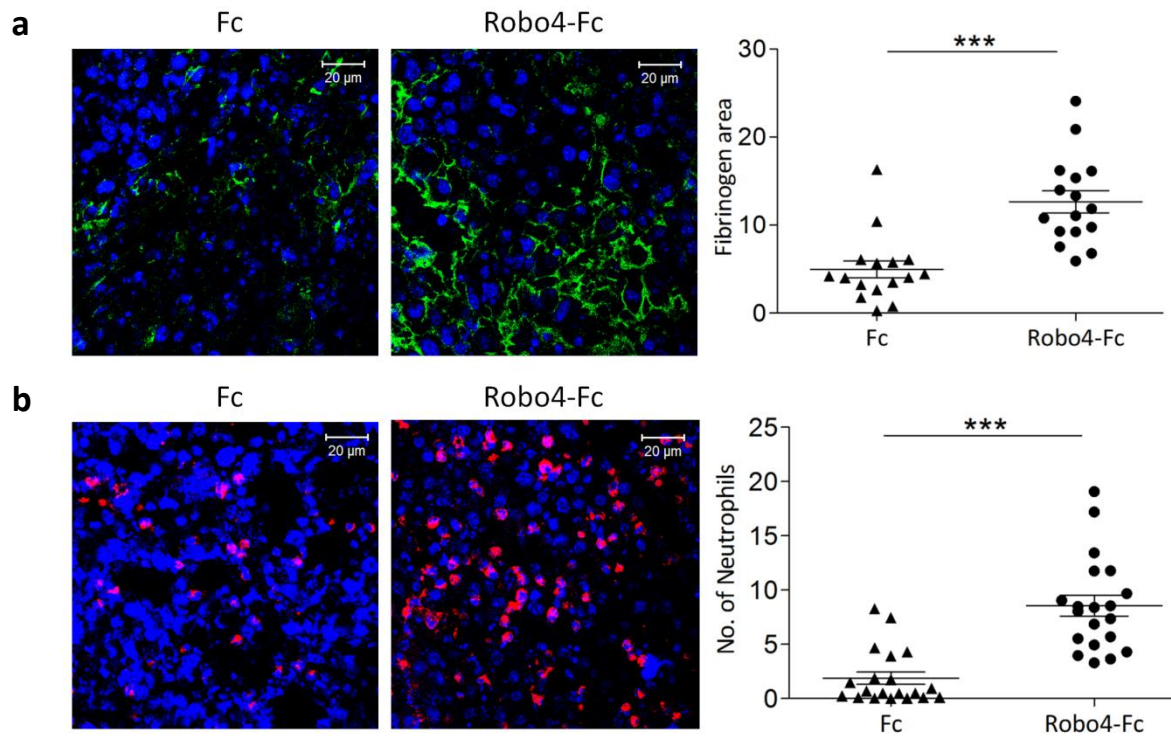


Figure 6.12 Staining of fibrinogen and neutrophils in Lewis lung tumour from control and Robo4 vaccinated mice. (a) Immunofluorescent staining of fibrinogen was performed using polyclonal fibrinogen antisera on 4 sections for 4 tumours per group. Quantification of the area positive for fibrinogen staining (green) determined using ImageJ. The mean and SEM are indicated ($p < 0.0001$, Mann-Whitney test). (b) Neutrophil invasion was assessed by immunofluorescent staining with monoclonal anti-Ly6G and Ly-6C antibody. The number of infiltrating neutrophils (red) was counted from 4 sections for each of 4 independent tumours. The mean and SEM are shown ($p < 0.0001$, Mann-Whitney test).

6.13 Soluble Robo4 conjugated to a carrier protein can induce a rapid protective antibody response in the absence of adjuvants

As strong adjuvants such as Freund's adjuvant cannot be used in humans, the efficiency of a milder conjugate vaccine immunization protocol was tested. Mice were primed with chicken gamma globulin (CGG). Five weeks later, after immunological memory had developed, mice were immunized with soluble Robo4-Fc chemically crosslinked to CGG without further adjuvants. Simultaneously tumor growth was induced by subcutaneous injection of Lewis lung carcinoma cells (**Figure 6.13a**). Vaccination of primed animals with Robo4-Fc crosslinked to CGG led to production of high levels of Robo4-specific IgG (**Figure 6.13b**) and significant and sustained growth inhibition of the tumour (**Figure 6.13c**). Instead of a prophylactic vaccine, these findings suggest the possibility of developing a treatment vaccine using carrier conjugated Robo4 as the immunogen.

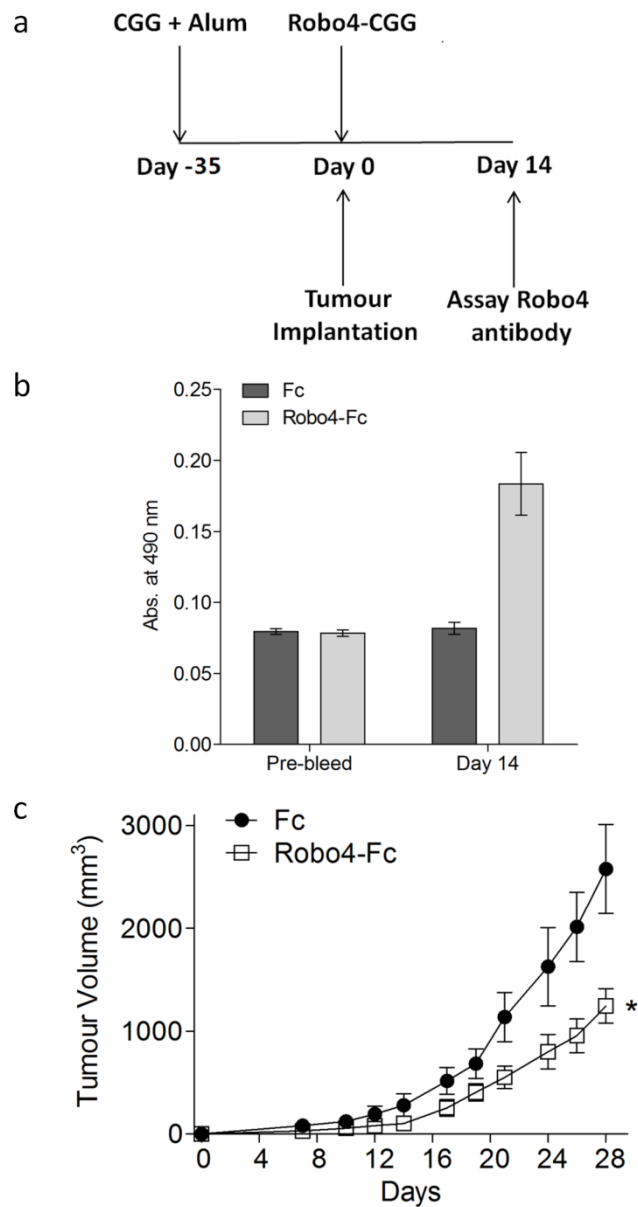


Figure 6.13 Induction of protective Robo4-specific antibody in carrier-primed animals (a) Mice receiving primary immunization i.p. with chicken gamma globulin (CGG) in alum [176] were reimmunised 5 weeks later subcutaneously with Robo4-Fc crosslinked to CGG [154]. Simultaneously 10^6 Lewis lung carcinoma cells were implanted subcutaneously. (b) Induction of Robo4-specific antibody two weeks post immunization with Robo4-CGG determined by ELISA. (c) Significant reduction in tumour growth in CGG primed and Robo4-Fc-CGG immunized animals compared to animals primed and Fc-CGG immunized ($P < 0.05$, $n = 6$ per group).

6.14 Tissue screen of Robo4 vaccinated mice

Although Robo4 vaccinated mice showed promising anti-angiogenic effects in the sponge implantation and tumour growth models, in the view of the therapeutic opportunity, it is essential to know whether the immune response against Robo4 impaired the normal vasculature. Organs including brain, heart, lung, liver, kidney and spleen were collected from both Robo4 immunized and control mice and H+E stained tissue sections.

As shown in **Figure 6.14**, the tissues from Robo4 immunized mice remained intact and exhibited no obvious difference to that from the control mice in terms of the morphology of tissues and the vasculature. During the immunization period, no weight loss, abnormal appearance or behavior was observed in Robo4 immunized mice. Taken together, targeting Robo4 may be a safe immunotherapeutic intervention.

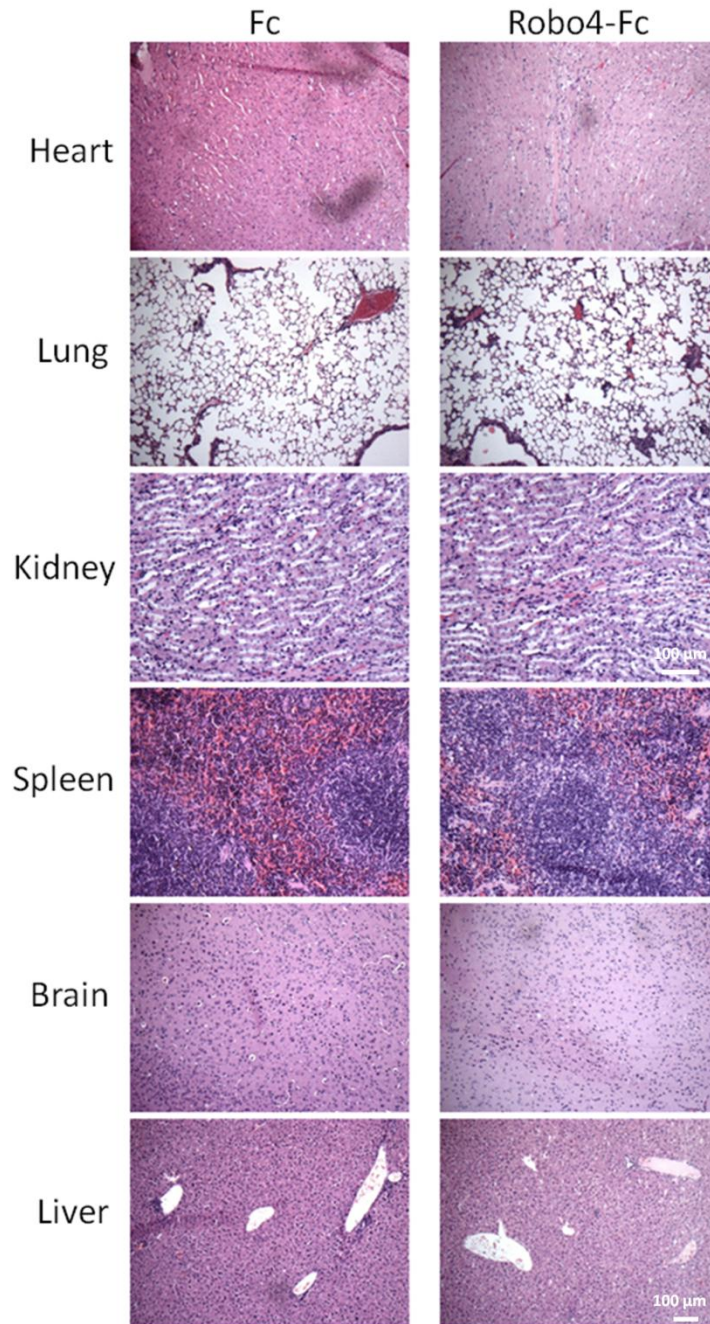


Figure 6.14 H+E staining of tissues from control and Robo4 vaccinated mice. Tissues including heart, lung, kidney, spleen, brain and liver were collected from control or Robo4 vaccinated mice. After fixation, paraffin embedding and sectioning, the tissues were stained with H+E.

6.15 Conclusions

Apart from chemotherapy and radiotherapy, immunotherapy has been a major research focus in cancer. Vaccination is an attractive approach to treat cancer, particularly in the context of vascular targeting. A well defined target is needed as an antigen for the vaccine. Robo4 is a pre-validated TEM that has been shown to be restricted to the vasculature in many cancer types. Robo4 was investigated as a vaccine immunogen in animal models of cancer. A strong antibody response was induced by vaccination of soluble mouse Robo4 protein with Freund's adjuvant, suggesting the immune tolerance to the self-antigen was successfully broken. The *in vivo* sponge implantation assay showed strong inhibition of angiogenesis in Robo4 vaccinated mice compared to control Fc vaccinated group. Robo4 vaccinated mice also showed retarded tumour growth in a Lewis lung carcinoma model. To explore the clinical possibility of a Robo4 vaccine, we developed an alternative immunization approach to avoid the use of strong adjuvants such as Freund's adjuvant. Mice were initially primed with CGG protein to develop immune memory and subsequently immunized with Robo4-CGG crosslinked complex in the absence of adjuvant. A strong antibody response was seen 14 days post-immunization. Tumour implanted on the day of immunization was inhibited in the Robo4 vaccinated mice compared with the control group. Histochemistry of organs derived from Robo4 vaccinated mice showed no apparent pathology. Taken together, these results suggest that vaccination against Robo4 holds promising therapeutic potential.

Chapter seven

Discussion

Discussion

Considerable effort has been invested in identifying and validating novel targets which are restricted to tumour vessels and known as Tumour Endothelial Markers [177]. The study which provided the first proof of principle that vascular targeting can be used to eradicate solid tumours in mice came from the work of Burrows and Thorpe in 1993 [63]. In 1997, these studies were extended when Huang and Thorpe reported that targeting the inducible truncated form of tissue factor (tTF) in the tumour vasculature of mice by an antibody-tTF complex resulted in significant tumour regressions [64]. In 2002, Thorpe's group proposed that the presence of anionic phospholipids on tumour vessels held potential for tumor vessel targeting and imaging [178] and more recently (2005), a monoclonal antibody against anionic phospholipids showed damage to the tumour vasculature and suppression of tumor growth in mouse models [179, 180]. The combined evidence strongly suggests that targeting molecules present in the tumour vasculature can lead to tumour shrinkage and cancer regression.

A number of approaches have been developed to identify TEMs. One of the most direct screens for TEMs has been the isolation of endothelium from normal and tumour colon followed by immediate extraction of RNA and conversion to SAGE libraries for transcriptome differentiation analysis [74]. Nine TEM's labeled TEM1 through TEM9 were identified from this work. However further studies showed that TEM1, also known as endosialin, was not expressed by endothelium but enriched in

tumour associated fibroblasts and pericytes [181]. However TEM1 retains potential as a tumour target and functionally, endosialin null mice show defective angiogenesis in orthotopically implanted colon tumours [83]. More recently, a monoclonal antibody targeting TEM8 was reported to inhibit pathological angiogenesis and tumour growth in multiple cancer models [182]. The EDB domain of fibronectin has been used in a clinical trial as an anti-cancer target [79]. The EDB domain is present only in fibronectin expressed in the foetus or tumours. Specific antibodies to the EDB domain have been used in several animal models to show an antitumour effect when coupled to TNF- α [183] interferon- γ [184] photosensitizer [185], interleukin 12 [186] interleukin 15, GM-CSF [187] or interleukin 2 [188]. Annexin A and Robo4 were also successfully identified and characterized as TEMs and have been reviewed [79]. Nevertheless, the expression profile of these targets is often not as specific and widespread as was expected and many putative TEMs to date have not entered clinical trials [22]. As a result, there exists an urgent need for new TEMs.

In **Chapter three**, a systematic approach was carried out to validate putative TEMs derived from a bioinformatics data mining prediction. Three candidates, CLEC14A, GBP4 and IKBKE were investigated.

It is shown here that CLEC14A is a novel TEM. This was shown on a human cancer tissue array by both immunofluorescence and immunohistochemical analysis. Immunofluorescent images of CLEC14A showed highly specific CLEC14A

expression on tumour vessels in a wide range of cancers and no or very low expression found in the adjacent healthy tissues. The co-localization with the human endothelial marker *Ulex* lectin confirmed its endothelial expression *in vivo*. The elevation of CLEC14A was also confirmed in endothelial isolates from hepatocellular carcinoma compared with that from healthy liver tissue [109]. Substantial CLEC14A expression was found across a range of common tumour types, including 100% of the ovarian and liver cancer, 90% of bladder and prostate cancer and 80% of breast cancer. The subcellular localization study of CLEC14A in HUVEC showed that it is mainly expressed on the cell membrane [109], which is a desirable property because cell surface proteins are easier to target. These collective findings confirm that CLEC14A is a novel TEM.

Guanylate binding proteins are the most abundant cellular proteins that belong to the GTPase superfamily. Seven members have been discovered in man: hGBP1-7 and all members are expressed by endothelial cells and can be induced by IFN- γ [88]. GBP1 has been closely studied in the last ten years and showed inhibitory effects on endothelial cell proliferation, migration and tube formation in response to inflammatory cytokines [90, 189]. In contrast, there are few publications on GBP4 and its expression profile and function remains unknown. Expression analysis in tumour / adjacent healthy tissues arrays showed that GBP4 is highly expressed on the tumour vascular, in some cases including the tumour cells. It is also of note that the expression of GBP4 was detected at a higher frequency in the adjacent healthy tissues

compared to CLEC14A. However, the term ‘adjacent healthy’ should be interpreted with some caution as the sections are from the same cancer patient. Therefore, when GBP4 expression was detected in adjacent healthy tissue, it may be due to the proximity of the tumour. In order to resolve the question of expression in healthy tissues, we performed a screen on tissue from healthy donors. No GBP4 expression was detected.

Since evidence shows that long-term inflammation contributes to the initiation and development of cancer [190], we have reason to suggest that the expression of GBP4 might be induced by inflammatory cytokines within the tumour microenvironment. To confirm this hypothesis, Dr. Mura performed a stimulation of IFN- γ or TNF- α on HUVEC and the results confirmed that the level of GBP4 indeed was strongly elevated in response to either IFN- γ or TNF- α treatment (unpublished data). However this result was partially contradictory to the finding from Sturzl’s group in 2007 where they reported GBP4 is only activated by IFN- γ but not by TNF- α [88].

In conclusion, GBP4 exhibits specificity to vessels throughout the tumour in a wide range of cancers with complete absence in healthy tissues. Although expression of GBP4 was detected in other cell types within or adjacent to the tumour, it remains a promising TEM that requires further investigation.

IKBKE is a relatively well-studied gene compared with CLEC14A and GBP4. The

expression profile of IKBKE suggests it is not a TEM due to its wide expression spectrum in healthy tissues. But interestingly, the expression of IKBKE was strongly detected in cells adjacent to the endothelium in healthy colon and healthy bladder tissues whereas in the case of carcinoma, IKBKE is enriched in the tumour vessels especially in the breast carcinomas, for which IKBKE is a validated oncogene [98]. Preliminary data showed that IKBKE siRNA knock down showed inhibition of HUVEC migration. This implies a role of IKBKE in controlling the transcription of genes that might be involved in endothelial cell migration. Although IKBKE is not a TEM in terms of its expression profile, it might play a role in mediating the motility of endothelial cells.

In **Chapter 4**, the functional role of CLEC14A in endothelial biology was explored. Blocking the transcription of CLEC14A by siRNA resulted in diminished endothelial cell migration in wound healing assays and reduced tube formation in a Matrigel assay [109]. Work by Rho et al. published simultaneously to our work independently confirmed these findings [191]. Interestingly, a similar inhibitory effect on migration was observed when either the endothelial specific gene ECSCR [192] or a pre-validated TEM Robo4 was knocked down in HUVEC [104], indicating a relationship between these endothelial specific genes and endothelial cell motility. Such a phenotype was also observed when polyclonal antiserum to CLEC14A was added to the assays, which prompted the idea of generating a monoclonal antibody to CLEC14A that can inhibit HUVEC migration. Indeed, amongst the five CLEC14A

monoclonal antibodies (CRT1-5), CRT3 showed modest but statistically significant inhibition in a dose dependent manner. This suggests that CRT3 can be used to investigate the effect on angiogenesis *in vivo*.

It has been shown that filopodia formation was strongly induced by ectopic overexpression of CLEC14A in 293T and CHO cells (R. Swain in [109]). As filopodia formation is a key feature of sprouting angiogenesis, one may speculate increased expression of CLEC14A could lead to an angiogenic phenotype. However, HUVEC migration was inhibited by overexpression of CLEC14A. These results suggest the expression level of CLEC14A in endothelial cells is critical for its motility. More interestingly, the same inhibitory effect was also observed when Robo4 was knocked down with siRNA or overexpressed in HUVEC [108].

Expression of CLEC14A in tumour vasculature suggests a role in pathological angiogenesis. However, CLEC14A also plays a role in physiological angiogenesis. Others have investigated the role of CLEC14A during zebrafish development. The data showed that CLEC14A expression begins at 5 hpf which coincides with the appearance of haemangioblasts [109]. The zebrafish ortholog of CLEC14A was previously identified as a putative endothelial specific gene by microarray analysis of zebrafish cloche mutants that fail to undergo haematopoiesis [193]. Also a recent study has shown that CLEC14A (called complement receptor C1qR-like gene) lies downstream of the transcription factor Etsrp, a factor required for vasculogenesis and

primitive myelopoiesis in the zebrafish [194]. This suggests that Etsrp may regulate hemangioblast migration by inducing CLEC14A expression. This is supported by data showing CLEC14A expression continues through the stages of development that involve angiogenesis. Furthermore, morpholino mediated knockdown of CLEC14A disrupts intersomitic vessels which are formed by sprouting angiogenesis from the dorsal aorta and this confirmed the role of CLEC14A in angiogenesis. Interestingly human CLEC14A mRNA injection rescued the vascular phenotype induced by knockdown of CLEC14A.

CLEC14A KO mice showed no defects during development, although Rho et al. showed that the mouse ortholog of CLEC14A is expressed in endothelial cells during development [191]. This contradicts the observation in CLEC14A knockdown zebrafish, however it is likely due to the difference in species. Interestingly, an *in vivo* tumour challenge experiment by others in the group showed a growth delay of a subcutaneous Lewis lung carcinoma tumour in the CLEC14A KO mice compared with that in WT mice. This suggests CLEC14A may be dispensable in physiological angiogenesis in the mouse yet playing an essential role in tumour angiogenesis. It is of note that a family member of CLEC14A, endosialin or TEM1 KO mice also display normal developmental angiogenesis unless challenged orthotopically with colon tumour fragment, in which tumour growth was retarded compared with WT [83]. No difference was observed in body weight or fertility between wild type and CLEC14A KO mice.

Many factors modulate the endothelial transcriptome in tumours, including hypoxia, oxidative stress, activation of growth factors and cytokines as well as low shear stress caused by the ill formed vessels within the tumour. Low shear stress and turbulent flow have been demonstrated as mechanical factors that regulate endothelial gene expression [195, 196]. Endothelial cells express 20000 genes of which 3 percent are regulated by shear stress [197]. SAGE analysis of endothelial cells cultured in static conditions or shear stress showed a marked differential expression in genes involved in cell proliferation, angiogenesis, extracellular matrix and cell-cell adhesion molecules and ATP synthesis [198]. Reduced shear stress strongly upregulates expression of CLEC14A and Robo4 mRNA in HUVEC cells [109]. In our zebrafish work, CLEC14A is expressed until 24 hpf when blood circulation begins. One explanation for the loss of CLEC14A at later time points could be that it is down regulated by shear stress. This hypothesis would be consistent with increased CLEC14A expression in the low flow environment of the tumour endothelium. In contrast, GBP4 is upregulated by shear stress at the RNA level in HUVEC (S. Durrant, unpublished work). Thus, these findings suggest a link between the induction of TEMs and the low shear stress environment that is associated with the tumour vasculature.

Lung cancer, as the leading cause of cancer related death, is still lacking a well-characterized vascular target. Although CLEC14A showed a high specificity and

a wide spectrum in tumours, its expression is low in lung cancer. In **Chapter 5**, expression profiling of lung endothelial cells isolated from NSCLC was performed using genomics technologies. A major obstacle that remains in the molecular profiling of endothelial cells is the difficulty of obtaining pure endothelial isolates. Previous molecular profiling work of lung endothelium was performed in mouse using *in vivo* fluorescent labeling of the vasculature to isolate ECs. In this study, Favre et al. isolated ECs from normal mouse lung and used the unpurified lung cells as the control, aiming at identifying endothelial specific genes [199]. A similar study was performed on colon endothelium which used long SAGE library sequencing to measure gene expression [74]. In this study, endothelial cells were isolated from human lung normal and tumour samples following downstream work involving deep sequencing and microarray technologies. Currently, deep sequencing technology has been intensively used in molecular profiling many tissue types and cell populations from different species. Yet not many studies have applied such technology to endothelium [200, 201], and not in the context of mRNA profiling of endothelial cells from lung cancer to identify putative vascular targets. Therefore our data provides novel insights into the molecular transcription signatures of endothelial cells isolated from fresh clinical samples.

Elevated MMP activity often associates with active angiogenesis and tumour growth in cancer [202]. MMP2 and MMP9 have been reported as being overexpressed in various solid tumours and have been associated with tumour grade and malignancy

and associated with increased metastasis in lung cancer [202]. In fact, the expression of MMP7 and MMP9 were previously found to be significantly upregulated in NSCLC compared with that of normal lung and benign lung tumour [203]. The MMPs expression profile is consistent with these previous findings and support the potential therapeutic use of MMP inhibitors for lung cancer. Deep sequencing data also provided a snapshot of a panel of angiogenic associated gene including VEGF-A, IL8, Ang2, EPHB2, TEM2, TEM4 and TEM7 being elevated in lung tumour endothelium, confirming that tumour angiogenesis is a result of combined effects caused by multiple angiogenic factors and receptors.

Differential gene expression analysis of deep sequencing combined with microarray of normal and tumour endothelium from multiple lung cancer patients has identified 13 putative lung TEMs. Six putative lung TEMs including ROS1, STEAP1, BIRC5, GJB2, PCDH7 and PROM2 were validated by real-time qPCR and immunohistochemistry, displaying endothelial expression on placental and lung cancer tissues.

ROS1 belongs to the sevenless subfamily of tyrosine kinase insulin receptor genes. ROS1 is a proto-oncogene and highly expressed in a variety of tumor cell lines [204-208]. Recently chromosomal rearrangement of ROS1 has been detected in a sub population of NSCLC patient [209-211]. Despite of intensive studies on ROS1 in lung cancer, no study regarding its role in the endothelial cell has been reported.

STEAP1 (six-transmembrane epithelial antigen of prostate 1) was the first member of a family of metalloredoxases identified as cell-surface antigens in prostate tissue [212, 213]. Its expression is highly increased in prostate, breast, bladder, colon, ovarian cancers and in Ewing's sarcoma [214], indicating STEAP1 may function as a universal tumor antigen. Alves and colleagues showed that STEAP1 peptides can be used to stimulate CD8⁺ T cells in healthy people, enabling them to recognize STEAP1 expressing tumor cells, suggesting that STEAP1 may be a useful target for cancer immunotherapy [215]. Similar to ROS1, research on STEAP1 was predominantly focused on its role in tumour cells. Its expression and function in endothelial cells and angiogenesis remains unexplored.

BIRC5 (baculoviral inhibitor of apoptosis repeat-containing 5) or survivin, belongs to the family of inhibitors of apoptosis. BIRC5 inhibits caspase activation to regulate apoptosis. Disruption of the BIRC5 signaling pathway leads to tumour cell apoptosis and growth delay. BIRC5 protein is present in a range of tumour cells and fetal tissues but is rarely detectable in healthy tissues [216]. One can speculate that the presence of BIRC5 on the lung tumour vasculature could be induced by the stressed endothelial cells which are struggling to survive in the abnormal tumour vasculature.

GJB2 (Gap junction beta-2) also known as connexin-26, belongs to the Connexins family. Connexins are essential for many physiological processes and embryonic

development including the microvasculature. Mutations in connexins can cause functional and developmental abnormalities. Defects in GJB2 lead to the most common form of congenital deafness [217]. Thus, most GJB2 studies have centered on this field and very little is known about GJB2 in association with endothelial cells and lung cancer.

PCDH7 and PROM2 are less studied genes compared with other identified targets. PCDH7 belongs to the protocadherin gene family, a subfamily of the cadherin superfamily. PCDH7 encodes a single transmembrane protein that is thought to function in cell-cell recognition and adhesion. PROM2 is a member of the prominin family of pentaspan membrane glycoproteins. The limited literature of these two targets makes them exceptionally attractive for further characterization.

From a technical point of view, investigation of laser microdissection technology in this report has demonstrated several critical points suggesting that such technology is not suitable for isolating lung endothelium: 1. Vessel visualization on the slides caused RNA degradation. 2. The vessel mural cells were impossible to separate from the endothelium and this would compromise the purity of the cell population. 3. Frozen normal lung slides showed poor morphology which was due to the cavities in the tissue. In contrast, the *Ulex*-bead isolation approach has been proven an effective approach to obtain a pure endothelial population from lung. Because of the significant increase in purity and amount of RNA, this approach permitted the 2nd generation

sequencing technology, which is a new technology and the results could be compared with microarray data.

The ineffectiveness of the common treatments for lung cancer prompted the search for alternative approaches for NSCLC. Although tyrosine kinase inhibitors of EGFR initially showed promising outcome in several trials, resistance was eventually developed in all patients [111]. The development of anti-angiogenic drugs such as VEGF (receptor) blockers has aroused general interest in the lung tumour vasculature. The use of such drugs in treating NSCLC patients has been investigated in early clinical trials. However, concerns have arisen from the inefficacy in tumour regression and lack of effective biomarkers for patient selection. Thus molecular profiling the tumour vasculature in lung cancer will not only enhance our understanding of molecules involved in this disease but also may provide biomarkers and targets that have therapeutic potential.

Evidence has been presented that vaccination to antigens over-expressed on the tumour vasculature holds therapeutic potential [132, 133]. For example, a significant delay in tumour growth and increased median survival rate by oral DNA vaccination against VEGFR2 has been observed in mice [134-136]. Similar effects were seen when mice were immunized with VEGFR1 or VEGFR2 derived peptides [137, 138]. In **Chapter 6**, investigation of a pre-validated TEM Robo4 as a cancer vaccine immunogen has been carried out. Robo4 was firstly characterized as a TEM in a wide

range of human carcinomas and absent in normal tissues in 2002 [73]. In 2005, Sukhatme's paper confirmed that Robo4 is a TEM in lung, liver and kidney [108]. Robo4 was reported to be expressed in mouse adult tissue including lung and brain by northern blot [107] however the expression level was not compared to that in tumours. A recent study has shown that the tumour vasculature in a mouse melanoma model can be imaged by magnetic resonance imaging (MRI) using Robo4 antibody coupled nanoparticles [218]. These findings, justify the attempt to induce an anti-Robo4 antibody response by vaccination and investigate its effect on angiogenesis and tumour growth.

Immune tolerance to Robo4 was successfully broken in mice using self-antigen, recombinant mouse Robo4 protein. This was the first attempt to induce a specific immune response against Robo4 *in vivo*. Protein immunization tends to induce Ig class switching to IgG1 isotype and this isotype is associated with T helper 2-type immunity [169]. After immunization, a high level of IgG1 was detected compared to other isotypes including IgG2b and IgG3. The subsequent sponge implantation experiment exhibited a dramatic anti-angiogenic effect. Thus, the immune response to Robo4 and most likely the Robo4-specific antibody, interrupted the development of new blood vessels within the implanted sponges. Delay in Lewis lung carcinoma growth and tumour vascular damage was presumably the result of Robo4 antibodies that attack the tumour endothelium by mediating antibody dependent cell-mediated cytotoxicity. During this process, effector cells including monocytes or NK cells were

directed to the tumour vasculature by crosslinking of their Fc receptors to the induced immunoglobulin, which subsequently led to apoptosis of the target cells [219]. Similar effects have been demonstrated for B cell expressed CD20 as the target antigen, in which monoclonal IgG1 antibody caused B cell depletion by interactions with Fc γ RIII [220], expressed on natural killer cells [221].

Instead of using Freund's adjuvant, conjugation of Robo4 to a foreign protein CGG resulted in a strong anti-Robo4 response and retarded tumour growth. This strategy overcame the absence of Robo4 specific T cell help due to central tolerance. In addition, pre-existing immunity to the CGG leads to rapid B cell activation through recruitment of help from CGG-specific memory T cells [176]. Hence conjugating Robo4 to carrier proteins routinely used in human conjugate vaccines such as tetanus or diphtheria toxoid, may produce a vaccine that would rapidly develop protective antibody responses.

The promise of anti-vascular immunisation in a clinical setting has been shown by tumour regression in some patients with brain tumours inoculated with glutaraldehyde-fixed human umbilical vein endothelial cells (HUVECs) which had been cultured for a number of passages prior to use. These patients developed HUVEC-specific antibodies which, although the antibodies were not characterized, may have recognized Robo4. Robo4 is expressed by HUVEC in tissue culture due to the lack of fluid shear stress [109]. The use of whole endothelial cell vaccines has the

advantage of presenting a set of identified or unknown targets to the immune system. However because of the same property, the expression or presentation level of the 'real targets' might be masked to a certain extent by other unrelated antigens.

A key consideration for vascular targeting strategies is the effect these treatments might have on the normal vasculature. While in the HUVEC-immunised patients no adverse effects were observed, gastrointestinal bleeding was observed in a pancreatic cancer trial using vaccination to peptides from VEGFR-1 [222]. Given the importance of VEGFR signalling in tumour angiogenesis, and the emergence of VEGF targeted therapies, such as bevacizumab, as approved anti-cancer therapies, significant effort has gone into immune targeting of this signalling pathway (reviewed in [166]). Though effective, in some cases wound healing was negatively affected. Indeed prolonged use of VEGF-based anti-angiogenics has highlighted a role for VEGF signalling in the maintenance of the normal vasculature [223].

Delta-like 4 is an endothelial expressed protein induced by hypoxia [224], it also plays a critical role in angiogenesis through its activation of Notch signalling [225]. DLL4 is expressed on the sprouting tip cells [226] and on vessels in a number of tumours, including breast cancer, colon cancer and glioblastoma [227-229], making it an attractive tumour vascular target. Vaccination against DLL4 using a DNA-based approach has shown anti-tumour effects [146], but its suitability as a target has been called into question as prolonged blockade of DLL4 signalling was found to actually

induce vascular neoplasms [230]. Vaccination of Robo4, as reported here shows there were no obvious delays in wound healing after sponge implantation, and histological analysis of heart, lung, kidney, spleen, brain or liver showed no differences between control and Robo4 vaccinated mice, which indicates that targeting Robo4 may be a safe immunotherapeutic intervention. It is worth mentioning that vaccination against self-antigen does not normally induce a permanent response. A recent study showed that antibody titres dropped to the baseline level seven months after the vaccination of EDB-fibronectin with Freund's adjuvant [231].

TEM expression varies in different tumour types [109]. The extra-domain B of fibronectin is expressed in a high percentage of certain brain tumours such as meningiomas and in a half of lung cancers, but in less than a quarter of the breast, colon and pancreatic cancers examined [232]. In an experimental mouse system this antigen was also successfully used to reduce tumour growth when used as an immunogen, with no obvious adverse effects [67]. But the applicability of this, and indeed any other TEM, as a therapeutic target will be limited to those tumour types found expressing it. Robo4 was found expressed in over 60% of pancreatic, bladder, prostate, stomach, lung and kidney cancer, and in a lower percentage of a number of other common tumour types, suggesting that a Robo4 targeted vaccination strategy may be effective in a variety of cancers, including cancer of the pancreas and lung which remain difficult to treat [233, 234]. Variation in TEM expression in different

tumour types justifies the concurrent study of several as targets for novel anti-cancer therapies.

Different strategies of immunotherapy have emerged to target the tumour vasculature. Abengoza et al. recently showed that EphrinB2 antibody treatment alone inhibited VEGF-mediated angiogenesis in a Matrigel plug assay and caused reduction in tumour vascular density and growth delay in a xenografted tumor model [235]. Photosensitizer conjugated antibody to EDB domain of fibronectin selectively disrupted tumour vasculature and led to complete tumour ablation in both mouse and human xenograft models [236]. Modified T cells such as the use of engineered chimeric antigen receptor (CAR) have also been investigated in vascular targeting. Chinnasamy and colleagues showed that transferred VEGFR2 CAR infected T cells resulted in tumour growth inhibition in multiple tumour models [66].

Compared to the current variety of immunotherapy in vascular targeting, vaccination is a practical approach that has clear advantages. Because of the simplicity, vaccination is considered more cost-effective compared to other immunotherapeutic approaches such as antibody conjugates or engineered T cells which are labor intensive. Secondly, vaccination of TEMs harnesses the body's own immune system to produce antibodies with anti-tumour effects which is less arduous for the patient than current popular approaches involving repeated infusion of therapeutic antibody. Depending on the type of delivery, it is possible to generate not only a humoral

response, but also cytotoxic T cell responses which can augment the anti-tumour effect [237].

The function of Robo4 in endothelial cells has been studied over the last ten years but remains controversial. Proposed functions fall broadly into two categories and have been reviewed in Legg et al. [102]. (i) A pro-filopodia, pro-migratory, pro-angiogenic role and (ii) an anti-migratory stabilization of the existing vasculature role. Thus, in support of a pro-angiogenic function, Sheldon et al. showed that Robo4 knockdown by siRNA inhibited endothelial cell migration, tube formation and overexpression of Robo4 strongly induced filopodia in endothelial cells [104]. Kaur et al. performed a modified Boyden chamber assay on Robo4 knockdown cells and found a similar effect [238]. In contrast, work originating primarily from the laboratory of Dean Li has used knockout mice to show that Robo4 stabilised the vasculature in for example retinal injury. Thus, in mouse models of retinal and choroidal vascular disease, Robo4 knockout mice showed higher vascular leakage and permeability in response to exogenously administered VEGF [239]. It is of interest that the endothelial transmembrane protein Unc5B has recently been shown to be a ligand for Robo4 [240]. When Robo4 binds Unc5B on an adjacent endothelial cell, Unc5B releases an anti-migratory stabilizing signal.

The apparently conflicting observations described above could be reconciled if the function of Robo4 were context dependant. We propose the working hypothesis that

in a tip cell, unligated Robo4 stimulates filopodia formation and migration, whereas in a phalanx cell it binds Unc5B on adjacent phalanx cells leading to an overall stabilization of the vasculature. Finally, the identification of Unc5B as a ligand of Robo4 could explain the inhibitory, anti-angiogenic effects of the extracellular domain of Robo4 previously described [106]. Unc5B is highly expressed on endothelial tip cells [241, 242] and binding of soluble Robo4 to Unc5B may initiate an inhibitory signal.

Appendix

Zhuang *et al.* publications

Oncogene (2011) 1–13
© 2011 Macmillan Publishers Limited All rights reserved 0950-9232/11
www.nature.com/onc



ORIGINAL ARTICLE

Identification and angiogenic role of the novel tumor endothelial marker CLEC14A

M Mura^{1,7}, RK Swain^{1,7}, X Zhuang^{1,7}, H Vorschmitt¹, G Reynolds², S Durant¹, JFJ Beesley¹, JMJ Herbert¹, H Sheldon³, M Andre³, S Sanderson³, K Glen⁴, N-T Luu⁴, HM McGettrick⁴, P Antczak⁵, F Falciani⁵, GB Nash⁴, Zs Nagy⁶ and R Bicknell^{1,3}

¹Angiogenesis Group, Centre for Cardiovascular Sciences, Institute for Biomedical Research, Schools of Immunity and Infection and Cancer Sciences, College of Medical and Dental Sciences, University of Birmingham, Birmingham, UK; ²Liver Laboratories, Institute for Biomedical Research, School of Immunity and Infection, College of Medical and Dental Sciences, University of Birmingham, Birmingham, UK; ³Cancer Research UK Angiogenesis Group, Institute of Molecular Medicine, University of Oxford, John Radcliffe Hospital, Oxford, UK; ⁴Centre for Cardiovascular Sciences, School of Clinical and Experimental Research, College of Medical and Dental Sciences, University of Birmingham, Birmingham, UK; ⁵School of Biosciences, University of Birmingham, Edgbaston, Birmingham, UK and ⁶Neurodegeneration and Repair Group, School of Clinical and Experimental Medicine, College of Medicine and Dentistry, University of Birmingham, Birmingham, UK

Advances in the Cellular and Molecular Biology of Angiogenesis



Shear stress, tip cells and regulators of endothelial migration

Xiaodong Zhuang^{*1}, Darren Cross[†], Victoria L. Heath^{*} and Roy Bicknell^{*1,2}

^{*}Angiogenesis Group, Institute for Biomedical Research, College of Medicine and Dentistry, University of Birmingham, Edgbaston, Birmingham B15 2TT, U.K., and [†]AstraZeneca plc, Mereside, Alderley Park, Macclesfield, Cheshire SK10 4TG, U.K.

References

1. Vandenbroucke, E., et al., *Regulation of endothelial junctional permeability*. Ann N Y Acad Sci, 2008. **1123**: p. 134-45.
2. Minshall, R.D. and A.B. Malik, *Transport across the endothelium: regulation of endothelial permeability*. Handb Exp Pharmacol, 2006(176 Pt 1): p. 107-44.
3. Sato, Y. and D.B. Rifkin, *Inhibition of endothelial cell movement by pericytes and smooth muscle cells: activation of a latent transforming growth factor-beta 1-like molecule by plasmin during co-culture*. J Cell Biol, 1989. **109**(1): p. 309-15.
4. Vanhoutte, P.M., et al., *Endothelial dysfunction and vascular disease*. Acta Physiol (Oxf), 2009. **196**(2): p. 193-222.
5. Carmeliet, P. and R.K. Jain, *Molecular mechanisms and clinical applications of angiogenesis*. Nature, 2011. **473**(7347): p. 298-307.
6. Chung, A.S. and N. Ferrara, *Developmental and pathological angiogenesis*. Annu Rev Cell Dev Biol, 2011. **27**: p. 563-84.
7. Gerhardt, H., et al., *VEGF guides angiogenic sprouting utilizing endothelial tip cell filopodia*. J Cell Biol, 2003. **161**(6): p. 1163-77.
8. Mazzone, M., et al., *Heterozygous deficiency of PHD2 restores tumor oxygenation and inhibits metastasis via endothelial normalization*. Cell, 2009. **136**(5): p. 839-51.
9. Risau, W., *Mechanisms of angiogenesis*. Nature, 1997. **386**(6626): p. 671-4.
10. Swift, M.R. and B.M. Weinstein, *Arterial-venous specification during development*. Circ Res, 2009. **104**(5): p. 576-88.
11. Adams, R.H. and K. Alitalo, *Molecular regulation of angiogenesis and lymphangiogenesis*. Nat Nat Rev Mol Cell Biol, 2007. **8**(6): p. 464-78.
12. Jain, R.K., *Molecular regulation of vessel maturation*. Nat Med, 2003. **9**(6): p. 685-93.
13. Potente, M., H. Gerhardt, and P. Carmeliet, *Basic and therapeutic aspects of angiogenesis*. Cell, 2011. **146**(6): p. 873-87.
14. Mignatti, P. and D.B. Rifkin, *Plasminogen activators and matrix metalloproteinases in angiogenesis*. Enzyme Protein, 1996. **49**(1-3): p. 117-37.
15. Moses, M.A., *The regulation of neovascularization of matrix metalloproteinases and their inhibitors*. Stem Cells, 1997. **15**(3): p. 180-9.
16. Lamalice, L., F. Le Boeuf, and J. Huot, *Endothelial cell migration during angiogenesis*. Circ Res, 2007. **100**(6): p. 782-94.
17. Makanya, A.N., R. Hlushchuk, and V.G. Djonov, *Intussusceptive angiogenesis and its role in vascular morphogenesis, patterning, and remodeling*. Angiogenesis, 2009. **12**(2): p. 113-23.
18. Burri, P.H., R. Hlushchuk, and V. Djonov, *Intussusceptive angiogenesis: its emergence, its characteristics, and its significance*. Dev Dyn, 2004. **231**(3): p. 474-88.
19. Fang, S. and P. Salven, *Stem cells in tumor angiogenesis*. J Mol Cell Cardiol, 2011. **50**(2): p. 290-5.
20. AMP-Lab, <http://www.amplab.de/angiogenesis.html>: p. Assay of angiogenesis.
21. Gimbrone, M.A., Jr., et al., *Tumor growth and neovascularization: an experimental model using the rabbit cornea*. J Natl Cancer Inst, 1974. **52**(2): p. 413-27.
22. Heath, V.L. and R. Bicknell, *Anticancer strategies involving the vasculature*. Nat Rev Clin

- Oncol, 2009. **6**(7): p. 395-404.
23. Chung, A.S., J. Lee, and N. Ferrara, *Targeting the tumour vasculature: insights from physiological angiogenesis*. Nat Rev Cancer, 2010. **10**(7): p. 505-14.
 24. Nussenbaum, F. and I.M. Herman, *Tumor angiogenesis: insights and innovations*. J Oncol, 2010. **2010**: p. 132641.
 25. Folkman, J., *Tumor angiogenesis: therapeutic implications*. N Engl J Med, 1971. **285**(21): p. 1182-6.
 26. Davidoff, A.M. and J.J. Kandel, *Antiangiogenic therapy for the treatment of pediatric solid malignancies*. Semin Pediatr Surg, 2004. **13**(1): p. 53-60.
 27. Kerbel, R. and J. Folkman, *Clinical translation of angiogenesis inhibitors*. Nat Rev Cancer, 2002. **2**(10): p. 727-39.
 28. Ferrara, N., *Vascular endothelial growth factor*. Arterioscler Thromb Vasc Biol, 2009. **29**(6): p. 789-91.
 29. Kim, K.J., et al., *Inhibition of vascular endothelial growth factor-induced angiogenesis suppresses tumour growth in vivo*. Nature, 1993. **362**(6423): p. 841-4.
 30. Ellis, L.M. and D.J. Hicklin, *VEGF-targeted therapy: mechanisms of anti-tumour activity*. Nat Rev Cancer, 2008. **8**(8): p. 579-91.
 31. Ferrara, N. and T. Davis-Smyth, *The biology of vascular endothelial growth factor*. Endocr Rev, 1997. **18**(1): p. 4-25.
 32. Hanahan, D. and J. Folkman, *Patterns and emerging mechanisms of the angiogenic switch during tumorigenesis*. Cell, 1996. **86**(3): p. 353-64.
 33. Ferrara, N., *VEGF and the quest for tumour angiogenesis factors*. Nat Rev Cancer, 2002. **2**(10): p. 795-803.
 34. Carmeliet, P., et al., *Abnormal blood vessel development and lethality in embryos lacking a single VEGF allele*. Nature, 1996. **380**(6573): p. 435-9.
 35. Ferrara, N., et al., *Heterozygous embryonic lethality induced by targeted inactivation of the VEGF gene*. Nature, 1996. **380**(6573): p. 439-42.
 36. Lohela, M., et al., *VEGFs and receptors involved in angiogenesis versus lymphangiogenesis*. Curr Opin Cell Biol, 2009. **21**(2): p. 154-65.
 37. Liu, Y., et al., *Hypoxia regulates vascular endothelial growth factor gene expression in endothelial cells. Identification of a 5' enhancer*. Circ Res, 1995. **77**(3): p. 638-43.
 38. Alitalo, K. and P. Carmeliet, *Molecular mechanisms of lymphangiogenesis in health and disease*. Cancer Cell, 2002. **1**(3): p. 219-27.
 39. Hirakawa, S., et al., *VEGF-A induces tumor and sentinel lymph node lymphangiogenesis and promotes lymphatic metastasis*. J Exp Med, 2005. **201**(7): p. 1089-99.
 40. Waltenberger, J., et al., *Different signal transduction properties of KDR and Flt1, two receptors for vascular endothelial growth factor*. J Biol Chem, 1994. **269**(43): p. 26988-95.
 41. Seetharam, L., et al., *A unique signal transduction from FLT tyrosine kinase, a receptor for vascular endothelial growth factor VEGF*. Oncogene, 1995. **10**(1): p. 135-47.
 42. Hiratsuka, S., et al., *Involvement of Flt-1 tyrosine kinase (vascular endothelial growth factor receptor-1) in pathological angiogenesis*. Cancer Res, 2001. **61**(3): p. 1207-13.
 43. Hiratsuka, S., et al., *MMP9 induction by vascular endothelial growth factor receptor-1 is involved in lung-specific metastasis*. Cancer Cell, 2002. **2**(4): p. 289-300.
 44. Kaplan, R.N., et al., *VEGFR1-positive haematopoietic bone marrow progenitors initiate the*

- pre-metastatic niche*. Nature, 2005. **438**(7069): p. 820-7.
45. Karkkainen, M.J., et al., *Vascular endothelial growth factor C is required for sprouting of the first lymphatic vessels from embryonic veins*. Nat Immunol, 2004. **5**(1): p. 74-80.
 46. Karkkainen, M.J., et al., *Missense mutations interfere with VEGFR-3 signalling in primary lymphoedema*. Nat Genet, 2000. **25**(2): p. 153-9.
 47. Ogawa, S., et al., *A novel type of vascular endothelial growth factor, VEGF-E (NZ-7 VEGF), preferentially utilizes KDR/Flk-1 receptor and carries a potent mitotic activity without heparin-binding domain*. J Biol Chem, 1998. **273**(47): p. 31273-82.
 48. Kiba, A., et al., *VEGFR-2-specific ligand VEGF-E induces non-edematous hyper-vascularization in mice*. Biochem Biophys Res Commun, 2003. **301**(2): p. 371-7.
 49. Zheng, Y., et al., *Chimeric VEGF-E(NZ7)/PlGF promotes angiogenesis via VEGFR-2 without significant enhancement of vascular permeability and inflammation*. Arterioscler Thromb Vasc Biol, 2006. **26**(9): p. 2019-26.
 50. William D. Figg, J.F., *Angiogenesis - An Integrative Approach From Science to Medicine*. 2008: p. 90.
 51. Ferrara, N., *VEGF as a therapeutic target in cancer*. Oncology, 2005. **69 Suppl 3**: p. 11-6.
 52. Kazazi-Hyseni, F., J.H. Beijnen, and J.H. Schellens, *Bevacizumab*. Oncologist, 2010. **15**(8): p. 819-25.
 53. Raja, M.S., et al., *Ranibizumab treatment for neovascular age-related macular degeneration in patients with good baseline visual acuity (better than 6/12): 12-month outcomes*. Br J Ophthalmol, 2010. **94**(11): p. 1543-5.
 54. Pieramici, D.J. and R.L. Avery, *Ranibizumab: treatment in patients with neovascular age-related macular degeneration*. Expert Opin Biol Ther, 2006. **6**(11): p. 1237-45.
 55. Friberg, T.R., et al., *Pegaptanib sodium as maintenance therapy in neovascular age-related macular degeneration: the LEVEL study*. Br J Ophthalmol, 2010. **94**(12): p. 1611-7.
 56. Hernandez-Pastor, L.J., et al., *Cost-effectiveness of ranibizumab compared with pegaptanib in neovascular age-related macular degeneration*. Graefes Arch Clin Exp Ophthalmol, 2010. **248**(4): p. 467-76.
 57. Crawford, Y. and N. Ferrara, *Tumor and stromal pathways mediating refractoriness/resistance to anti-angiogenic therapies*. Trends Pharmacol Sci, 2009. **30**(12): p. 624-30.
 58. Claes, A. and W. Leenders, *Vessel normalization by VEGF inhibition. A complex story*. Cancer Biol Ther, 2008. **7**(7): p. 1014-6.
 59. Carmeliet, P. and R.K. Jain, *Principles and mechanisms of vessel normalization for cancer and other angiogenic diseases*. Nat Rev Drug Discov, 2011. **10**(6): p. 417-27.
 60. Ebos, J.M., et al., *Accelerated metastasis after short-term treatment with a potent inhibitor of tumor angiogenesis*. Cancer Cell, 2009. **15**(3): p. 232-9.
 61. Paez-Ribes, M., et al., *Antiangiogenic therapy elicits malignant progression of tumors to increased local invasion and distant metastasis*. Cancer Cell, 2009. **15**(3): p. 220-31.
 62. Loges, S., et al., *Silencing or fueling metastasis with VEGF inhibitors: antiangiogenesis revisited*. Cancer Cell, 2009. **15**(3): p. 167-70.
 63. Burrows, F.J. and P.E. Thorpe, *Eradication of large solid tumors in mice with an immunotoxin directed against tumor vasculature*. Proc Natl Acad Sci U S A, 1993. **90**(19): p. 8996-9000.
 64. Huang, X., et al., *Tumor infarction in mice by antibody-directed targeting of tissue factor to tumor vasculature*. Science, 1997. **275**(5299): p. 547-50.

65. He, J., et al., *Antiphosphatidylserine antibody combined with irradiation damages tumor blood vessels and induces tumor immunity in a rat model of glioblastoma*. Clin Cancer Res, 2009. **15**(22): p. 6871-80.
66. Chinnasamy, D., et al., *Gene therapy using genetically modified lymphocytes targeting VEGFR-2 inhibits the growth of vascularized syngenic tumors in mice*. J Clin Invest, 2010. **120**(11): p. 3953-68.
67. Huijbers, E.J., et al., *Vaccination against the extra domain-B of fibronectin as a novel tumor therapy*. FASEB J, 2010. **24**(11): p. 4535-44.
68. Siemann, D.W., *The unique characteristics of tumor vasculature and preclinical evidence for its selective disruption by Tumor-Vascular Disrupting Agents*. Cancer Treat Rev, 2011. **37**(1): p. 63-74.
69. Dachs, G.U. and D.J. Chaplin, *Microenvironmental control of gene expression: implications for tumor angiogenesis, progression, and metastasis*. Semin Radiat Oncol, 1998. **8**(3): p. 208-16.
70. Helmlinger, G., et al., *Interstitial pH and pO₂ gradients in solid tumors in vivo: high-resolution measurements reveal a lack of correlation*. Nat Med, 1997. **3**(2): p. 177-82.
71. Padera, T.P., et al., *Pathology: cancer cells compress intratumour vessels*. Nature, 2004. **427**(6976): p. 695.
72. Bicknell, R. and A.L. Harris, *Novel angiogenic signaling pathways and vascular targets*. Annu Rev Pharmacol Toxicol, 2004. **44**: p. 219-38.
73. Huminiecki, L., et al., *Magic roundabout is a new member of the roundabout receptor family that is endothelial specific and expressed at sites of active angiogenesis*. Genomics, 2002. **79**(4): p. 547-52.
74. St Croix, B., et al., *Genes expressed in human tumor endothelium*. Science, 2000. **289**(5482): p. 1197-202.
75. Ho, M., et al., *Identification of endothelial cell genes by combined database mining and microarray analysis*. Physiol Genomics, 2003. **13**(3): p. 249-62.
76. Oh, P., et al., *Subtractive proteomic mapping of the endothelial surface in lung and solid tumours for tissue-specific therapy*. Nature, 2004. **429**(6992): p. 629-35.
77. Huminiecki, L. and R. Bicknell, *In silico cloning of novel endothelial-specific genes*. Genome Res, 2000. **10**(11): p. 1796-806.
78. Herbert, J.M., et al., *A novel method of differential gene expression analysis using multiple cDNA libraries applied to the identification of tumour endothelial genes*. BMC Genomics, 2008. **9**: p. 153.
79. Neri, D. and R. Bicknell, *Tumour vascular targeting*. Nat Rev Cancer, 2005. **5**(6): p. 436-46.
80. Zelensky, A.N. and J.E. Gready, *The C-type lectin-like domain superfamily*. FEBS J, 2005. **272**(24): p. 6179-217.
81. Drickamer, K., *C-type lectin-like domains*. Curr Opin Struct Biol, 1999. **9**(5): p. 585-90.
82. Cambi, A. and C. Figdor, *Necrosis: C-type lectins sense cell death*. Curr Biol, 2009. **19**(9): p. R375-8.
83. Nanda, A., et al., *Tumor endothelial marker 1 (Tem1) functions in the growth and progression of abdominal tumors*. Proc Natl Acad Sci U S A, 2006. **103**(9): p. 3351-6.
84. Greenlee, M.C., S.A. Sullivan, and S.S. Bohlsion, *CD93 and related family members: their role in innate immunity*. Curr Drug Targets, 2008. **9**(2): p. 130-8.

85. Maruyama, I., C.E. Bell, and P.W. Majerus, *Thrombomodulin is found on endothelium of arteries, veins, capillaries, and lymphatics, and on syncytiotrophoblast of human placenta*. J Cell Biol, 1985. **101**(2): p. 363-71.
86. Esmon, C.T., *Thrombomodulin as a model of molecular mechanisms that modulate protease specificity and function at the vessel surface*. FASEB J, 1995. **9**(10): p. 946-55.
87. McCormick, S.M., et al., *DNA microarray reveals changes in gene expression of shear stressed human umbilical vein endothelial cells*. Proc Natl Acad Sci U S A, 2001. **98**(16): p. 8955-60.
88. Tripal, P., et al., *Unique features of different members of the human guanylate-binding protein family*. J Interferon Cytokine Res, 2007. **27**(1): p. 44-52.
89. Naschberger, E., et al., *Nuclear factor-kappaB motif and interferon-alpha-stimulated response element co-operate in the activation of guanylate-binding protein-1 expression by inflammatory cytokines in endothelial cells*. Biochem J, 2004. **379**(Pt 2): p. 409-20.
90. Guenzi, E., et al., *The helical domain of GBP-1 mediates the inhibition of endothelial cell proliferation by inflammatory cytokines*. EMBO J, 2001. **20**(20): p. 5568-77.
91. Lipnik, K., et al., *Interferon gamma-induced human guanylate binding protein 1 inhibits mammary tumor growth in mice*. Mol Med. **16**(5-6): p. 177-87.
92. Guimaraes, D.P., et al., *Interferon-inducible guanylate binding protein (GBP)-2: a novel p53-regulated tumor marker in esophageal squamous cell carcinomas*. Int J Cancer, 2009. **124**(2): p. 272-9.
93. Fellenberg, F., et al., *GBP-5 splicing variants: New guanylate-binding proteins with tumor-associated expression and antigenicity*. J Invest Dermatol, 2004. **122**(6): p. 1510-7.
94. Hayden, M.S. and S. Ghosh, *Signaling to NF-kappaB*. Genes Dev, 2004. **18**(18): p. 2195-224.
95. Tenover, B.R., et al., *Multiple functions of the IKK-related kinase IKKepsilon in interferon-mediated antiviral immunity*. Science, 2007. **315**(5816): p. 1274-8.
96. Fitzgerald, K.A., et al., *IKKepsilon and TBK1 are essential components of the IRF3 signaling pathway*. Nat Immunol, 2003. **4**(5): p. 491-6.
97. Sharma, S., et al., *Triggering the interferon antiviral response through an IKK-related pathway*. Science, 2003. **300**(5622): p. 1148-51.
98. Boehm, J.S., et al., *Integrative genomic approaches identify IKBKE as a breast cancer oncogene*. Cell, 2007. **129**(6): p. 1065-79.
99. Hutti, J.E., et al., *Phosphorylation of the tumor suppressor CYLD by the breast cancer oncogene IKKepsilon promotes cell transformation*. Mol Cell, 2009. **34**(4): p. 461-72.
100. Guo, J.P., et al., *Deregulation of IKBKE is associated with tumor progression, poor prognosis, and cisplatin resistance in ovarian cancer*. Am J Pathol, 2009. **175**(1): p. 324-33.
101. Kidd, T., et al., *Roundabout controls axon crossing of the CNS midline and defines a novel subfamily of evolutionarily conserved guidance receptors*. Cell, 1998. **92**(2): p. 205-15.
102. Legg, J.A., et al., *Slits and Roundabouts in cancer, tumour angiogenesis and endothelial cell migration*. Angiogenesis, 2008. **11**(1): p. 13-21.
103. Zhuang, X., et al., *Shear stress, tip cells and regulators of endothelial migration*. Biochem Soc Trans, 2011. **39**(6): p. 1571-5.
104. Sheldon, H., et al., *Active involvement of Robo1 and Robo4 in filopodia formation and endothelial cell motility mediated via WASP and other actin nucleation-promoting factors*. FASEB J, 2009. **23**(2): p. 513-22.
105. Kaur, S., et al., *Silencing of directional migration in roundabout4 knockdown endothelial cells*.

- BMC Cell Biol, 2008. **9**: p. 61.
106. Suchting, S., et al., *Soluble Robo4 receptor inhibits in vivo angiogenesis and endothelial cell migration*. FASEB J, 2005. **19**(1): p. 121-3.
 107. Park, K.W., et al., *Robo4 is a vascular-specific receptor that inhibits endothelial migration*. Dev Dev Biol, 2003. **261**(1): p. 251-67.
 108. Seth, P., et al., *Magic roundabout, a tumor endothelial marker: expression and signaling*. Biochem Biophys Res Commun, 2005. **332**(2): p. 533-41.
 109. Mura, M., et al., *Identification and angiogenic role of the novel tumor endothelial marker CLEC14A*. Oncogene, 2012. **31**(3): p. 293-305.
 110. Lanza, K.S.B.A.H.S.G.M., *MR Angiogenesis Imaging with Robo4- versus avbeta3- targeted Nanoparticles in the B16/F10 Mouse Melanoma Model*. 2010.
 111. Lovly, C.M. and D.P. Carbone, *Lung cancer in 2010: One size does not fit all*. Nat Rev Clin Oncol, 2011. **8**(2): p. 68-70.
 112. Gimbrone, M.A., Jr., R.S. Cotran, and J. Folkman, *Human vascular endothelial cells in culture. Growth and DNA synthesis*. J Cell Biol, 1974. **60**(3): p. 673-84.
 113. Jaffe, E.A., et al., *Culture of human endothelial cells derived from umbilical veins. Identification by morphologic and immunologic criteria*. J Clin Invest, 1973. **52**(11): p. 2745-56.
 114. Durr, E., et al., *Direct proteomic mapping of the lung microvascular endothelial cell surface in vivo and in cell culture*. Nat Biotechnol, 2004. **22**(8): p. 985-92.
 115. Kaneko, T., et al., *Gene expression analysis of immunostained endothelial cells isolated from formaldehyde-fixated paraffin embedded tumors using laser capture microdissection--a technical report*. Microsc Res Tech, 2009. **72**(12): p. 908-12.
 116. Kinnecom, K. and J.S. Pachter, *Selective capture of endothelial and perivascular cells from brain microvessels using laser capture microdissection*. Brain Res Brain Res Protoc, 2005. **16**(1-3): p. 1-9.
 117. Cunnea, P., et al., *Gene expression analysis of the microvascular compartment in multiple sclerosis using laser microdissected blood vessels*. Acta Neuropathol, 2010. **119**(5): p. 601-15.
 118. Hormia, M., V.P. Lehto, and I. Virtanen, *Identification of UEA I-binding surface glycoproteins of cultured human endothelial cells*. Cell Biol Int Rep, 1983. **7**(6): p. 467-75.
 119. Holthofer, H., et al., *Ulex europaeus I lectin as a marker for vascular endothelium in human tissues*. Lab Invest, 1982. **47**(1): p. 60-6.
 120. Cha, M.S., D.K. Rah, and K.H. Lee, *Isolation and pure culture of microvascular endothelial cells from the fetal skin*. Yonsei Med J, 1996. **37**(3): p. 186-93.
 121. Grimwood, J., R. Bicknell, and M.C. Rees, *The isolation, characterization and culture of human decidual endothelium*. Hum Reprod, 1995. **10**(8): p. 2142-8.
 122. Jackson, C.J., et al., *Binding of human endothelium to Ulex europaeus I-coated Dynabeads: application to the isolation of microvascular endothelium*. J Cell Sci, 1990. **96** (Pt 2): p. 257-62.
 123. Rafii, S., et al., *Isolation and characterization of human bone marrow microvascular endothelial cells: hematopoietic progenitor cell adhesion*. Blood, 1994. **84**(1): p. 10-9.
 124. Schatz, F., et al., *Human endometrial endothelial cells: isolation, characterization, and inflammatory-mediated expression of tissue factor and type 1 plasminogen activator inhibitor*. Biol Reprod, 2000. **62**(3): p. 691-7.

125. Rohrbeck, A. and J. Borlak, *Cancer genomics identifies regulatory gene networks associated with the transition from dysplasia to advanced lung adenocarcinomas induced by c-Raf-1*. PLoS PLoS One, 2009. **4**(10): p. e7315.
126. Slevin, M., et al., *Identification of a 'snapshot' of co-expressed angiogenic markers in laser-dissected vessels from unstable carotid plaques with targeted arrays*. J Vasc Res, 2010. **47**(4): p. 323-35.
127. Buckanovich, R.J., et al., *Use of immuno-LCM to identify the in situ expression profile of cellular constituents of the tumor microenvironment*. Cancer Biol Ther, 2006. **5**(6): p. 635-42.
128. Metzker, M.L., *Sequencing technologies - the next generation*. Nat Rev Genet, 2010. **11**(1): p. 31-46.
129. Tavakoli, J. and J.B. Aragon-Ching, *Mechanisms of drug resistance to vascular endothelial growth factor (VEGF) inhibitors*. Anticancer Agents Med Chem, 2010. **10**(8): p. 593-600.
130. Cheever, M.A. and C.S. Higano, *PROVENGE (Sipuleucel-T) in prostate cancer: the first FDA-approved therapeutic cancer vaccine*. Clin Cancer Res, 2011. **17**(11): p. 3520-6.
131. Abul K. Abbas, A.H.L., *Basic Immunology - Functions and Disorders of the Immune System*. 2007: p. 179-180.
132. Wada, S., et al., *Rationale for antiangiogenic cancer therapy with vaccination using epitope peptides derived from human vascular endothelial growth factor receptor 2*. Cancer Res, 2005. **65**(11): p. 4939-46.
133. Zhou, H., et al., *T cell-mediated suppression of angiogenesis results in tumor protective immunity*. Blood, 2005. **106**(6): p. 2026-32.
134. Petrovan, R.J., et al., *DNA vaccination against VEGF receptor 2 reduces atherosclerosis in LDL LDL receptor-deficient mice*. Arterioscler Thromb Vasc Biol, 2007. **27**(5): p. 1095-100.
135. Reisfeld, R.A., et al., *DNA vaccines designed to inhibit tumor growth by suppression of angiogenesis*. Int Arch Allergy Immunol, 2004. **133**(3): p. 295-304.
136. Reisfeld, R.A., et al., *DNA vaccines suppress tumor growth and metastases by the induction of anti-angiogenesis*. Immunol Rev, 2004. **199**: p. 181-90.
137. Ishizaki, H., et al., *Inhibition of tumor growth with antiangiogenic cancer vaccine using epitope peptides derived from human vascular endothelial growth factor receptor 1*. Clin Cancer Res, 2006. **12**(19): p. 5841-9.
138. Dong, Y., et al., *Identification of H-2Db-specific CD8+ T-cell epitopes from mouse VEGFR2 that can inhibit angiogenesis and tumor growth*. J Immunother, 2006. **29**(1): p. 32-40.
139. Lyons, J.M., 3rd, et al., *The role of VEGF pathways in human physiologic and pathologic angiogenesis*. J Surg Res, 2010. **159**(1): p. 517-27.
140. He, Q.M., et al., *Inhibition of tumor growth with a vaccine based on xenogeneic homologous fibroblast growth factor receptor-1 in mice*. J Biol Chem, 2003. **278**(24): p. 21831-6.
141. Ramage, J.M., et al., *Identification of an HLA-A*0201 cytotoxic T lymphocyte epitope specific to the endothelial antigen Tie-2*. Int J Cancer, 2004. **110**(2): p. 245-50.
142. Lee, S.H., et al., *Endoglin (CD105) is a target for an oral DNA vaccine against breast cancer*. Cancer Immunol Immunother, 2006. **55**(12): p. 1565-74.
143. Lou, Y.Y., et al., *Immunogene therapy of tumors with a vaccine based on the ligand-binding domain of chicken homologous integrin beta3*. Immunol Invest, 2002. **31**(1): p. 51-69.
144. Holmgren, L., et al., *A DNA vaccine targeting angiogenin inhibits angiogenesis and suppresses tumor growth*. Proc Natl Acad Sci U S A, 2006. **103**(24): p. 9208-13.

145. Wood, L.M., et al., *Targeting tumor vasculature with novel Listeria-based vaccines directed against CD105*. *Cancer Immunol Immunother*, 2011. **60**(7): p. 931-42.
146. Haller, B.K., et al., *Therapeutic efficacy of a DNA vaccine targeting the endothelial tip cell antigen delta-like ligand 4 in mammary carcinoma*. *Oncogene*, 2010. **29**(30): p. 4276-86.
147. Stura E.A., F.G.G., Wilson I.A, *Crystallization of Antibodies and Antibody-Antigen Complexes*. *Immunomethods*, 1993. **3**: p. 164-179.
148. Dwyer, M.A., et al., *Expression and characterization of a DNase I-Fc fusion enzyme*. *J Biol Chem*, 1999. **274**(14): p. 9738-43.
149. Trapnell, C., L. Pachter, and S.L. Salzberg, *TopHat: discovering splice junctions with RNA-Seq*. *Bioinformatics*, 2009. **25**(9): p. 1105-11.
150. Li, H., et al., *The Sequence Alignment/Map format and SAMtools*. *Bioinformatics*, 2009. **25**(16): **25**(16): p. 2078-9.
151. Anders, S. *HTSeq: Analysing high-throughput sequencing data with Python*. 2010; Available from: <http://www-huber.embl.de/users/anders/HTSeq/doc/overview.html>.
152. Anders, S. and W. Huber, *Differential expression analysis for sequence count data*. *Genome Biol*, 2010. **11**(10): p. R106.
153. Attia, M.A. and D.W. Weiss, *Immunology of spontaneous mammary carcinomas in mice. V. Acquired tumor resistance and enhancement in strain A mice infected with mammary tumor virus*. *Cancer Res*, 1966. **26**(8): p. 1787-800.
154. Garside, P., et al., *Visualization of specific B and T lymphocyte interactions in the lymph node*. *Science*, 1998. **281**(5373): p. 96-9.
155. Andersen, C.L., J.L. Jensen, and T.F. Orntoft, *Normalization of real-time quantitative reverse transcription-PCR data: a model-based variance estimation approach to identify genes suited for normalization, applied to bladder and colon cancer data sets*. *Cancer Res*, 2004. **64**(15): p. 5245-50.
156. Jacobs, J.P., C.M. Jones, and J.P. Baille, *Characteristics of a human diploid cell designated MRC-5*. *Nature*, 1970. **227**(5254): p. 168-70.
157. Verissimo, A.R., et al., *Functionally defining the endothelial transcriptome, from Robo4 to ECSCR*. *Biochem Soc Trans*, 2009. **37**(Pt 6): p. 1214-7.
158. Taraboletti, G. and R. Giavazzi, *Modelling approaches for angiogenesis*. *Eur J Cancer*, 2004. **40**(6): p. 881-9.
159. Liang, C.C., A.Y. Park, and J.L. Guan, *In vitro scratch assay: a convenient and inexpensive method for analysis of cell migration in vitro*. *Nat Protoc*, 2007. **2**(2): p. 329-33.
160. Lloyd, K.C., *A knockout mouse resource for the biomedical research community*. *Ann N Y Acad Acad Sci*, 2011. **1245**(1): p. 24-6.
161. Clement-Ziza, M., et al., *Stabilization of RNA during laser capture microdissection by performing experiments under argon atmosphere or using ethanol as a solvent in staining solutions*. *RNA*, 2008. **14**(12): p. 2698-704.
162. Fleige, S., et al., *Comparison of relative mRNA quantification models and the impact of RNA integrity in quantitative real-time RT-PCR*. *Biotechnol Lett*, 2006. **28**(19): p. 1601-13.
163. Fleige, S. and M.W. Pfaffl, *RNA integrity and the effect on the real-time qRT-PCR performance*. *Mol Aspects Med*, 2006. **27**(2-3): p. 126-39.
164. Sottile, J., *Regulation of angiogenesis by extracellular matrix*. *Biochim Biophys Acta*, 2004. **1654**(1): p. 13-22.

165. Wang, D., J.C. Anderson, and C.L. Gladson, *The role of the extracellular matrix in angiogenesis in malignant glioma tumors*. Brain Pathol, 2005. **15**(4): p. 318-26.
166. Matejuk, A., et al., *Vaccines targeting the neovasculature of tumors*. Vasc Cell, 2011. **3**(1): p. 7.
167. Grone, J., et al., *Robo1/Robo4: differential expression of angiogenic markers in colorectal cancer*. Oncol Rep, 2006. **15**(6): p. 1437-43.
168. Marlow, R., et al., *Vascular Robo4 restricts proangiogenic VEGF signaling in breast*. Proc Natl Acad Sci U S A, 2010. **107**(23): p. 10520-5.
169. Toellner, K.M., et al., *T helper 1 (Th1) and Th2 characteristics start to develop during T cell priming and are associated with an immediate ability to induce immunoglobulin class switching*. J Exp Med, 1998. **187**(8): p. 1193-204.
170. Plunkett, M.L. and J.A. Hailey, *An in vivo quantitative angiogenesis model using tumor cells entrapped in alginate*. Lab Invest, 1990. **62**(4): p. 510-7.
171. Dellian, M., et al., *Quantitation and physiological characterization of angiogenic vessels in mice: effect of basic fibroblast growth factor; vascular endothelial growth factor/vascular permeability factor; and host microenvironment*. Am J Pathol, 1996. **149**(1): p. 59-71.
172. Shojaei, F., et al., *Tumor refractoriness to anti-VEGF treatment is mediated by CD11b+Gr1+ myeloid cells*. Nat Biotechnol, 2007. **25**(8): p. 911-20.
173. Benny, O., et al., *An orally delivered small-molecule formulation with antiangiogenic and anticancer activity*. Nat Biotechnol, 2008. **26**(7): p. 799-807.
174. Allport, J.R. and R. Weissleder, *Murine Lewis lung carcinoma-derived endothelium expresses markers of endothelial activation and requires tumor-specific extracellular matrix in vitro*. Neoplasia, 2003. **5**(3): p. 205-17.
175. Tyagi, N., et al., *Fibrinogen induces endothelial cell permeability*. Mol Cell Biochem, 2008. **307**(1-2): p. 13-22.
176. Toellner, K.-M., et al., *Immunoglobulin switch transcript production in vivo related to the site and time of antigen-specific B cell activation*. Journal of Experimental Medicine, 1996. **183**(5): p. 2303-2312.
177. Nanda, A. and B. St Croix, *Tumor endothelial markers: new targets for cancer therapy*. Curr Opin Oncol, 2004. **16**(1): p. 44-9.
178. Ran, S., A. Downes, and P.E. Thorpe, *Increased exposure of anionic phospholipids on the surface of tumor blood vessels*. Cancer Res, 2002. **62**(21): p. 6132-40.
179. Huang, X., M. Bennett, and P.E. Thorpe, *A monoclonal antibody that binds anionic phospholipids on tumor blood vessels enhances the antitumor effect of docetaxel on human breast tumors in mice*. Cancer Res, 2005. **65**(10): p. 4408-16.
180. Ran, S., et al., *Antitumor effects of a monoclonal antibody that binds anionic phospholipids on the surface of tumor blood vessels in mice*. Clin Cancer Res, 2005. **11**(4): p. 1551-62.
181. MacFadyen, J.R., et al., *Endosialin (TEM1, CD248) is a marker of stromal fibroblasts and is not selectively expressed on tumour endothelium*. FEBS Lett, 2005. **579**(12): p. 2569-75.
182. Chaudhary, A., et al., *TEM8/ANTXR1 blockade inhibits pathological angiogenesis and potentiates tumoricidal responses against multiple cancer types*. Cancer Cell, 2012. **21**(2): p. 212-26.
183. Borsi, L., et al., *Selective targeted delivery of TNFalpha to tumor blood vessels*. Blood, 2003. **102**(13): p. 4384-92.
184. Ebbinghaus, C., et al., *Engineered vascular-targeting antibody-interferon-gamma fusion*

- protein for cancer therapy*. Int J Cancer, 2005. **116**(2): p. 304-13.
185. Fabbrini, M., et al., *Selective occlusion of tumor blood vessels by targeted delivery of an antibody-photosensitizer conjugate*. Int J Cancer, 2006. **118**(7): p. 1805-13.
 186. Gafner, V., E. Trachsel, and D. Neri, *An engineered antibody-interleukin-12 fusion protein with enhanced tumor vascular targeting properties*. Int J Cancer, 2006. **119**(9): p. 2205-12.
 187. Kaspar, M., E. Trachsel, and D. Neri, *The antibody-mediated targeted delivery of interleukin-15 interleukin-15 and GM-CSF to the tumor neovasculature inhibits tumor growth and metastasis*. Cancer Res, 2007. **67**(10): p. 4940-8.
 188. Wagner, K., et al., *The targeted immunocytokine L19-IL2 efficiently inhibits the growth of orthotopic pancreatic cancer*. Clin Cancer Res, 2008. **14**(15): p. 4951-60.
 189. Guenzi, E., et al., *The guanylate binding protein-1 GTPase controls the invasive and angiogenic capability of endothelial cells through inhibition of MMP-1 expression*. EMBO J, 2003. **22**(15): p. 3772-82.
 190. Schetter, A.J., N.H. Heegaard, and C.C. Harris, *Inflammation and cancer: interweaving microRNA, free radical, cytokine and p53 pathways*. Carcinogenesis. **31**(1): p. 37-49.
 191. Rho, S.S., et al., *Clec14a is specifically expressed in endothelial cells and mediates cell to cell adhesion*. Biochem Biophys Res Commun, 2011. **404**(1): p. 103-8.
 192. Armstrong, L.J., et al., *ECSM2, an endothelial specific filamin a binding protein that mediates chemotaxis*. Arterioscler Thromb Vasc Biol, 2008. **28**(9): p. 1640-6.
 193. Sumanas, S., T. Joraniak, and S. Lin, *Identification of novel vascular endothelial-specific genes by the microarray analysis of the zebrafish cloche mutants*. Blood, 2005. **106**(2): p. 534-41.
 194. Gomez, G.A., et al., *Discovery and characterization of novel vascular and hematopoietic genes downstream of etsrp in zebrafish*. PLoS One, 2009. **4**(3): p. e4994.
 195. Wasserman, S.M. and J.N. Topper, *Adaptation of the endothelium to fluid flow: in vitro analyses analyses of gene expression and in vivo implications*. Vasc Med, 2004. **9**(1): p. 35-45.
 196. Matharu, N.M., et al., *Inflammatory responses of endothelial cells experiencing reduction in flow after conditioning by shear stress*. J Cell Physiol, 2008. **216**(3): p. 732-41.
 197. Ando, J. and K. Yamamoto, *Vascular mechanobiology: endothelial cell responses to fluid shear stress*. Circ J, 2009. **73**(11): p. 1983-92.
 198. Chu, T.J. and D.G. Peters, *Serial analysis of the vascular endothelial transcriptome under static static and shear stress conditions*. Physiol Genomics, 2008. **34**(2): p. 185-92.
 199. Favre, C.J., et al., *Expression of genes involved in vascular development and angiogenesis in endothelial cells of adult lung*. Am J Physiol Heart Circ Physiol, 2003. **285**(5): p. H1917-38.
 200. Voellenkle, C., et al., *Deep-sequencing of endothelial cells exposed to hypoxia reveals the complexity of known and novel microRNAs*. RNA, 2012. **18**(3): p. 472-84.
 201. Guduric-Fuchs, J., et al., *Deep sequencing reveals predominant expression of miR-21 amongst the small noncoding RNAs in retinal microvascular endothelial cells*. J Cell Biochem, 2012.
 202. John, A. and G. Tuszynski, *The role of matrix metalloproteinases in tumor angiogenesis and tumor metastasis*. Pathol Oncol Res, 2001. **7**(1): p. 14-23.
 203. Safranek, J., et al., *Expression of MMP-7, MMP-9, TIMP-1 and TIMP-2 mRNA in lung tissue of patients with non-small cell lung cancer (NSCLC) and benign pulmonary disease*. Anticancer Res, 2009. **29**(7): p. 2513-7.
 204. Birchmeier, C., et al., *Characterization of ROS1 cDNA from a human glioblastoma cell line*. Proc Natl Acad Sci U S A, 1990. **87**(12): p. 4799-803.

205. Birchmeier, C., S. Sharma, and M. Wigler, *Expression and rearrangement of the ROS1 gene in human glioblastoma cells*. Proc Natl Acad Sci U S A, 1987. **84**(24): p. 9270-4.
206. Maxwell, M., et al., *Overexpression of the ros1 gene in primary human gliomas may contribute to malignant progression*. Int J Oncol, 1996. **8**(4): p. 713-8.
207. Sharma, S., et al., *Characterization of the ros1-gene products expressed in human glioblastoma cell lines*. Oncogene Res, 1989. **5**(2): p. 91-100.
208. Zhao, J.F. and S. Sharma, *Expression of the ROS1 oncogene for tyrosine receptor kinase in adult adult human meningiomas*. Cancer Genet Cytogenet, 1995. **83**(2): p. 148-54.
209. *ROS1 Gene Rearrangement Is Identified in NSCLC*. Cancer Discov, 2012. **2**(2): p. OF9.
210. Bergethon, K., et al., *ROS1 rearrangements define a unique molecular class of lung cancers*. J Clin Oncol, 2012. **30**(8): p. 863-70.
211. Janne, P.A. and M. Meyerson, *ROS1 rearrangements in lung cancer: a new genomic subset of lung adenocarcinoma*. J Clin Oncol, 2012. **30**(8): p. 878-9.
212. Yang, D., et al., *Murine six-transmembrane epithelial antigen of the prostate, prostate stem cell antigen, and prostate-specific membrane antigen: prostate-specific cell-surface antigens highly expressed in prostate cancer of transgenic adenocarcinoma mouse prostate mice*. Cancer Res, 2001. **61**(15): p. 5857-60.
213. Hubert, R.S., et al., *STEAP: a prostate-specific cell-surface antigen highly expressed in human prostate tumors*. Proc Natl Acad Sci U S A, 1999. **96**(25): p. 14523-8.
214. Gomes, I.M., C.J. Maia, and C.R. Santos, *STEAP Proteins: From Structure to Applications in Cancer Therapy*. Mol Cancer Res, 2012. **10**(5): p. 573-87.
215. Alves, P.M., et al., *STEAP, a prostate tumor antigen, is a target of human CD8+ T cells*. Cancer Immunol Immunother, 2006. **55**(12): p. 1515-23.
216. Sah, N.K., et al., *Structural, functional and therapeutic biology of survivin*. Cancer Lett, 2006. **244**(2): p. 164-71.
217. Apps, S.A., W.A. Rankin, and A.P. Kurmis, *Connexin 26 mutations in autosomal recessive deafness disorders: a review*. Int J Audiol, 2007. **46**(2): p. 75-81.
218. Boles, K.S., et al., *MR angiogenesis imaging with Robo4- vs. $\{\alpha\}V\{\beta\}3$ -targeted nanoparticles in a B16/F10 mouse melanoma model*. FASEB J.
219. JV, R., *Fc receptors*. Fundamental Immunology, 2003: p. 685-700.
220. Hamaguchi, Y., et al., *Antibody isotype-specific engagement of Fc γ receptors regulates B lymphocyte depletion during CD20 immunotherapy*. J Exp Med, 2006. **203**(3): p. 743-53.
221. Nimmerjahn, F. and J.V. Ravetch, *Fc γ receptors: old friends and new family members*. Immunity, 2006. **24**(1): p. 19-28.
222. Nagayama, H., et al., *Gastrointestinal bleeding during anti-angiogenic peptide vaccination in combination with gemcitabine for advanced pancreatic cancer*. Clin J Gastroenterol, 2010. **3**(6): p. 307-317.
223. Kamba, T. and D.M. McDonald, *Mechanisms of adverse effects of anti-VEGF therapy for cancer*. Br J Cancer, 2007. **96**(12): p. 1788-95.
224. Mailhos, C., et al., *Delta4, an endothelial specific notch ligand expressed at sites of physiological and tumor angiogenesis*. Differentiation, 2001. **69**(2-3): p. 135-44.
225. Noguera-Troise, I., et al., *Blockade of Dll4 inhibits tumour growth by promoting non-productive non-productive angiogenesis*. Nature, 2006. **444**(7122): p. 1032-7.
226. Hellstrom, M., et al., *Dll4 signalling through Notch1 regulates formation of tip cells during*

- angiogenesis*. Nature, 2007. **445**(7129): p. 776-80.
227. Jubb, A.M., et al., *Expression of vascular Notch ligands Delta-like 4 and Jagged-1 in glioblastoma*. Histopathology, 2012. **60**(5): p. 740-7.
 228. Jubb, A.M., et al., *Expression of vascular notch ligand delta-like 4 and inflammatory markers in breast cancer*. Am J Pathol, 2010. **176**(4): p. 2019-28.
 229. Jubb, A.M., et al., *Expression of delta-like ligand 4 (Dll4) and markers of hypoxia in colon cancer*. Br J Cancer, 2009. **101**(10): p. 1749-57.
 230. Yan, M., et al., *Chronic DLL4 blockade induces vascular neoplasms*. Nature, 2010. **463**(7282): p. E6-7.
 231. Huijbers, E.J., et al., *The non-toxic and biodegradable adjuvant Montanide ISA 720/CpG can replace Freund's in a cancer vaccine targeting ED-B--a prerequisite for clinical development*. Vaccine, 2012. **30**(2): p. 225-30.
 232. Carnemolla, B., et al., *A tumor-associated fibronectin isoform generated by alternative splicing of messenger RNA precursors*. J Cell Biol, 1989. **108**(3): p. 1139-48.
 233. Onn, A. and R.S. Herbst, *Molecular targeted therapy for lung cancer*. Lancet, 2005. **366**(9496): p. 1507-8.
 234. Xiong, H.Q., K. Carr, and J.L. Abbruzzese, *Cytotoxic chemotherapy for pancreatic cancer: Advances to date and future directions*. Drugs, 2006. **66**(8): p. 1059-72.
 235. Abengozar, M.A., et al., *Blocking ephrin-B2 with highly specific antibodies inhibits angiogenesis, lymphangiogenesis, and tumor growth*. Blood, 2012.
 236. Palumbo, A., et al., *A chemically modified antibody mediates complete eradication of tumours by selective disruption of tumour blood vessels*. Br J Cancer, 2011. **104**(7): p. 1106-15.
 237. Guojun, W., et al., *A novel vaccine targeting gastrin-releasing peptide: efficient inhibition of breast cancer growth in vivo*. Endocr Relat Cancer, 2008. **15**(1): p. 149-59.
 238. Kaur, S., et al., *Robo4 signaling in endothelial cells implies attraction guidance mechanisms*. J Biol Chem, 2006. **281**(16): p. 11347-56.
 239. Jones, C.A., et al., *Robo4 stabilizes the vascular network by inhibiting pathologic angiogenesis and endothelial hyperpermeability*. Nat Med, 2008. **14**(4): p. 448-53.
 240. Koch, A.W., et al., *Robo4 maintains vessel integrity and inhibits angiogenesis by interacting with UNC5B*. Dev Cell, 2011. **20**(1): p. 33-46.
 241. Lu, X., et al., *The netrin receptor UNC5B mediates guidance events controlling morphogenesis of the vascular system*. Nature, 2004. **432**(7014): p. 179-86.
 242. Larrivee, B., et al., *Activation of the UNC5B receptor by Netrin-1 inhibits sprouting angiogenesis*. Genes Dev, 2007. **21**(19): p. 2433-47.